SCIENTIFIC NOTEBOOK #432E

Randall Fedors
GHGC
TEF KTI

Volume VII – Cold Trap

Sept 02, 2002 started
Volume VII, pages 1-150

Volume VII – TEF Cold Trap **9/6/02** RF

Initial Entry

The cold trap laboratory experiment has been setup and running test phases. Data from this experiment is recorded in Jim Prikryl's scientific notebook (#337). This notebook will contain developments and interpretations of the experiment and the resulting data. Data from the cold trap experiment will help evaluate DOE's model for the cold trap, particularly with regards to thermal scaling, airflow patterns, and condensation rates.

Collaborators: Jim Prikryl, Franklin Dodge, Stefan Mayer, Lauren Browning, Steve Green

Computers: WinNT box is called bubo in Bldg 189, Room A214
Sun is Spock (used for plotting in Tecplot 8)

The pc in my office (called bubo) is:
Primary computer running WindowsNT 4.00.1381 is called bubo (Acer, x86 Family 6 Model 4 Stepping 2; AT compatible with 512 MBytes RAM).

Software on bubo (I can't remember any upgrades since last February 2002):

ArcView version 3.2a
Adobe Acrobat & Distiller version 5.0
Adobe Illustrator 8.0
Adobe Photoshop version 5.0.2
Corpscon version 5.11.08 (U.S. Army Corps of Engineers)
ENVI version 3.6
Excel 97 SR-2
HYDRUS-2D version 2.05
Lahey/Fujitsu Fortran 95 version 5.0
MathCad 2000
Mathematica version 4.2.0.0
NIST Standard Reference Database 10, version 2.2
Sigma Plot2000 version 6.00
Word 97 SR-2
Word Perfect version 8.00

UNIX (use uname –X on SUNs and uname -msR) as of March 2003
SGI: Io with a IP27 cpu board, 64-bit, running IRIX64 version 6.5 6.5.14m
ERDAS Imagine version 8.5
Earth Vision 5.1 (Dynamic Graphics)
SUN:
Spock is a SUN sparc Ultra 4 (4 cpu), 64-bit,
running SunOS version (Kernel ID) Generic_108528-17 release 5.8

fortran 77 version 5.0 (SUN Workshop Compiler FORTRAN 77 version 5.0)

Estimates of Thermal Properties

Initial computational fluid dynamics modeling will use an effective material for the ceramic/sand/Lexan composite. Hence, an effective thermal conductivity is needed.

Effective thermal conductivity was needed for the materials in the laboratory setup. Approximate values are acceptable for the individual materials, The effective thermal conductivity data is below. Assuming the radial condition with the radius determined from the thickness of each material (saturated ceramic, partially saturated sand, lexan, silica insulation) immediately above the cylinder: Quartz, which is the primary component of the fine sand has a thermal conductivity of 0.19 K/m-K and water is 0.606 W/m-K (Kreith and Bohn, Principles of Heat Transfer, Brooks/Cole Publishing,2001; or Incropera and DeWitt, Fundamentals of Heat and Mass Transfer, Wiley, 2002). With a porosity of 0.35, the weighted thermal conductivity of the sand would be 0.24 W/m-K. A similar method was used to estimate the ceramic, though the thermal conductivity of ceramic was set to 0, thus water in the pores supplies all the conductance.

Thermal Conductivity (W/m*K)	Thickness, delta y (cm)	where y is the distance (layer thickness)
0.212	0.675	ceramic (conduction only in water phase, 35% porosity)
0.24	8.305	sand (saturation with water assumed)
0.008	1.27	lexan (web source, www.sdplastics.com/polycarb.htm)
0.210	10.25	Total/bulk property (calculated as a thickness-weighted mean)

I'll ignore the insulation for now, since we're measuring temperatures inside and outside the insulation. There is an small <2 °C difference, and the temperature patterns track fairly well.

Note that the sand thermal conductivity, and the uncertainty of saturation in the sand above the cylinder, is very important to the conductance of heat away from the drift. We need explore ways of measuring the dry and wet thermal conductivity of the sand. Measuring in the lab will be expensive to develop the right configuration. Sending out to a known expert is cheaper but carries the QA requirement of auditing the lab (likely a university lab, which generally do not have formal QA procedures written down).

The ceramic assumption (nonconductive) requires further literature search. The ceramic is Kellundite, an alumina-bonded ceramic. The alumina-bonded part could impart some thermal conductance capability, though ceramics are in general non-conductors. The lexan thickness is small and far from the action (the thermal effect is significantly dampened where the lexan is in place. The sand thermal conductivity has a narrow range based on typical values from the literature. Therefore, I will use the temperature data from the sand profiles to make sure that the ceramic is a non-conductor when dry.

To estimate the thermal conductivity of a sand (30-40% porosity, Prikryl notebook #337), use a 1-D model for thermal flux. The thermal flux between two different sections, in series, are equal. If one-dimensional heat flow is assumed, then the heat flux J $=K_{th}$ * temperature gradient; where the temperature gradient is ΔTemperature / distance, and K_{th} is the thermal conductivity of each material. If the thermal conductivity of one material is known with confidence, then the thermal

conductivity of the other material can be estimated if temperature data is available. Using a FiberFrax insulation thermal conductivity of 0.035 W/mK with thickness of insulation=0.0254 m, and the temperature gradients extracted from steady state conditions for the highest power setting in cttest#11 for across the insulation is ΔT=-3.1 C, and across the sand is DT=-2.93 and –0.78 C for the profiles at 57.15 cm and 46.99 cm, the thermal conductivity of the sand would be 0.144 and 0.72 W/mK. These, of course are rough calculations because the same temperature gradient across the insulation was used at both profile locations, and because of the dimensionality issue, and because the thermocouples in the sand were not ideally placed for such a calculation, and .... This range includes the previously estimated 0.24 W/mK, the method used to get that number is generally not a satisfying approach.

Power to Heater

Don Bannon checked data for the power calibrations for the transformer on the cold trap experiment. The first time the calibration was done, the transformer was started just for the calibration. I'll call this the cold calibration. I had Don re-do some points on the calibration when the transformer had been running for a few days; I'll call this one the hot calibration. The "cold" and "hot" power noted below refer to use of the cold or hot calibration to predict watts for cttest11. The times correspond to the temperature slice data I gave you earlier today.

cold trap test 11 (cttest11)

Time (hrs)	cold Power (W)	hot Power (W)
457	3.627	3.370
735	5.607	5.251
925	1.351	1.246

Even though there were fewer calibration points for the hot calibration, I am inclined to go with those data.

Calculations done in
E:\TEF-kti\ColdTrap\TestData\cttest11.xls, worksheet "PowerCalib"

Sigma Plot 2000 version 6.00 was used for the regression of transformer settings and measured power (watts) using cubic polynomials. The regression coefficients are

August 2, 2002 calibration		
y = y0 +ax + bx^2 +cx^3 where x is setting (%) and y is predicted power		
-0.111316	y0	adj R^2 = .99992
0.0286087	a	
0.00755699	b	
1.79E-05	c	
quadratic		
0.457096	y0	adj R^2 = .9997
-0.0624643	a	little poorer on low end and high end
0.0101054	b	

August 20, 2002 calibration		
y = y0 +ax + bx^2 +cx^3 where x is setting (%) and y is predicted power		
0.00578097	y0	adj R^2 = .99995
0.0102372	a	
0.00755941	b	
1.70E-05	c	

Details of the calibration measurements by Don Bannon are in the following table

Calibration with the help of Don Bannon on August 2, 2002
using Don's equipment
Transformer was off for a few days
(cold) prior to calibration
Heater element: 100W
OMEGALUX, 3/8 inch sheath

Power (watts) = Voltage (volts) *
Current (amps)
voltage is the difference in electrical potential between 2 points, current is what flows between those 2 points

Equipment used:	Fluke 87	**Staco Energy Products Co.**
Wavetek 27XT S/N 971004157 Calibrated: 17 JUL 02	S/N 61880517 Calibrated: 11 MAR 02	**Type 3PN1010 Variable Autotransformer**

8/20/02 Transformer, cold calibration						**8/20/02** Transformer, hot calibration			
				2-Aug	20-Aug				
Percent of Max. Output	A.C. volts	Current amps	Power watts	Estimated Power watts	Estimated Power watts	Percent of Max. Output	A.C. volts	Current amps	Power watts
0	0.51	0.003	0.0017	-1.11E-01	5.78E-03				
1	1.44	0.010	0.0138	-7.51E-02	2.36E-02				
2	2.53	0.017	0.0435	-2.37E-02	5.66E-02	2	2.51	0.017	0.0419
3	3.53	0.025	0.0893	4.30E-02	1.05E-01				
4	4.56	0.032	0.1477	1.25E-01	1.69E-01				
5	5.56	0.040	0.2207	2.23E-01	2.48E-01	5	5.71	0.038	0.2164
6	6.57	0.047	0.3081	3.36E-01	3.43E-01				
7	8.02	0.057	0.4595	4.65E-01	4.54E-01				
8	9.11	0.065	0.5922	6.10E-01	5.80E-01				
9	10.13	0.072	0.7324	7.71E-01	7.23E-01				
10	11.15	0.080	0.8875	9.48E-01	8.81E-01	10	10.90	0.076	0.8306
12	13.70	0.098	1.3385	1.35E+00	1.25E+00				
14	15.63	0.111	1.7412	1.82E+00	1.68E+00				
16	17.74	0.127	2.2441	2.35E+00	2.17E+00				
18	20.10	0.145	2.9065	2.96E+00	2.74E+00				
20	22.10	0.159	3.5161	3.63E+00	3.37E+00	20	22.40	0.165	3.7050
22	24.60	0.177	4.3468	4.37E+00	4.07E+00				
24	26.60	0.191	5.0806	5.18E+00	4.84E+00				

26	28.50	0.209	5.9565	6.06E+00	5.68E+00				
28	31.00	0.224	6.9440	7.01E+00	6.59E+00				
30	33.60	0.242	8.1312	8.03E+00	7.57E+00	30	33.00	0.220	7.2600
32	35.70	0.256	9.1392	9.13E+00	8.63E+00				
34	37.70	0.271	10.2167	1.03E+01	9.76E+00				
36	40.30	0.289	11.6467	1.15E+01	1.10E+01				
38	42.40	0.304	12.8896	1.29E+01	1.22E+01				
40	45.00	0.322	14.4900	1.43E+01	1.36E+01	40	44.10	0.310	13.6710
42	47.50	0.339	16.1025	1.57E+01	1.50E+01				
44	48.90	0.348	17.0172	1.73E+01	1.65E+01				
46	51.40	0.367	18.8638	1.89E+01	1.81E+01				
48	53.40	0.379	20.2386	2.07E+01	1.98E+01				
50	55.90	0.398	22.2482	2.25E+01	2.15E+01				
52	58.50	0.424	24.8040	2.43E+01	2.34E+01				
54	60.60	0.438	26.5428	2.63E+01	2.53E+01				
56	62.60	0.451	28.2326	2.83E+01	2.73E+01				
58	65.40	0.471	30.8034	3.05E+01	2.93E+01				
60	67.80	0.486	32.9508	3.27E+01	3.15E+01	60	66.90	0.470	31.4430
65	73.20	0.525	38.4300	3.86E+01	3.73E+01				
70	79.30	0.569	45.1217	4.51E+01	4.36E+01				
75	85.30	0.611	52.1183	5.21E+01	5.04E+01	75	84.20	0.600	50.5200
80	91.50	0.654	59.8410	5.97E+01	5.79E+01				
85	97.10	0.694	67.3874	6.79E+01	6.59E+01				
90	103.30	0.738	76.2354	7.67E+01	7.45E+01				
95	109.50	0.787	86.1765	8.62E+01	8.37E+01				
100	115.30	0.839	96.7367	9.62E+01	9.36E+01	100	114.10	0.820	93.5620
FULL Clockwise	116.80	0.853	99.6304			FULL Clockwise	115.60	0.840	97.1040

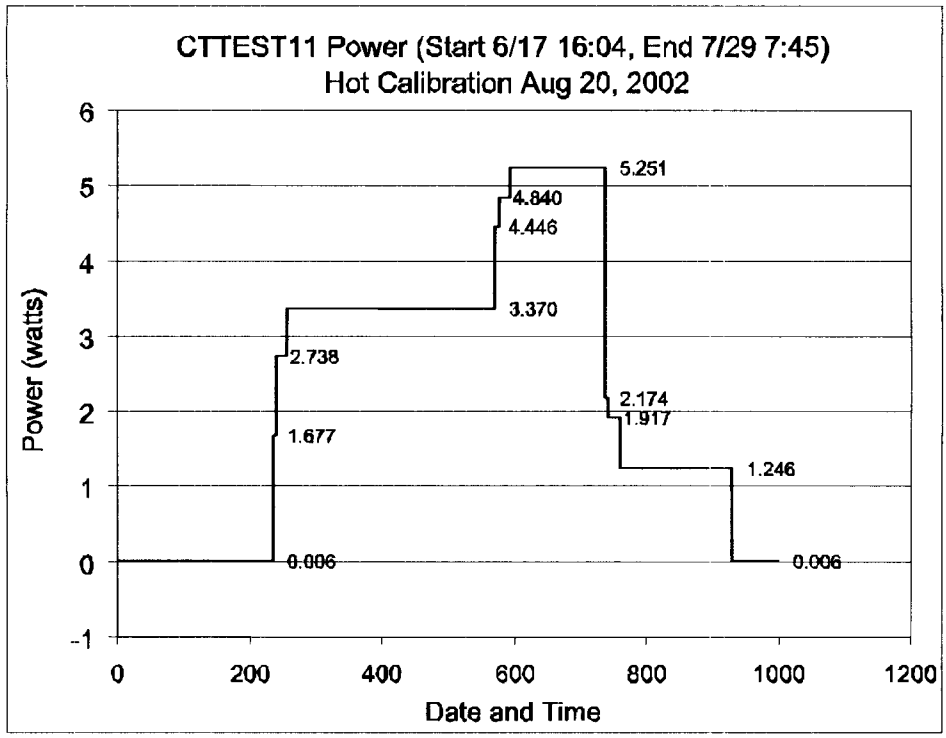

The figures on this page plot the same data, just at different resolution. The regression fit to the calibration data was based on the full range, transformer settings from 0 to 100. The upper figure displays the range expected for most of our cold trap experiments using the desktop model (~1% scale).

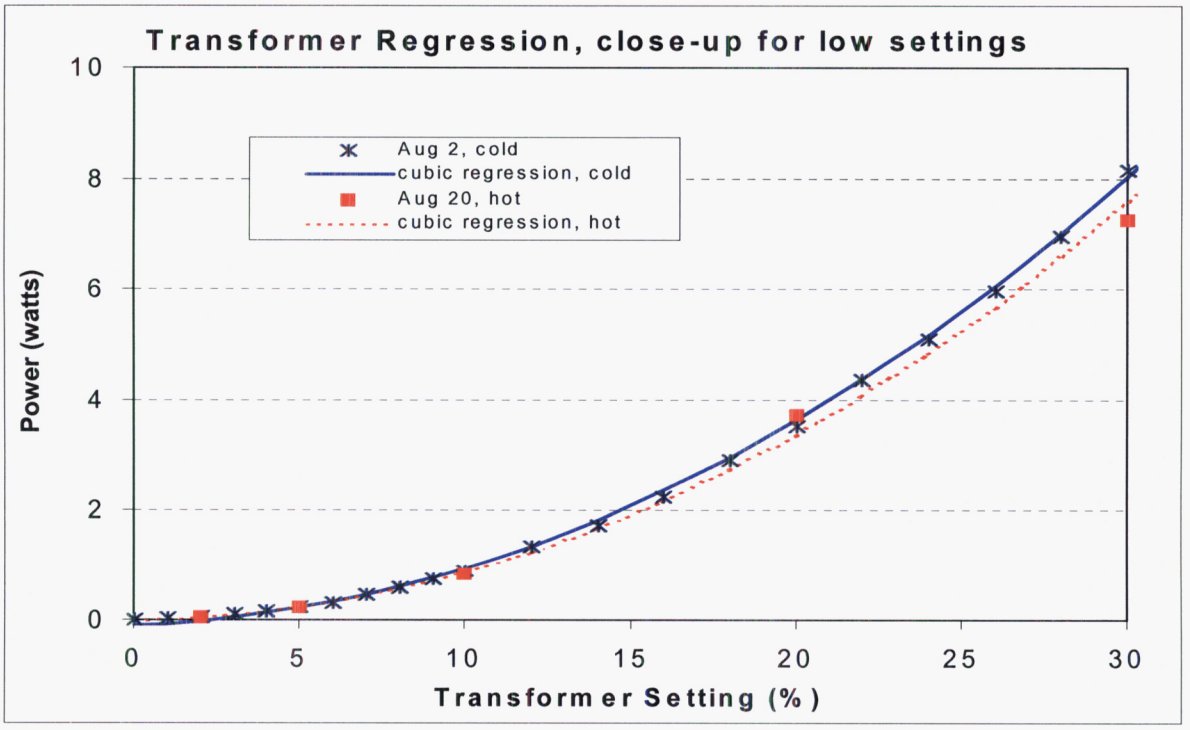

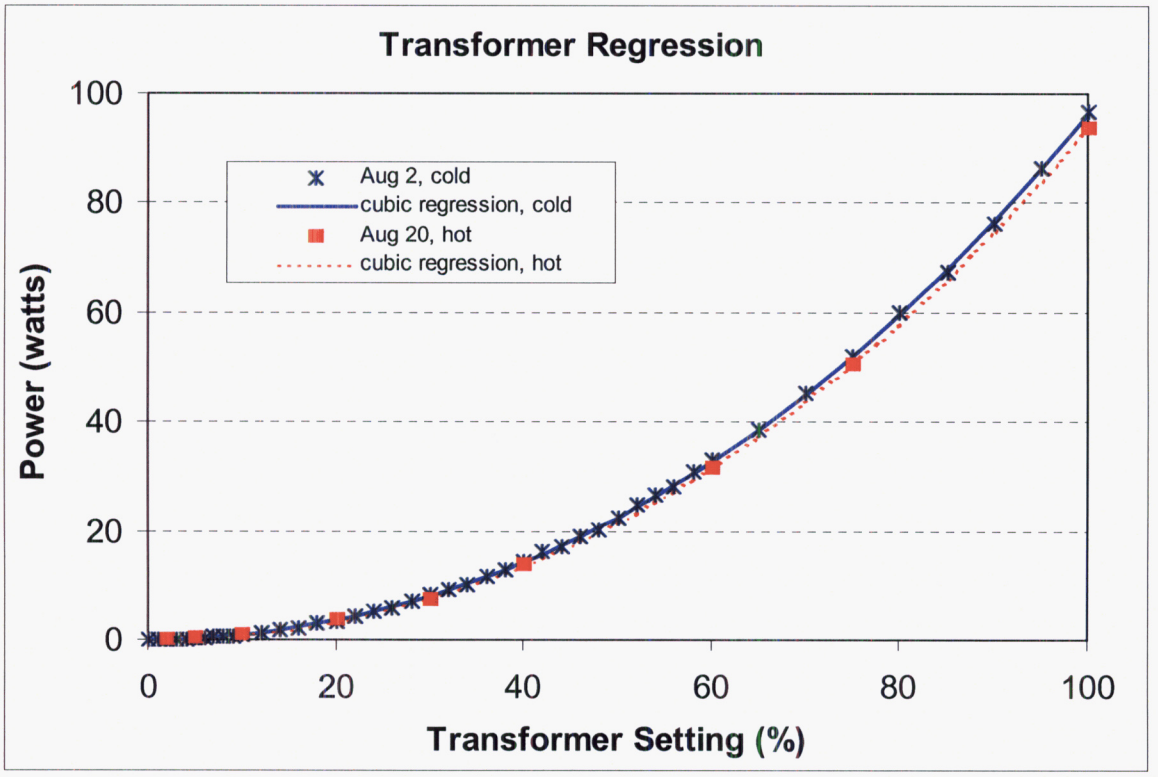

RF 9/16/02

Frank Dodge's MathCad sheet:
bubo: E:\TEF-kti\ColdTrap\AnalyticalSoln\coldTrapModelProblem-2000ver.mcd
This file is run using MathCad 2000 on bubo.

ANALYSIS OF COLD-TRAP EXPERIMENT

This is an analysis of a "model" problem tha is meant to aid in designing and interpreting the Cold Trap experiment. It replaces the actual cylindrical experiment drift with a two-dimensional drift. the model probelm also replaces the heater by a uniform hot wall. The object of the analysis is to predict the magnitudes of the overall circulation in the drift and the rate at which moisture might be condensed on a target near the cold wall.
Various values of the parameters can be input (as indicated by the **red text** below) to investigate their effects.

The overall geometry of the model problem is shown in the illustration.

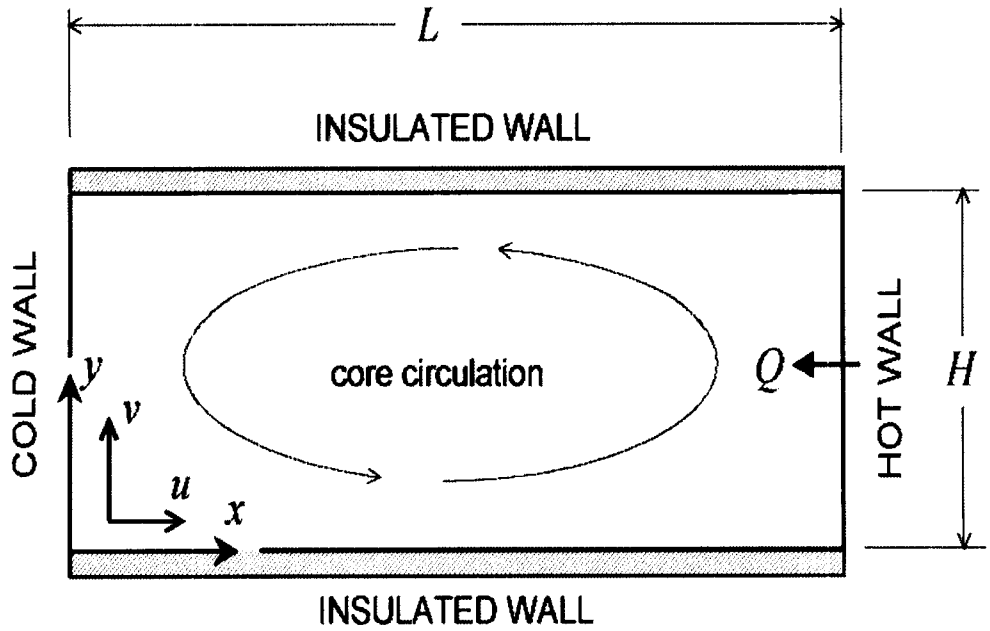

The main assumptions used in the *flow* analysis are:

2-D x,y geometry
heat Q added at the hot wall and removed at the cold wall
walls at $y = 0$ and $y = H$ are insulated
steady flow
Boussinesq approximation is used to estimate buyoyancy effects
The equations of motion are made nondimensional using the following scheme

$X = x/L$ $\quad Y = y/H$ = non-dimensional coordinates
$U = u\,(\nu_0 L)(g\beta_0 H^3 \Delta T_0)^{-1}$ = non-dimensional velocity in x-direction
$V = v\,(\nu_0 L^2)(g\beta_0 H^4 \Delta T_0)^{-1}$ = non-dimensional velocity in y-direction
$\theta = (T - T_c)/\Delta T_0$ = non-dimensional temperature

The symbols are defined as:

ΔT_0 = temperature difference between hot and cold walls
T = air temperature at time t at location x,y

T_c = temperature of the cold wall at $x = 0$
g = gravitational acceleration
β_o = thermal expansion coeffcient of air at the reference temperature
ν_o = kinematic viscosity of air at the reference temperature

Other symobls that will be used subsequently are defined as:

α_o = thermal diffusivity of air, $k_o/\rho_o C_{po}$, at the reference temperature
δ^* = boundary layer thickness parameter
ρ_o = density of air at the reference temperature
C_{po} = specific heat of air at the reference temperature
k_o = thermal conductivity of air at the reference temperature
p = pressure
Pr = Prandtl number, ν_o/α_o
Q = heat input at hot wall (per unit width of the drift)
Ra = Rayleigh number, $g\beta_o H^3 \Delta T_o/(\alpha_o \nu_o)$
t = time

With these definitions and non-dimensional variables, we expect that the **non-dimensional variables will have a maximum value of one and a minimum of zero**:

$0 <= x <= 1$ $0 <= y <= 1$ $0 <= |U| <= 1$ $0 <= |V| <= 1$ $0 <= |\theta| <= 1$

GOVERNING DIFFERENTIAL EQUATIONS

The circulatory flow within the 2-D drift is governed by the following diffferenital equations, which express the conservation of mass, momentum, and energy requirements:

conservation of mass:

$$\frac{\partial U}{\partial X} + \frac{\partial V}{\partial Y} = 0$$

combined *x* and *y* conservation of momentum (combining the equations eliminates pressure as a variable)

$$\left(\frac{H}{L}\right)^4 \left(\frac{Ra}{Pr}\right)\left[\frac{\partial}{\partial X}\left(U\frac{\partial U}{\partial X} + V\frac{\partial U}{\partial Y}\right)\right] - \left(\frac{H}{L}\right)^2 \left(\frac{Ra}{Pr}\right)\left[\frac{\partial}{\partial Y}\left(U\frac{\partial V}{\partial X} + V\frac{\partial V}{\partial Y}\right)\right] =$$

$$\frac{\partial \theta}{\partial X} - \frac{\partial^3 U}{\partial Y^3} + \left(\frac{H}{L}\right)^2 \left[\frac{\partial}{\partial Y}\left(\frac{\partial^2 V}{\partial X \partial Y} - \frac{\partial^2 U}{\partial X^2}\right)\right] + \left(\frac{H}{L}\right)^4 \frac{\partial^3 V}{\partial X^3}$$

conservation of energy

$$Ra\left(\frac{H}{L}\right)^2 \left(U\frac{\partial \theta}{\partial X} + V\frac{\partial \theta}{\partial Y}\right) = \frac{\partial^2 \theta}{\partial Y^2} + \left(\frac{H}{L}\right)^2 \frac{\partial \theta}{\partial X^2}$$

The **boundary conditions** for these differential equations are expressed as:

$U = V = 0$ for $X = 0$ and $X = 1$, and for $Y = 0$ and $Y = 1$ ("no - slip")

$\frac{\partial \theta}{\partial Y} = 0$ for $Y = 0$ and $Y = 1$ (insulated walls)

$\theta = 0$ for $X = 0$; $\theta = 1$ for $X = 1$

Considering the form of these equations and the fact that $(H/L)^2 << 1$, it is natural to try to find a **solution expressed in powers of $(H/L)^2$** since higher order terms can be negelected. Thus, we assume:

$$U = U_o + \left(\frac{H}{L}\right)^2 U_1 + \left(\frac{H}{L}\right)^4 U_2 + \ldots$$

$$V = V_o + \left(\frac{H}{L}\right)^2 V_1 + \left(\frac{H}{L}\right)^4 V_2 + \ldots$$

$$\theta = \theta_o + \left(\frac{H}{L}\right)^2 \theta_1 + \left(\frac{H}{L}\right)^4 \theta_2 + \ldots$$

These expressions are substituted into the differential equations for mass, momentum, and energy conservation given above. We collect the terms in powers of the parameter $(H/L)^2$. Since $(H/L)^2$ in principle can have any value, it is necessary that the expressions multiplied by the various powers of $(H/L)^2$ must each be satisfied individually. This process gives the following set of differential equations.

Zeroth order $(H/L)^0$ equations

$$\frac{\partial U_o}{\partial X}+\frac{\partial V_o}{\partial Y}=0$$

$$\frac{\partial \Theta_o}{\partial X}-\frac{\partial^3 U_o}{\partial Y^3}=0$$

$$\frac{\partial^2 \Theta_o}{\partial Y^2}=0$$

First order $(H/L)^2$ equations

$$\frac{\partial U_1}{\partial X}+\frac{\partial V_1}{\partial Y}=0$$

$$-\frac{Ra}{Pr}\left[\frac{\partial}{\partial Y}\left(U_o\frac{\partial U_o}{\partial X}+V_o\frac{\partial U_o}{\partial Y}\right)\right]=\frac{\partial \theta_1}{\partial X}-\frac{\partial^3 U_1}{\partial Y^3}+\frac{\partial^3 V_o}{\partial X\partial Y^2}-\frac{\partial^3 U_o}{\partial Y\partial X^2}$$

$$Ra\left(U_o\frac{\partial \theta_o}{\partial X}+V_o\frac{\partial \theta_o}{\partial Y}\right)=\frac{\partial^2 \theta_o}{\partial X^2}+\frac{\partial^2 \theta_1}{\partial Y^2}$$

Second order $(H/L)^4$ equations

$$\frac{\partial U_2}{\partial X}+\frac{\partial V_2}{\partial Y}=0$$

$$\frac{Ra}{Pr}\left[\frac{\partial}{\partial X}\left(U_o\frac{\partial U_o}{\partial X}+V_o\frac{\partial U_o}{\partial Y}\right)\right]-\frac{Ra}{Pr}\left[\frac{\partial}{\partial Y}\left(U_o\frac{\partial U_1}{\partial X}+V_o\frac{\partial U_1}{\partial Y}+U_1\frac{\partial U_o}{\partial X}+V_1\frac{\partial U_o}{\partial Y}\right)\right]=$$

$$\frac{\partial \Theta_2}{\partial X}-\frac{\partial^3 U_2}{\partial Y^3}+\frac{\partial^3 V_1}{\partial X\partial Y^2}-\frac{\partial^3 U_1}{\partial Y\partial X^2}+\frac{\partial^3 V_o}{\partial X^3}$$

$$Ra\left(U_o\frac{\partial \theta_1}{\partial X}+V_o\frac{\partial \theta_1}{\partial Y}+U_1\frac{\partial \theta_o}{\partial X}+V_1\frac{\partial \theta_o}{\partial Y}\right)=\frac{\partial^2 \theta_2}{\partial Y^2}+\frac{\partial^2 \theta_1}{\partial X^2}$$

The third and higher order equations are similar to the second order equations.

SOLUTION TO DIFFERENTIAL EQUATIONS FOR THE <u>CORE</u> FLOW

The solution of the differential equations correct through the first order terms is:

$$U(K_1,Y):=\frac{1}{6}\cdot K_1\cdot\left(Y^3-\frac{3}{2}\cdot Y^2+\frac{1}{2}\cdot Y\right)$$

$$V(K_1,Y):=0$$

$$\theta(K_1,K_2,Ra,H,L,X,Y):=K_2+K_1\cdot X+\frac{1}{120}\cdot Ra\cdot K_1^{\,2}\cdot\left(\frac{H}{L}\right)^2\cdot\left(Y^5-\frac{5}{2}\cdot Y^4+\frac{5}{3}\cdot Y^3\right)$$

where K_1 and K_2 are integration constants to be determined.

These equations represent the <u>core</u> flow away from the $X = 0$ and $X = 1$ ends of the channel. Note that U is not identically zero at $X = 0$ and $X = 1$ as the boundary conditions require. However, the average value of U across the channel height is zero, so the $X = 0$ and $X = 1$ boundary conditions are satisfied in an average sense. Similarly, the temperature θ is not constant at either the hot end or the cold end. The way the solutions are corrected to meet the boundary more exactly is described later.

HEAT FLOW FROM HOT END TO COLD END OF CHANNEL

The net heat flow from the hot end of the channel to the cold end is a combination of conduction through the air and the energy carried by the flow. It is given by the following integral. Note that the integral does not depend on position X in the channel.

$$Q = \int_0^H \left(k_o \frac{\partial T}{\partial X} - \rho_o C_{po} u T \right) dy$$

Carrying out the integration gives

$$Q(k_o, H, L, Ra, K_1, \Delta T_o) := k_o \cdot \Delta T_o \cdot \left(\frac{H}{L}\right) \cdot \left[K_1 + \frac{K_1^{\,3}}{362880} \cdot \left(\frac{H}{L} \cdot Ra\right)^2 \right]$$

EVALUATION OF INTEGRATION CONSTANTS TO MEET BOUNDARY CONDITIONS

A simple way to evaluate K_1 and K_2 is to set the average value of θ equal to 0 at $X = 0$ and equal to 1 at $X = 1$. This procedure gives $K_1 = 1$ and $K_2 = 0$. This satisfies the boundary conditions at X = 0 and X = 1 only in an average sense. We can do better by correcting the previous expressions by including the equations for higher powers of $(H/L)^2$ or we can consider the end effects separately by a boundary layer approach. The boundary layer approach is selected because it converges more quickly. Furthermore, an "integral" formulation is used. The boundary layer thickness at the end walls is denoted by δ. From symmetry, δ is the same on the cold wall and the hot wall. Thus, we will impose symmetry about the center of the drift and consider just the cold wall. The end conditions are denoted by the subscript "*e*."

The symmetry condition of θ = 0.5 for X=0.5, Y = 0.5 requires that:

$$K_2 + \frac{1}{2} K_1 + Ra \left(\frac{H}{L}\right)^2 \frac{K_1}{1440} = \frac{1}{2}$$

The boundary conditions at the cold wall are: (a) all velocities be zero; and (b) the temperature be constant and equal to the cold wall temperature. These conditions require that:

$$U_e = V_e = \theta_e = 0 \qquad \frac{\partial \theta_e}{\partial Y} = 0 \qquad \text{at} \quad X = 0$$

There are also conditions required to match the boundary layer to the core flow at the edge of the boundary layer and to make the boundary layer flow merge smoothly with the core flow; these conditions are expressed as:

$$U_e = U \qquad V_e = V = 0 \qquad \theta_e = \theta \qquad \text{at } X = \delta$$

$$\frac{\partial U_e}{\partial X} = \frac{\partial U}{\partial X} \qquad \frac{\partial V_e}{\partial X} = \frac{\partial V}{\partial X} = 0 \qquad \frac{\partial \theta_e}{\partial X} = \frac{\partial \theta}{\partial X} \qquad \text{at} \quad X = \delta$$

For an "integral" solution, we assume physically reasonable functions for the velocities and temperature, which are then made to satisfy the governing equations in an integral sense. The unknown in these functions is the boundary layer thickness, δ.

Suitable fundtional forms for the velocities and temperature that satisfy all the above B.C.s are:

$$U_e = K_1 \left(Y^3 - \frac{3}{2} Y^2 + \frac{1}{2} Y \right) \left(\frac{X}{\delta}\right)^2 \left[1 - \frac{4}{3} \left(\frac{X}{\delta}\right) + \frac{1}{2} \left(\frac{X}{\delta}\right)^2 \right]$$

$$V_e = \frac{K_1}{2\delta} \left(Y^4 - 2Y^3 + Y^2 \right) \left(\frac{X}{\delta}\right) \left(1 - \frac{X}{\delta}\right)^2$$

$$\theta_e = \left[K_2 + K_1 X + \frac{Ra}{120} K_1^2 \left(\frac{H}{L}\right)^2 \left(Y^5 - \frac{5}{2} Y^4 + \frac{5}{3} Y^3 \right) \right] \left(\frac{X}{\delta}\right) \left(2 - \frac{X}{\delta}\right)$$

Furthermore, the expressions for U_e and V_e satisfy the conservation of mass differential equation. Thus, only the conservation of momentum and conservation of energy equations remain to be satisfied. These equations are put into an integral form by integrating them across the boundary layer thickness. The result, for example, for the **conservation of energy** differential equation is:

$$Ra \left(\frac{H}{L}\right) \int_0^\delta \int_0^1 U_e \frac{\partial \theta_e}{\partial X} dX dY + Ra \left(\frac{H}{L}\right)^2 \int_0^\delta \int_0^1 V_e \frac{\partial \theta_e}{\partial Y} dX dY = \int_0^\delta \int_0^1 \left[\left(\frac{H}{L}\right)^2 \frac{\partial^2 \theta_e}{\partial X^2} + \frac{\partial^2 \theta_e}{\partial Y^2} \right] dX d$$

Some of the integrations can be done by parts to give the final result:

$$Ra\int_0^1 U_e\theta_e\big|_{X=\delta}\,dY = K_1 - \int_0^1 \left.\frac{\partial\theta_e}{\partial Y}\right|_{X=\delta} dY$$

Similarly, the **conservation of momentum** integral reduces to:

$$\int_0^1 \theta_e\big|_{X=\delta}\,dY - \int_0^\delta \left.\frac{\partial^2 U_e}{\partial Y^2}\right|_{Y=0}^{Y=1} dX - \left(\frac{H}{L}\right)^4 \int_0^1 \left.\frac{\partial^2 V_e}{\partial X^2}\right|_{X=0}^{X=\delta} dY = 0$$

By substituting in the previous functional expressions and performing the integrations, we derive the following two equations that relate the unknown parameters:

$$\frac{2}{5}\left(\frac{H}{L}K_1\right)\left[\frac{1}{4} - (\delta')^4\right] = \left[K_2 + \frac{Ra}{1440}\left(\frac{H}{L}K_1\right)^2\right](\delta')^3$$

$$\frac{Ra^2}{725{,}760}\left(\frac{H}{L}K_1\right)^3 \delta' = K_2 + \frac{Ra}{1440}\left(\frac{H}{L}K_1\right)^2$$

where $\delta' = \delta(L/H)$ is a scaled boundary layer thickness that is more convenient for numerical work since it is not so small as δ.

These two expressions and the previous expression for the symmetry condition are sufficient to determine the three unknowns: K_1, K_2, and δ'.

NUMERICAL RESULTS

Input values for drift dimensions, air properties, and desired temperature difference from the hot end to the cold end of the drift (properties are evaluated at about 60 deg C).

Air viscosity:

$$\nu_o := 0.191\cdot\frac{cm^2}{s}$$

Air diffusivity:

$$\alpha_o := 0.268\cdot\frac{cm^2}{s}$$

Air conductivity:

$$k_o := 0.000283\cdot\frac{watt}{cm\cdot K}$$

Drift height:

$H := 5\cdot cm$

Drift length:

$L := 24\cdot 2.54\cdot cm$

Gravity:

$$g := 980\cdot\frac{cm}{s^2}$$

Cold wall temperature:

$T_c := 295\cdot K$

Temperature difference:

$\Delta T_o := 32\cdot K$

Computed parameters

Air expansion coefficient:

$$\beta_o := \frac{1}{T_c + \Delta T_o}$$

$$\beta_o = 3.058 \times 10^{-3} \frac{1}{K}$$

Rayleigh number:

$$Ra := \frac{g \cdot \beta_o \cdot H^3 \cdot \Delta T_o}{\nu_o \cdot \alpha_o}$$

$$Ra = 2.342 \times 10^5$$

Equations are solved by inputting guesses and then finding the solution

(Because of limitations in Mathcad's font selection for equations, δ' will be replaced by δ_x for numerical work)

Guesses:

$K_1 := 1$

$K_2 := 0$

$\delta_x := 1$

Given

$$K_2 + 0.5 \cdot K_1 + \left(\frac{H}{L} \cdot K_1\right)^2 \cdot \frac{Ra}{1440} = 0.5$$

(symmetry condition)

$$0.4 \cdot \left(\frac{H}{L} \cdot K_1\right) \cdot \left(0.25 - \delta_x^4\right) = \delta_x^3 \cdot \left[K_2 + \left(\frac{H}{L} \cdot K_1\right)^2 \cdot \frac{Ra}{1440}\right]$$

(conservation of energy)

$$\left(\frac{H}{L} \cdot K_1\right)^3 \cdot \frac{Ra^2 \cdot \delta_x}{725760} = K_2 + \left(\frac{H}{L} \cdot K_1\right)^2 \cdot \frac{Ra}{1440}$$

(conservation of momentum)

$$\begin{pmatrix} KK_1 \\ KK_2 \\ \delta\delta \end{pmatrix} := \text{Find}(K_1, K_2, \delta_x)$$

(This is MathCad's solution technique)

$K_1 := KK_1$

$K_2 := KK_2$

$\delta_x := \delta\delta$

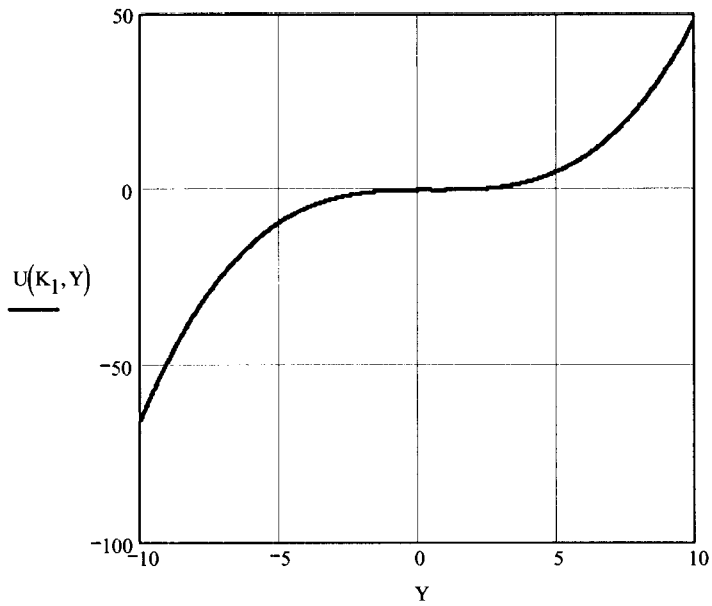

The numerical results are:

$K_1 = 0.339$

$K_2 = 0.204$

$\delta_x = 0.203$

PLOTS OF CORE FLOW AND TEMPERATURE

Plotting range:

$Y := 0, .02 .. 1$

X-velocity (non-dimensional)

(Velocity in upper half of the drift is from the hot end to the cold end, and in the reverse direction for the lower half)

Peak velocity (dimensional) from the graph:

$$u_{max} := 0.0016 \cdot \left(\frac{g \cdot \beta_o \cdot H^3 \cdot \Delta T_o}{\nu_o \cdot L} \right)$$

$$u_{max} = 0.016 \frac{m}{s}$$

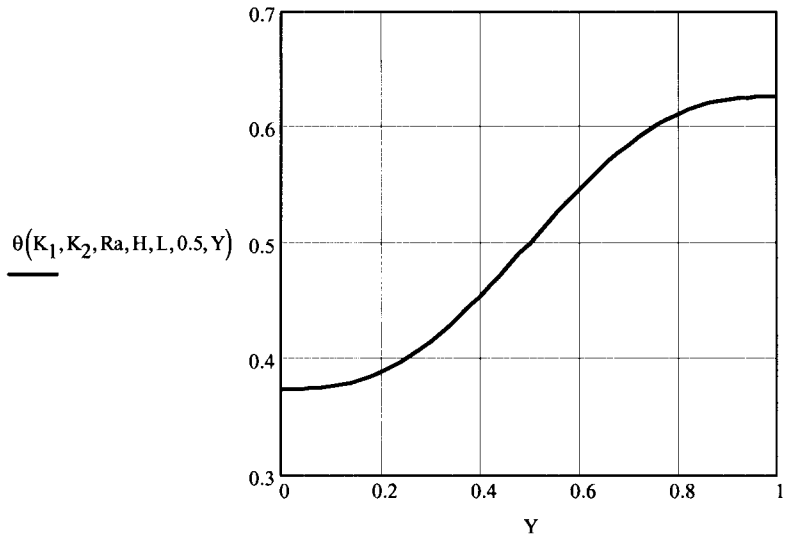

Nondimensional temperature distribution at X = 0.5

PLOTS OF FLOW AND TEMPERATURE IN THE END WALL REGION

Definition of end-wall X and Y velocities:

$$U_e(K_1,\delta_x,X,Y) := K_1\cdot\left(Y^3-\frac{3}{2}\cdot Y^2+\frac{1}{2}\cdot Y\right)\cdot\left(\frac{X}{\delta_x}\right)^2\cdot\left[1-\frac{4}{3}\cdot\left(\frac{X}{\delta_x}\right)+\frac{1}{2}\left(\frac{X}{\delta_x}\right)^2\right]$$

$$V_e(K_1,\delta_x,X,Y) := \frac{K_1}{2\cdot\delta_x}\cdot\left(\frac{X}{\delta_x}\right)\cdot\left(1-\frac{X}{\delta_x}\right)^2\cdot\left(Y^4-2\cdot Y^3+Y^2\right)$$

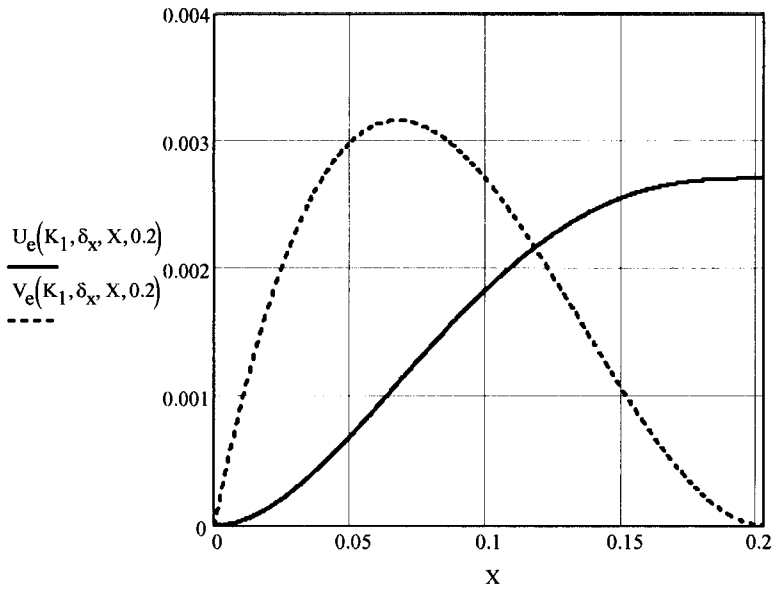

Plot of velocities in the end wall region $0 < X < \delta_x$ at the Y elevation that corresponds to the peak core flow velocity. Note that the X-velocity

blends smoothly to the core velocity for $X = \delta_X$ and the the V-velocity decreases to zero at $X = \delta_X$.

Definition of end-wall temperature distribution:

$$\theta_e(K_1, K_2, Ra, \delta_X, H, L, X, Y) := \left(\frac{X}{\delta_X}\right)\cdot\left(2 - \frac{X}{\delta_X}\right)\cdot\theta(K_1, K_2, Ra, H, L, X, Y)$$

$\theta_e(K_1, K_2, Ra, \delta_X, H, L, X, 0.5)$

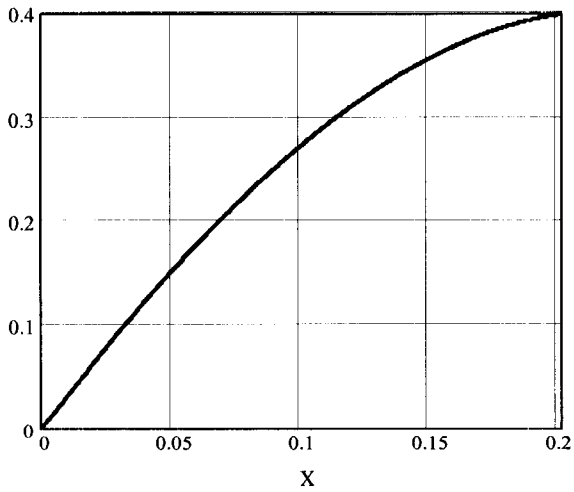

Plot of end wall temperature for $Y = 0.5$. Not that the temp. gradually increases from its value at $X = \delta_X$ to a value of 0.5 at $X = 0.5$, for this value of $Y = 0.5$.

MOISTURE TRANSPORT

The moisture transport is computed using the following observations and assumptions.

1. The flow from the hot end to the cold end carries wetter air to the cold end.
2. The reverse flow from the cold end to the hot end carries drier air back to the hot end
3. The air has a 100% relative humidity a the hot end. When the air gets to the cold end, if will be supersaturated and some moisture will condense on the target. The air will still have a 100% relative humidity but because it is colder, the actual mass of water in the air will be less.
4. The air flow from one end to the other is equal to the average density of the air times the average velocity in either the upper (hot to cold) or lower (cold to hot) half of the tube. Same air flow rate occurs in the circular channel as in the 2-D channel

INPUT FROM THERMODYNAMICS AND FROM THE STEAM TABLES

Relative humidity:

$RH := 1$

Moisture vapor pressures at various temperatures (curve fit to the steam table data over a range of temperatures):

$A := 0.0259 \cdot K^{-1}$

$B := 460 \cdot K$

$C := 0.075 \cdot psi$

$$PV(T) := C \cdot e^{A\cdot\left(\frac{9}{5}T - B\right)}$$

psia

Partial pressure of the air in the air-moisture mixture:

$P_o := 14.7 \cdot psi$

$P(T) := P_o - PV(T)$

psia

Absolute humidity of the air at temperature T

$\omega_o := 0.622 \cdot \frac{gm}{gm}$

$\omega(T) := \omega_o \cdot \frac{PV(T)}{P(T)} \cdot RH$

grams of moisture per gram of dry air

Average density of the dry air for cold air at temperature T and hot air at temperature T+ΔT:

$R := 41.65 \cdot \frac{cm^3 \cdot psi}{K \cdot gm}$

$\rho(T, \Delta T) := \frac{(P(T + \Delta T) + P(T))}{(2 \cdot T + \Delta T) \cdot R}$

grams per cubic centimeter

AIR MASS FLOW RATE

Reference air velocity:

$U_c(\Delta T) := \frac{g \cdot \beta_o \cdot H^3 \cdot \Delta T}{6 \cdot \nu_o \cdot L}$

Average velocity in the hot or cold half of the channel (by integrating the core velocity distribution):

$U_{ave}(\Delta T) := \frac{1}{32} \cdot U_c(\Delta T) \cdot K_1$

$U_{ave}(\Delta T_o) = 1.819 \frac{cm}{s}$

Mass flow rate of air in the upper or lower half of the channel:

$m_{air}(T, \Delta T) := \rho(T, \Delta T) \cdot U_{ave}(\Delta T) \cdot \frac{\pi}{4} \cdot \frac{H^2}{2}$

$m_{air}(T_c, \Delta T_o) = 0.018 \frac{gm}{s}$

MOISTURE FLOW RATE

The amount of moisture condensed on the target is the difference in the absolute humidities at the hot and cold ends of the channel times the flow rate of dry air.

$m_{cond}(T, \Delta T) := m_{air}(T, \Delta T) \cdot (\omega(T + \Delta T) - \omega(T))$

gram moisture per second

$m_{cond}(T_c, \Delta T_o) = 1.533 \times 10^{-3} \frac{gm}{s}$

CONDENSED MOISTURE PER HOUR

*The amount of moisture condensed **per hour** on the target can be no larger than:*

$M := 3600 \cdot s \cdot m_{cond}(T_c, \Delta T_o)$

$M = 5.518\,gm$

end of Dodge's MathCad file

9/20/02 RF

Measured and Calculation of Condensation Example

Condensation collected off the cold endwall of the desktop experiment is described in Jim Prikryl's scientific notebook. I used Frank's MathCad sheet to estimate condensation. Since the computational fluid dynamics model is not fully developed yet, these should be considered examples when discussing in the cold-trap uncertainty, which is the topic of the GSA presentation.

These calculations were stored and plotted in:
bubo: E:\TEF-kti\ColdTrap\Test-11\cttest11.xls (in the "steady summary" worksheet)

		in top	in top	discretized		To get the calculated entries in columns 2, 3,4,and 5, the variables Tc, H, and L were set and ΔT was varied	
		average	average	cold end			
	water rate	air flow	air flow	cell			
Δ T, C	g/hr	rate, cm/s	rate, m/s	g/hr			
1	0.007322	0.176	0.00176			Parameters set in Frank's MathCad file	
2	0.028	0.324	0.00324	5.26E-03		ΔT (C) =	variable
3	0.058	0.44	0.0044	1.07E-02		Tc (C) =	295
5	0.148	0.648	0.00648	2.71E-02		H (cm) =	5
8	0.344	0.877	0.00877	6.49E-02		L (cm) =	60.96
10	0.515	1.002	0.01002	9.86E-02			
15	1.099	1.255	0.01255	2.13E-01			
20	1.941	1.455	0.01455	3.74E-01			
25	3.114	1.622	0.01622	5.98E-01			
32	5.518	1.819	0.01819	1.08E+00			

Figure 092002-1 is a plot of the bulk airflow rate in the top portion (~half) of the drift as a function of temperature gradient. These values of airflow rate are ballpark agreement with the CFD values attained to date. Figure 092002-2 is the corresponding plot of condensation rate as a function of temperature gradient. Remember that this condensation rate is an integrated value for the entire drift. The uncertainty to emphasize in the GSA presentation is that the estimated value for the entire drift is 50 times larger than the amount collected at the cold endwall (heat sink). Does this mean that most of the water has condensed somewhere between the heat sink and the heater? We have visually observed condensation on objects dangling from the drift crown part way down the drift, and on thermocouples and anemometers. Or, doe this mean that evaporation (boundary-layer resistance) is reducing the available water to the hot air, and thus the relative humidity does not reach 100% until far down the drift length? Or, of course, do we have significant measurement error? This needs further development of our tools, particularly the CFD simulations.

The temperature gradients are highly uncertain, since we don't have a bulk temperature value for the air mass exiting the heater region. Obviously, the choices of the temperature at the heater cartridge surface or at the driftwall do not make sense. Visual estimates of maximum in-drift and average heat-sink wall temperatures were used. The integrated temperature in the area near the end of the heater cartridge is approximated using the nearest thermocouple (maximum temperature is from thermocouple above the heater cartridge).

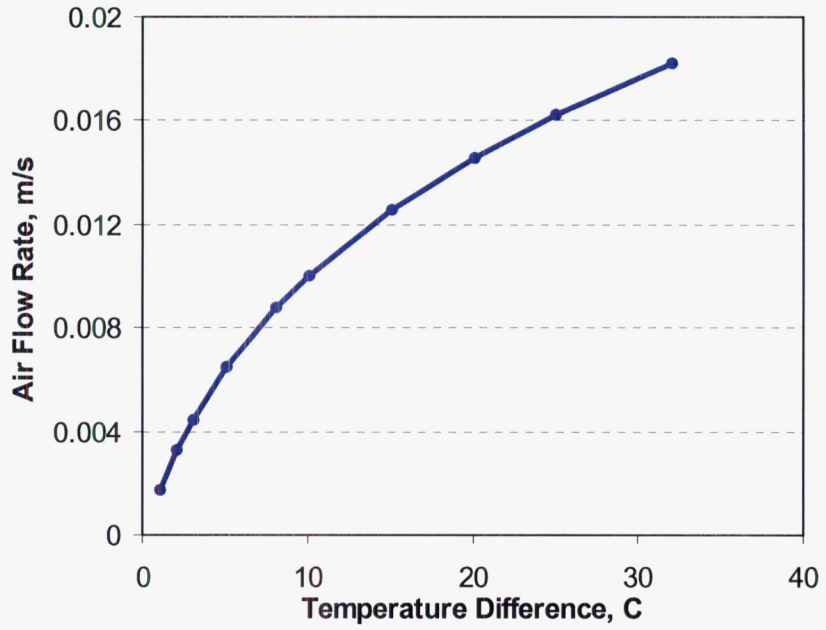

Figure 092002-1

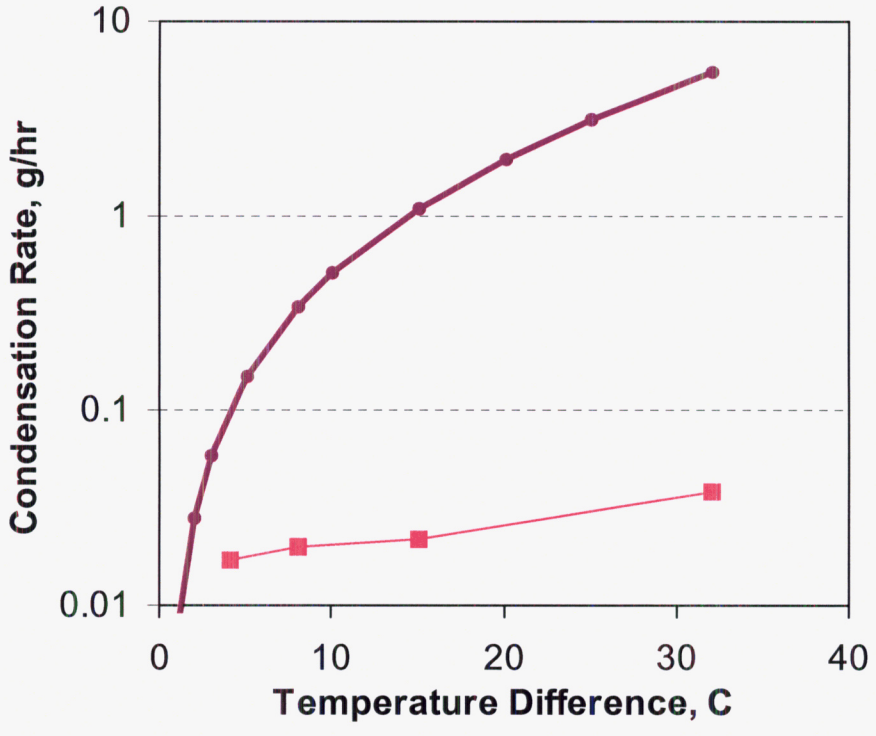

Figure 092002-2

9/26/02 RF

Frank's scaling memo is included below because he does not have a scientific notebook:

==========

MEMO

DATE: September 3, 2002
TO: Randy Fedors
FROM: Frank Dodge
SUBJECT: Comments on the thermal scaling methods for the Atlas Natural Convection Test Plan

This memo is relevant to the thermal scaling methods described in the document entitled "Atlas Natural Convection Test Plan" prepared by W. Lowry, Science & Engineering Associates, dated January 2, 2002. The Atlas test plan describes the experiments used to investigate natural convection heat transfer, temperature distributions, and air flow in several reduced-scale models of a representative drift at Yucca Mountain under post-closure (non-ventilated) conditions. In brief, the tests are concerned with the characteristics of natural convection created by a set of electrical heaters (simulated waste packages) located inside a large concrete pipe (simulated drift). Two different geometric scales (25% and 44% of full scale) were employed with the aim of determining the effects, if any, of the geometric size of the model drift on the test results; these particular geometric scales were apparently selected to allow standard-size concrete culverts to be used.

The design of an experiment that uses sub-scale models to investigate behavior in a full-scale prototype should be based on the requirements of *similitude*. These requirements state that all the important *dimensionless* parameters must be the same for the model and the prototype. Analytically, the similitude requirements are comparable to formulating the problem as a set of, say, differential equations initial conditions, and boundary conditions in dimensionless form so as to make the analytical solution independent of the geometric dimensions of the problem. For a natural convection problem, similitude requires that not only must the geometric configuration be preserved between the model and the prototype but also the dimensionless parameters that govern the flow and the heat transfer must be preserved. These additional parameters include the Grashof number Gr and the Prandtl number Pr, defined as:

$$Gr = \frac{g\beta L^3}{\gamma^2}\Delta T_{ref} \qquad Pr = \frac{\rho\gamma C_p}{k} \tag{1}$$

Here, g = acceleration of gravity, β = thermal expansion coefficient of the fluid (e.g., air), L = characteristic length (e.g., drift diameter D), γ = kinematic viscosity of the fluid, ρ = density of the fluid, C_p = specific heat of the fluid, k = thermal conductivity of the fluid, and ΔT_{ref} = a reference temperature difference (e.g., temperature difference between a heater surface T_s and a wall boundary T_w). Equating the model values of these parameters to the full scale values gives the requirements for fixing, as an example, the value of ΔT_{ref} for the model in terms of the value of ΔT_{ref} of the prototype. Using these results also allows the heat addition rate of, for example, the model heaters to be determined.

The Atlas tests do not employ this kind of similitude because, as the scaling report points out, , the ΔT_{ref} for a reduced geometric scale model would have to be equal to ΔT_{ref} for the full scale divided by the geometric scale factor cubed; the resulting value for, say, the heater wall temperature T_s would be considerably too large to be practical. (Another option in principle would be to use a fluid for the model tests that has a much smaller value for kinematic viscosity than air to lower the value of T_s, but this is also not likely to be practical.) Instead, the Atlas tests were scaled such that the heat transfer coefficient h from the heater to the air was supposed to be equal to the full scale value. It is known from many previous well-established experiments that the heat transfer coefficient for natural convection is of the form:

$$h = \frac{k}{L}A(Gr)^n(Pr)^m \tag{2}$$

where k is the thermal conductivity of the fluid, A is a numerical coefficient (dimensionless), and n and m are exponents (dimensionless). For many natural convection situations, in which the flow is turbulent, the exponent n is

close to equal to 1/3. When this is the case the characteristic length L of the problem cancels out of the right hand side of Eq. (2) to give:

$$h = Ak(Pr)^m \left(\frac{g\beta}{\gamma^2}\right)^{1/3} (\Delta T_{ref})^{1/3} \tag{3}$$

Consequently, the heat transfer rate $q = hA(T_s - T_a)$ from the heater to the fluid should be reduced in proportion to the geometric scale factor since (1) the surface area A of the heater is reduced in proportion to the geometric scale factor and (2) h from Eq. (3) is equal to the full scale coefficient; here T_a is the average or bulk temperature of the fluid far from the heater. Thus, the heater power in the model scale tests should apparently be reduced similarly.

But since the model tests were not conducted strictly in accordance with the requirements of similitude, the tests are *distorted*, and the conclusions that appear to follow from Eqs. (2) and (3) are not necessarily so straight forward. For example, the flow field in the model tests will not have the same scaled velocities as would the full-scale prototype because the Grashof number is too small in the model tests by a factor of the geometric scale factor cubed. This flow field distortion will influence the temperature distributions and the heat transfer rates. As an example, the natural convection flow and temperature distributions for a two dimensional analog of the Atlas test configuration are given by the following coupled differential equations:

$$Gr\left(\frac{H}{L}\right)^4\left[\frac{\partial}{\partial X}\left(U\frac{\partial U}{\partial X}+V\frac{\partial U}{\partial Y}\right)\right]-Gr\left(\frac{H}{L}\right)^2\left[\frac{\partial}{\partial Y}\left(U\frac{\partial V}{\partial X}+V\frac{\partial V}{\partial Y}\right)\right]= \frac{\partial\theta}{\partial X}-\frac{\partial^3 U}{\partial Y^3}+\left(\frac{H}{L}\right)^2\left[\frac{\partial}{\partial Y}\left(\frac{\partial^2 V}{\partial X\partial Y}-\frac{\partial^2 U}{\partial X^2}\right)\right]+\left(\frac{H}{L}\right)^4\frac{\partial^3 V}{\partial X^3} \tag{4a}$$

$$\frac{Gr}{\Pr}\left(\frac{H}{L}\right)^2\left(U\frac{\partial\theta}{\partial X}+V\frac{\partial\theta}{\partial Y}\right)=\frac{\partial^2\theta}{\partial Y^2}+\left(\frac{H}{L}\right)^2\frac{\partial^2\theta}{\partial Y^2} \tag{4b}$$

Here, X and Y are the dimensionless coordinates with X being along the drift axis, H and L are dimensionless lengths with L being along the dimensionless drift length, U and V are the dimensionless velocities, and θ is the dimensionless temperature. It is clear from these equations that neither the flow field nor the temperature distribution will be duplicated in a sub-scale test unless the Grashof number Gr and the Prandtl number Pr are both kept equal to their prototype values. (One exception to this is a case when Gr is very large in which case the right hand side of both equations can be ignored and the Grashof number cancels out of the equations. What constitutes "large Gr" depends on the problem but it probably corresponds to fully turbulent flow which generally requires $Gr > 10^{10}$.)

The potential misconceptions in the Atlas scaling are the assumptions that $\Delta T_{ref} = T_s - T_w$ is the same for the model as for the prototype, and that the temperature difference $T_s - T_a$ in Eq. (3) is also equal to the prototype value. The wall temperature T_w can certainly be controlled to be equal to the prototype value but the heater surface temperature T_s and the bulk fluid temperature T_a both "float" in accordance with the dynamics of the problem and cannot be determined not in advance; instead they are determined by the need to transfer the heat generated q from the heater to the fluid. It is likely that neither T_w or T_a will be exactly equal to the prototype since the flow field in the sub-scale tests will have a smaller dimensionless velocity than the prototype and the natural convection heat transfer will therefore be less effective. (That is, T_s will likely be higher than the prototype temperature and the circulatory flow along the drift axis will be less pronounced.) Consequently, the assumption that h and q are the same in the model tests as in the prototype may not be valid.

The magnitude of the distortions in the Atlas test can only be quantified by conducting tests at two different scales – as was done – and comparing the measured results in terms of dimensionless variables. The figure indicates one way that this might be accomplished. For example, a fluid temperature T_a is measured at a representative point (or points) and plotted in an appropriate dimensionless form against the geometric scale factor. The hypothetical

dimensionless test measurements are indicated by the small open circles in the figure. If the value of the dimensionless temperature does not vary or varies only slightly when the scale factor changes from 25% to 44%, then one can be reasonably confident that the same dimensionless value applies to the full scale prototype. If, however, the values do change with scale factor, some method of extrapolating the measurements to full scale must be determined. As shown in the figure, the dimensionless measurements can just be extrapolated by a straight line – although there is little theoretical justification for doing so. A better method, if it is feasible, is to use a computer code such as FLUENT to predict one of the measured points, say the one at 25% scale; this would more than likely involve adjusting some of the parameters in the code ("calibrating" the code). The reference prediction of the calibrated code is shown by the large open square in the figure. Then the calibrated code would be exercised again to predict the other measured data point; the only changes allowed in the code would be those parameters that depend on geometry, and none of the "calibration" parameters determined on the basis of the first point should be changed. If this second prediction is reasonably close to the other measured value, as shown by the small open square in the figure, one would have confidence in using the code to predict the full scale value (also shown by the small open square for a 100% scale factor). But if the second prediction is not reasonably close, as shown by the darkened square in the figure, then the full scale prediction would likely not be reliable.

If representative fluid velocities could be measured, a similar procedure could be used to determine the prototype fluid velocities by scaling up the dimensionless velocities from the tests. One logical dimensionless velocity for this purpose is:

$$U = u\frac{\gamma}{g\beta L^3 \Delta T_{ref}} \tag{5}$$

where u is the measured velocity and U is the dimensionless velocity; the characteristic length L might be chosen as the diameter of the drift. The velocity field is important in determining the transport of moisture along the drift length and thus in determining whether condensation might occur on cooler objects, similar to our Cold Trap experiment.

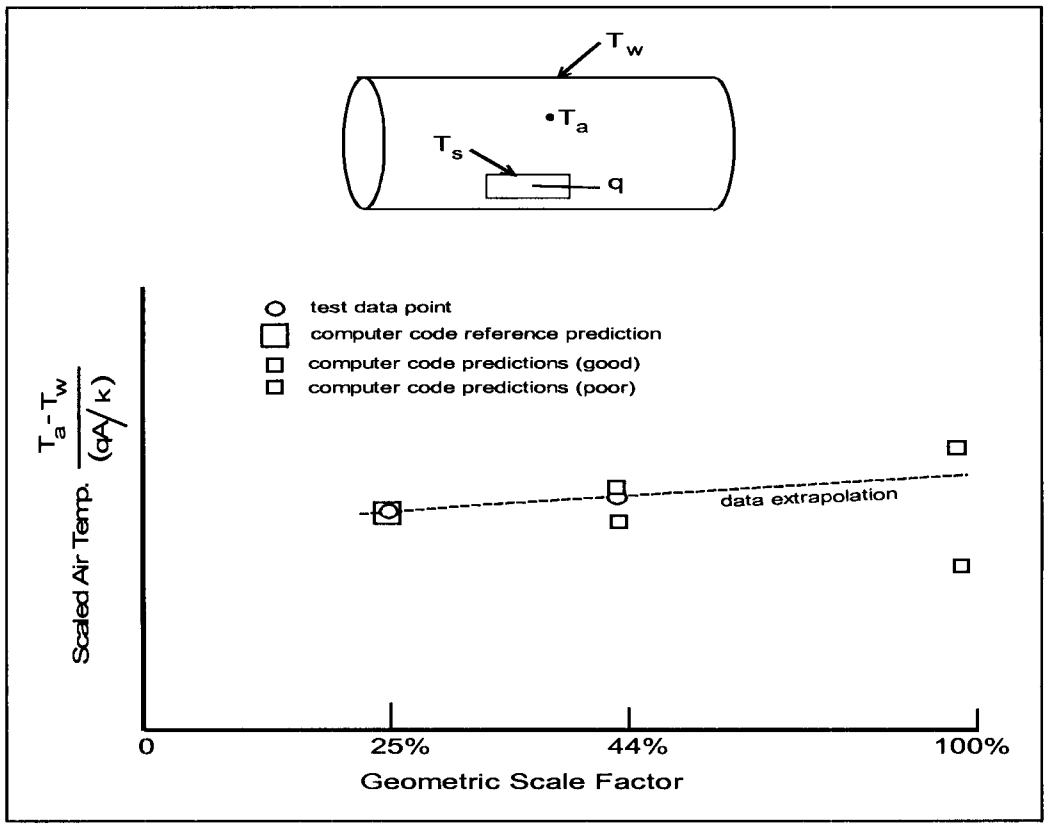

GSA Presentation on Uncertainties Cold Trap Process in Drifts

Example figures were created to illustrate flow patterns that likely will drive condensation in drifts.

The interplay between:

- strong local temperature variations leading to prominence of cross-sectional flow patterns
- strong large-scale temperature variations leading to prominence of axial flow

These were illustrated with the following two figures. Figure 092602-1 is conceptual sketch and Figure 092602-2 is from one of Steve Green's test runs for comparing Frank's analytical solution to computational fluid dynamics simulations. The actual test run doesn't matter since the figure is only needed to help visualize approximate cross-sectional flow away from the heaters/waste packages. Of course, this misrepresents heating near eccentrically located cylinders in drifts.

The flow patterns when considering eccentrically located cylinders in drifts are better reflected by Steve Green's CFD simulations of the actual desktop cold trap experiment. Figure 092602-3 shows a cross-section from a mid-drift location (far from the heater cartridge) and a cross-section at the end where the heater cartridge is located. Again, the CFD model is not yet refined adequately enough to hang our hats on it, but the general flow patterns in these plots will be used only to comment on the interplay between the axial and cross-sectional airflow.

Figure 092602-1

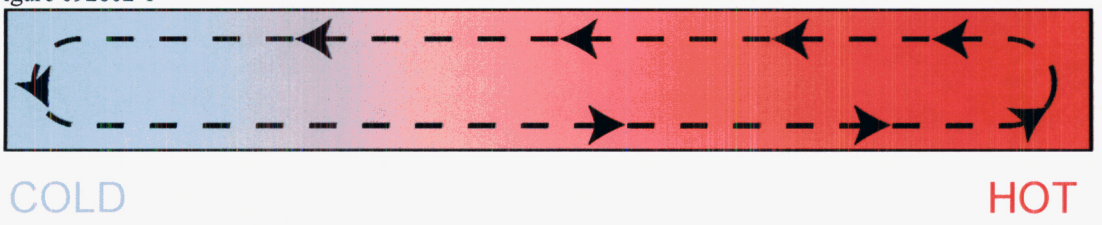

Figure 092602-2

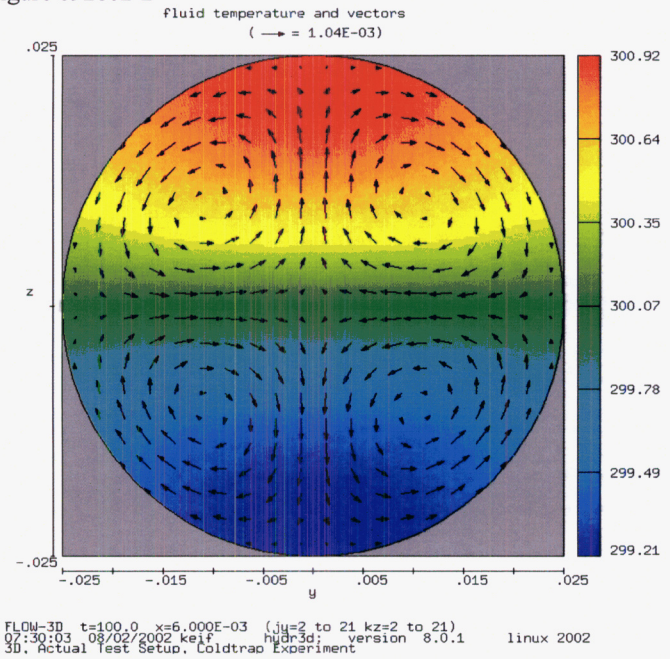

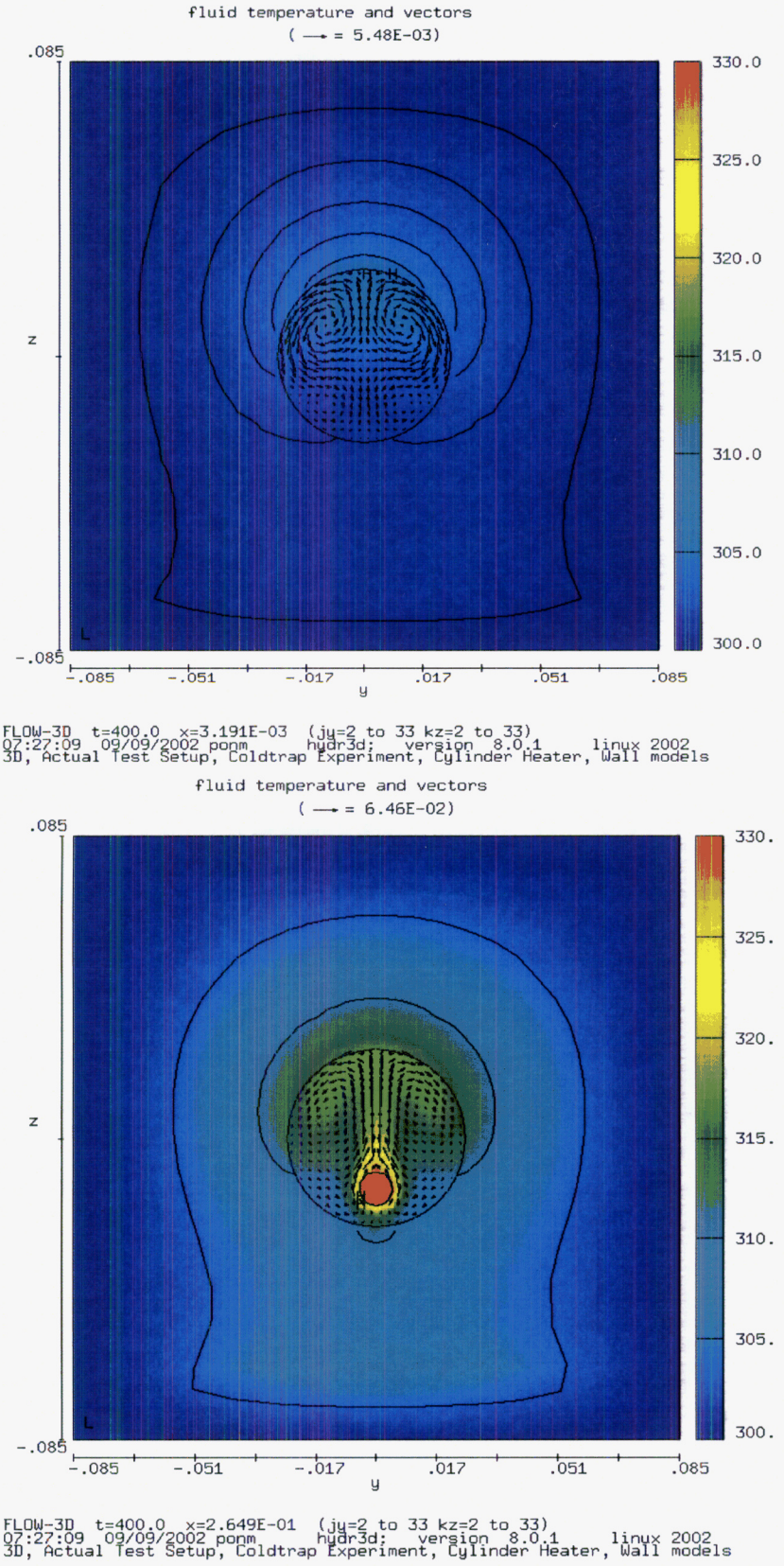

Figure 092602-3. Cross-sectional temperatures at the mid-drift and heater-end of the desktop experiment.

The effect of including the sand in the preliminary CFD modeling can better be illustrated by the axial flow patterns. Frank's analytical solution assumes a no flux boundary condition at the top and bottom of the 2-D drift (axial cross-section). We know, however, that there is heat flux out the drift walls, and furthermore, that it varies along the drift. This variation in heat flux out the *drift wall is another factor controlling the temperature variation along the drift (in-drift). Other* factors affecting the temperature distribution along the drift are conduction (small effect in the air, but more prominent in the wallrock – both parallel and perpendicular to the driftwall), convection, thermal radiation (for now, we have assumed the low absolute temperatures and small temperature differences make radiation less important than convection), latent heat transfer (evaporation, transport, condensation elsewhere). The importance of including the ceramic cylinder and the sand ("wallrock") in Steve Green's CFD simulations are illustrated by the difference in the two plots of Figure 092602-4. The top plot has a no heat flux boundary condition similar to the b.c. in Frank's analytical solution. The flow vectors maintain their magnitude throughout most of the length of the drift. The bottom plot includes the heat transfer in the ceramic and sand wallrock. Again, these are preliminary CFD results that are only used to illustrate a concept. Here, the axial airflow vector magnitudes taper off.

Figure 092602-4

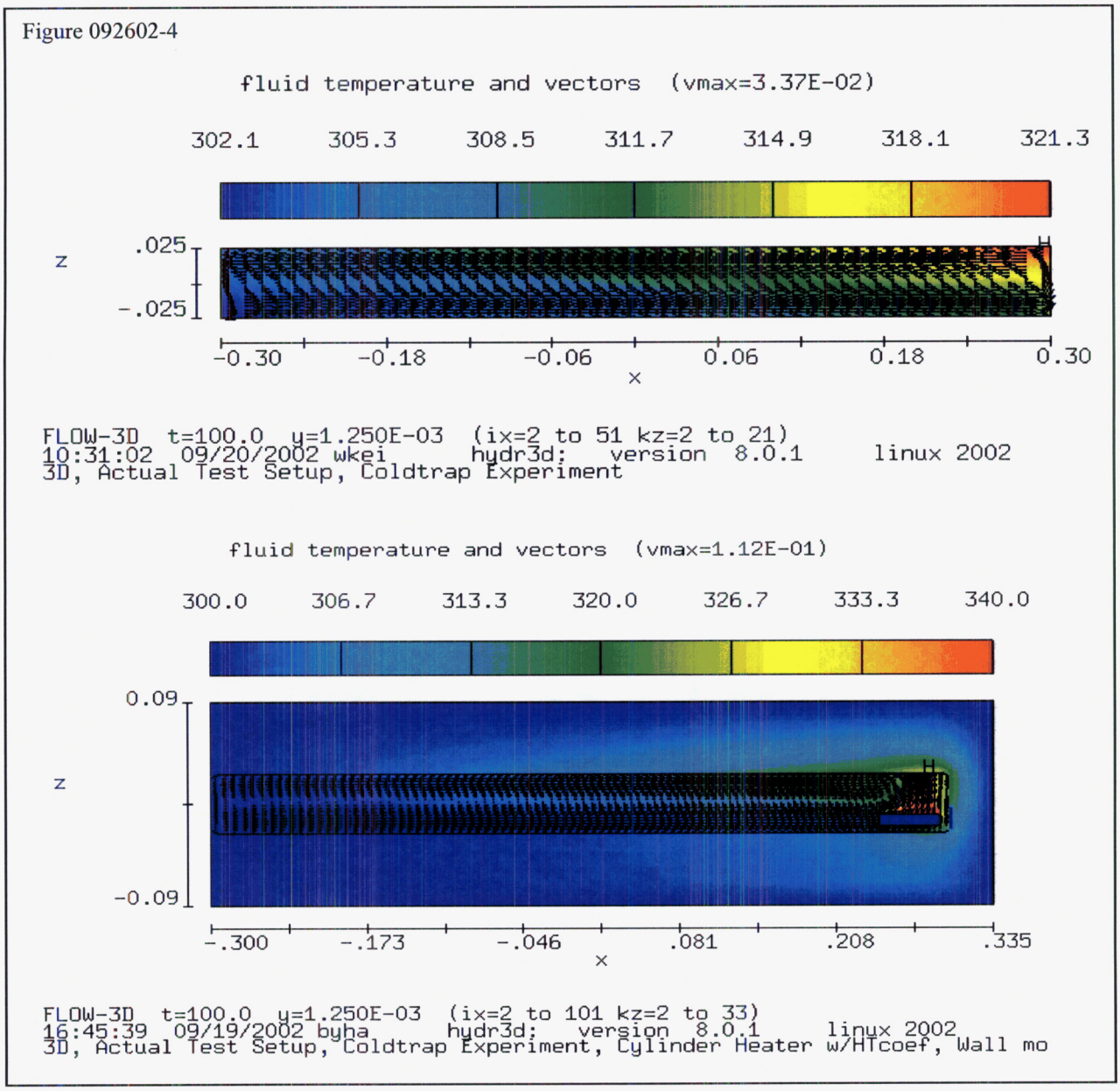

10/28/03 RF

Frank updated his last memo with some examples illustrating the scaling problem, though the figure is not included.

MEMO

DATE: September 3, 2002 October 28
TO: Randy Fedors
FROM: Frank Dodge
SUBJECT: Comments on the thermal scaling methods for the Atlas Natural Convection Test Plan

This memo is relevant to the thermal scaling methods described in the document entitled "Atlas Natural Convection Test Plan" prepared by W. Lowry, Science & Engineering Associates, dated January 2, 2002. The Atlas test plan describes the experiments used to investigate natural convection heat transfer, temperature distributions, and air flow in several reduced-scale models of a representative drift at Yucca Mountain under post-closure (non-ventilated) conditions. In brief, the tests are concerned with the characteristics of natural convection created by a set of electrical heaters (simulated waste packages) located inside a large concrete pipe (simulated drift). Two different geometric scales (25% and 44% of full scale) were employed with the aim of determining the effects, if any, of the geometric size of the model drift on the test results; these particular geometric scales were apparently selected to allow standard-size concrete culverts to be used.

The design of an experiment that uses sub-scale models to investigate behavior in a full-scale prototype should be based on the requirements of *similitude*. These requirements state that all the important *dimensionless* parameters must be the same for the model and the prototype. Analytically, the similitude requirements are comparable to formulating the problem as a set of, say, differential equations, initial conditions, and boundary conditions in dimensionless form so as to make the analytical solution independent of the geometric dimensions and fluid physical properties of the problem. For a natural convection problem, similitude requires that not only must the geometric configuration be preserved between the model and the prototype but also the dimensionless parameters that govern the flow and the heat transfer must be preserved. These additional parameters include the Grashof number *Gr* and the Prandtl number *Pr*, defined as:

$$Gr = \frac{g\beta L^3}{\gamma^2}\Delta T_{ref} \qquad Pr = \frac{\rho\gamma C_p}{k} \tag{1}$$

Here, g = acceleration of gravity, β = thermal expansion coefficient of the fluid (e.g., air), L = characteristic length (e.g., drift diameter D), γ = kinematic viscosity of the fluid, ρ = density of the fluid, C_p = specific heat of the fluid, k = thermal conductivity of the fluid, and ΔT_{ref} = a reference temperature difference (e.g., temperature difference between a heater surface T_s and a wall boundary T_w). As an alternative to the Grashof number, some investigators use the Rayleigh number. The Rayleigh number is the product of the Grashof number and the Prandtl number.

The requirements for scale model tests are determined by equating the model values of the Grashof and Prandtl number to the full scale values. This equality will, for example, determine the required value of ΔT_{ref} for the model in terms of the value of ΔT_{ref} of the prototype, the geometric scale factor λ (ratio of the characteristic dimension of the model to the full scale characteristic dimension), and the model and full-scale fluid properties. A similar procedure would determine the required heat addition rate of the model heaters.

The Atlas tests do not employ this kind of similitude because, as the scaling report points out, the ΔT_{ref} for a reduced geometric scale model would have to be equal to the full scale ΔT_{ref} divided by λ^3. This gives a value for, say, the heater wall temperature T_s that is considerably too large to be practical. (Another option in principle would be to use a fluid for the model tests that has a much smaller value for kinematic viscosity than air to lower the value of T_s, but this is also not likely to be practical.) Instead, the Atlas tests were scaled such that the heat transfer coefficient h from the heater to the air was *supposed* to be equal to the full scale value. It is known from many previous and well-established experiments that the heat transfer coefficient for *unconfined* natural convection is of the form:

$$h = \frac{k}{L} A(Gr)^n (Pr)^m \tag{2}$$

Here k is the thermal conductivity of the fluid, A is a numerical coefficient (dimensionless), and n and m are exponents (dimensionless). For many unconfined natural convection situations in which the flow is turbulent, the exponent n is close to equal to 1/3. When this is the case the characteristic length L of the problem cancels out of the right hand side of Eq. (2) to give:

$$h = Ak(Pr)^m \left(\frac{g\beta}{\gamma^2} \right)^{1/3} (\Delta T_{ref})^{1/3} \tag{3}$$

This relation was used in the Atlas report to show that the rate of heat generation by the heater should be reduced in proportion to the reduction in heater surface area, or in effect by λ^2 for sub-scale tests. This conclusion follows from the fact that the heat generation rate is numerically equal to the heat transfer rate $q = hA(T_s - T_a)$ from the heater to the air, and h from Eq. (3) is equal to the full scale coefficient and the surface area A of the heater is reduced in proportion to λ^2. Here T_a is the average or bulk temperature of the fluid far from the heater. It should be noted that these relations apply strictly to unconfined natural convection where T_a is independent of either the surface temperature of the heater or the heating rate. In the Atlas scaling method, T_a was taken to be the drift wall temperature T_w and this was assumed to be held at a known constant value. In a sense, the Atlas scaling method is overdefined since more parameters are assumed to be fixed (h, T_s, and T_w) than it is possible to hold constant.

Since the model tests were not conducted strictly in accordance with the requirements of similitude, the tests are *distorted*, and the conclusions that follow from Eqs. (2) and (3) are not necessarily so straight forward. For example, the flow field in the model tests and in a full-scale prototype would not yield identical values of the *scaled* (dimensionless) air velocities because the Grashof number is too small in the model tests by a factor equal to the geometric scale factor cubed. This flow field distortion will influence the temperature distributions and the heat transfer rates. To estimate the magnitude of the distortions on the heat transfer, an analogous problem was investigated by an analytical model having a closed form solution. The analogous problem is a two dimensional drift in which one vertical end walls is held at a high temperature and the other vertical end wall is held at a lower temperature. This problem was solved in closed form, and the heat transfer rate from the hot wall to the cold wall was determined. The heating sets up a natural convection flow in the drift that transports energy from the hot wall to the cold wall, so the heat transfer is not by conduction but by convection, and in this sense it is analogous to the Atlas tests.

For the full scale case, the height of the drift was assumed to 5 meters and the length was assumed to be 40 meters. The temperature difference ΔT between the hot wall and the cold wall was assumed to be 30°C. The Rayleigh number for this situation is 2.786×10^{11}. The heat flux q from the hot wall to the cold wall was computed from the analytical model to be 13.53 watt/m^2. The heat transfer coefficient $h = q/\Delta T$ thus has a value of 0.451 watt/m^2-°C.

For a 44% scale model, the drift height is 2.42 m and the length was reduced in proportion. If the model has the same $\Delta T = 30$°C as the prototype, the Rayleigh number is 2.373×10^{10}. The heat flux from the hot wall to the cold wall was computed to be 18.78 watt/m^2. Hence, the heat transfer coefficient is 18.78watt/m^2/30°C = 0.626 watt/m^2-°C, which is 39% larger than the full scale value. If, instead, the heat flux is maintained at the full scale value of 13.53 watt/m^2, the required value of ΔT is 23°C, and the heat transfer coefficient is 13.53/23 = 0.588 watt/m^2-°C, which is 30.3% larger than the full scale value. The Rayleigh number for this case is 1.857×10^{10}. In order the make the heat transfer coefficient equal to its full scale value of 0.451 watt/m^2-°C, the ΔT has to be reduced to about 6 °C, and the heat flux is only 2.7 watt/m^2 instead of the full scale value of 13.53 watt/m^2. It is apparent that the full scale values of heat flux, temperature difference, and heat transfer coefficient cannot all be maintained at the full scale values.

For a 25% scale model, the drift height is 1.375 m and the length was reduced in proportion. If the model has the same $\Delta T = 30$°C as the prototype, the Rayleigh number is 4.353×10^9. The heat flux from the hot wall to the cold wall was computed to be 23.53 watt/m^2. Hence, the heat transfer coefficient is 23.53 watt/m^2/30°C = 0.784 watt/m^2-°C, which is 74% larger than the full scale value. If, instead, the heat flux is maintained at the full scale value of 13.53 watt/m^2, the required value of ΔT is 19°C, and the heat transfer coefficient is 13.53/19 = 0.711 watt/m^2-°C, which is 57% larger than the full scale value. The Rayleigh number for this case is 1.857×10^{10}. In order the make the heat transfer coefficient equal to its full scale value of 0.451 watt/m^2-°C, the ΔT has to be

reduced to about 2 °C, and the heat flux is only 0.9 watt/m^2 instead of the full scale value of 13.53 watt/m^2. It is again apparent that the full scale values of heat flux, temperature difference, and heat transfer coefficient cannot all be maintained at the full scale values.

These results from the analytical model for a confined natural convection problem somewhat analogous to the Atlas tests indicate that the heat transfer coefficient increases with a decrease in the geometric scale factor of the situation rather than remain constant. This trend is in agreement with published literature [e.g., Kuehn and Goldstein, *An Experimental Study of Natural Convection Heat Transfer in Concentric and Eccentric Horizontal Concentric Annuli*, **Trans. ASME, J. Heat Transfer, 100**, Nov. 1978, pp. 635-640.]. Since the Atlas tests were apparently conducted by maintaining identical values of the heat flux q for both the 44% and the 25% models, the value of the heat transfer coefficients inferred from the tests may be too small, perhaps by a considerable percentage. The Atlas test results could, however, still be used to validate computer simulations, and for this purpose the temperature measurements from two different geometric scales would be extremely valuable.

---

last entry this page 10/28/03 RF

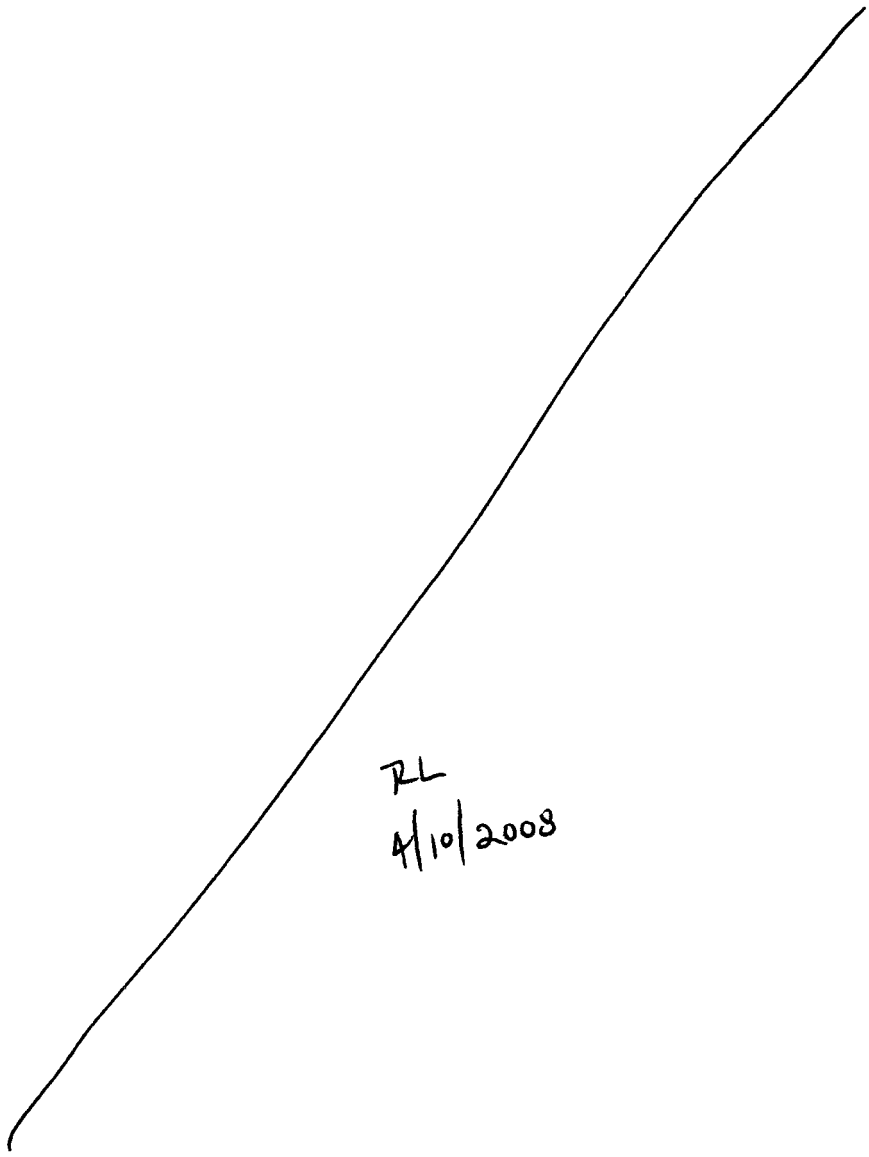

Volume VII – TEF Cold Trap

4/8/03 RF

Collaborators (SciNtbk#):

David Walter (#576e) Division 18 - new since initial entry for this notebook
Steve Svedeman (none) Division 18 - new since initial entry for this notebook
Steve Green (536e) Division 18
Frank Dodge (none) Division 18
Jim Prikryl (#554. laboratory data collection)
Don Bannon (none) Division 10

Software and computers still the same as noted on page 1 of this scientific notebook volume Mostly EXCEL 97 SR-2 on Windows NT system, Adobe Illustrator (to manipulate figures for the report), and Tecplot 8.0-1-0 on Spock (SunOS).

Desktop Experimental Setup

bubo E:\TEF-kti\ColdTrap\Desktop\desktop_dimen_centered.ai and desktop_dimen-1.ai

To create uniformity in coordinate systems, and to alleviate some confusion by David Walter in comparing computational fluid dynamics (CFD) results with measured data, we decided to use a coordinate system centered on the drift (center of the laboratory drift). This makes David's comparisons straightforward, because he likes to model with this arrangement. The confusion caused me to re-measure the desktop setup. The figures VII-29 and VII-30 on Volume VII page 29 and 30 contain the same information; page 29 has the actual measurements, page 30 has the distances labeled in the fashion needed by David Walter. David used these figures for siting the comparison with the measured thermocouple temperatures, and to create his own figures using some other drawing package.

The translation from Jim Prikryl's measured locations (referred to as the old locations here) for thermocouples to the coordinate system used for comparing CFD results is as follows:

$X=z_{old}$, $Y=x_{old}$; $Z=y_{old}$; center tunnel = 0,0,0
-30.5 = shift (cm) for X
0 = shift (cm) for Y
2.5 = shift (cm) for Z

Figure VII-29. Measured distance of desktop cold-trap model. K_{th} values are approximate.

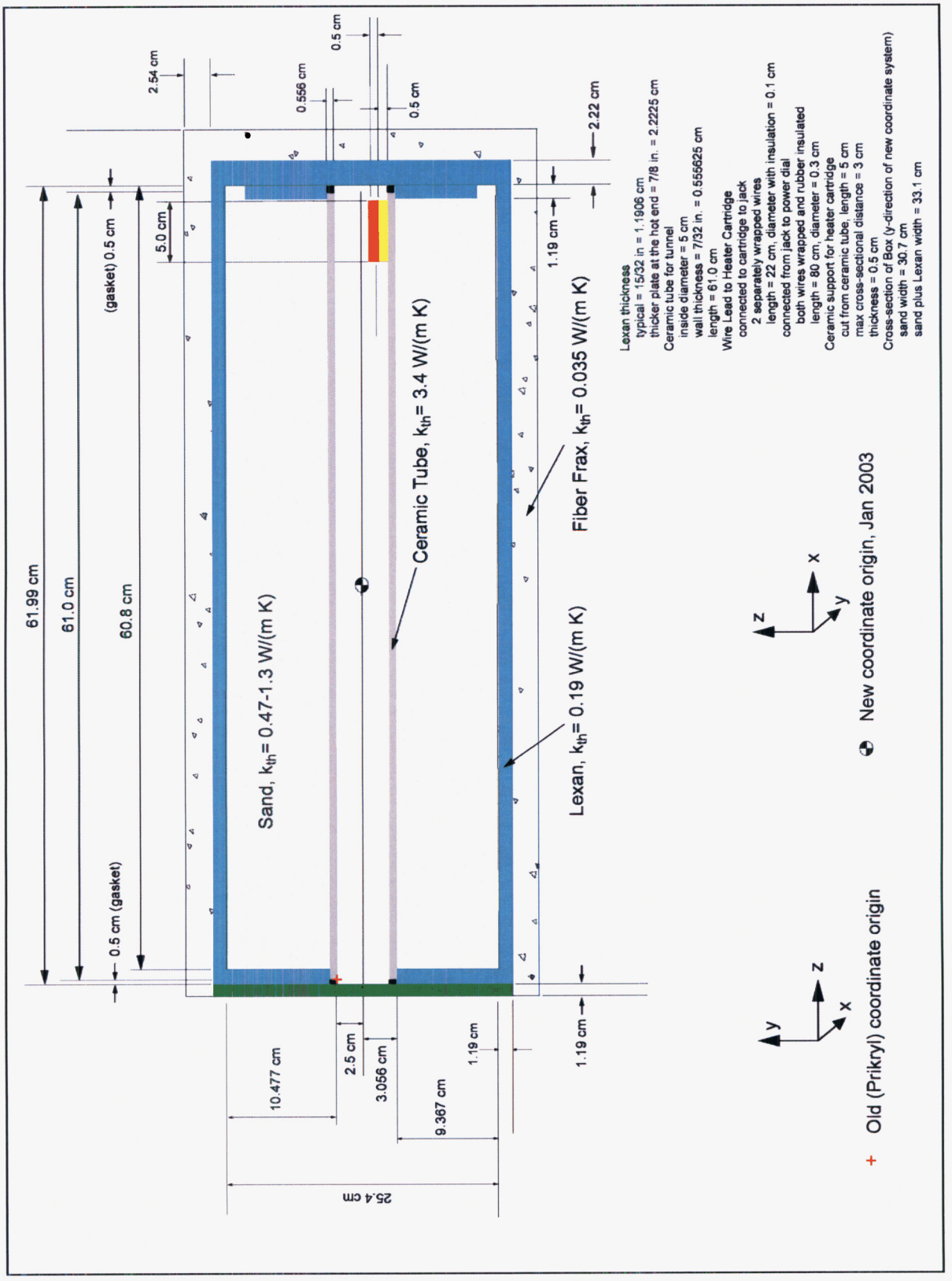

Figure VII-30. Measured distance of desktop cold-trap model.

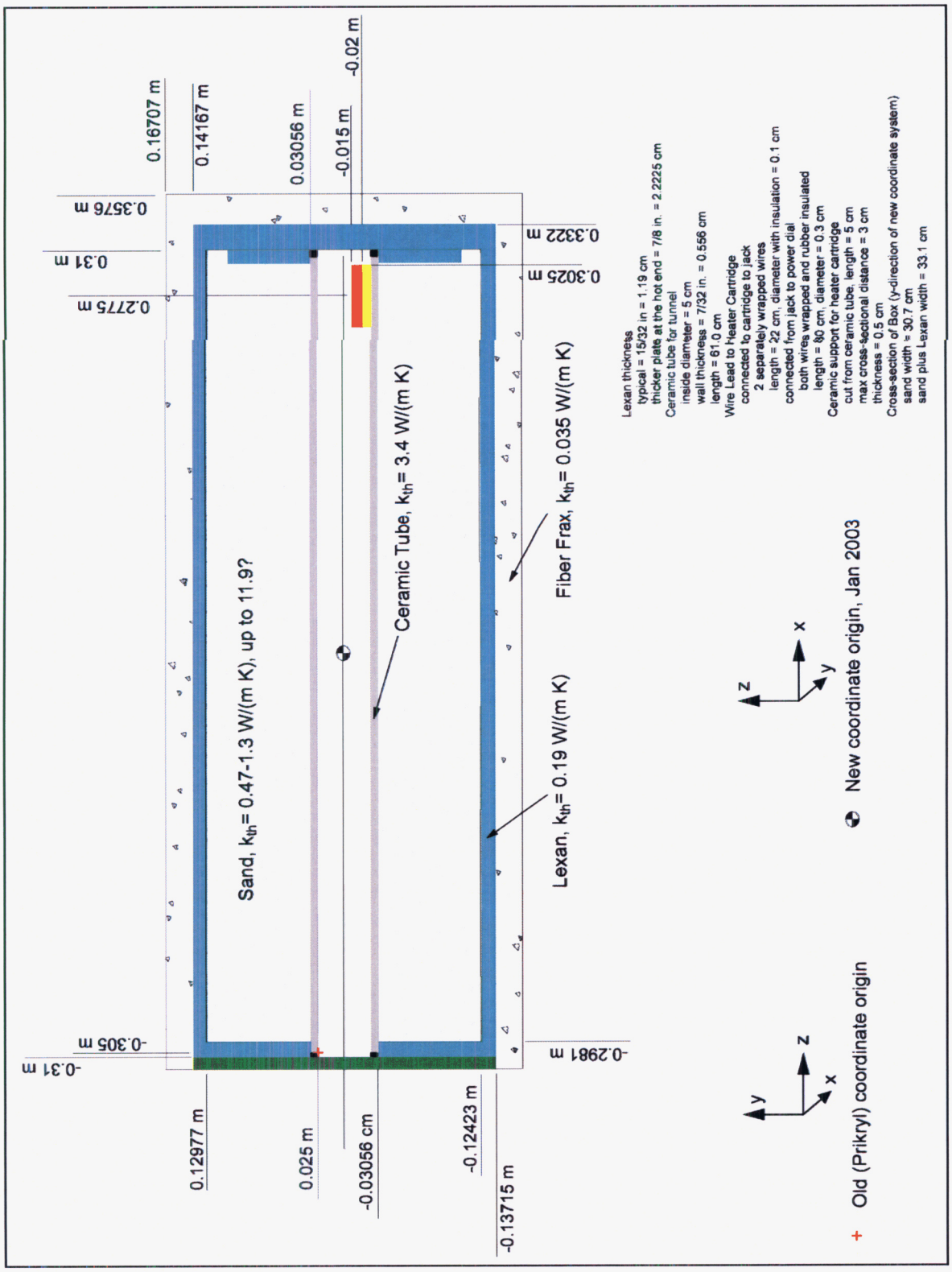

Sand Conductivity

bubo E:\TEF-kti\ColdTrap\Sand\sand.xls
bubo E:\TEF-kti\ColdTrap\Dwalter_tests11and14.xls worksheet "cttest11&14"

Difficulties in matching CFD simulations with measured data have driven David Walter to distraction. This section describes some additional analyses that were done to support the calibrated values of sand thermal conductivity in the wet desktop laboratory model.

The approach taken was to look for supporting analyses for the literature and calibrated values of thermal conductivity. In summary:
(i) 1-D heat transfer approximation across the lexan and insulation was used with the measured temperatures,
(ii) estimations of water saturation levels above the cylinder (noting that thermal conductivity of the sand is a function of water saturation, and
(iii) lab measured values were obtained (Blackwell).

<u>One-Dimensional Heat Transfer in Sand</u>

Calculations of heat transfer were recorded in
bubo E:\TEF-kti\ColdTrap\Dwalter_tests11and14.xls worksheet "cttest11&14"
The table below (Table VII-32) is taken from the worksheet. The second line of the table contains the 1-D equation for estimating the thermal conductivity from the rearranged heat flux equation.

$$k_{sand} = \left[k_{FF/LX}\right] \cdot \left[\Delta T / distance\right]$$

where k is thermal conductivity and FF/LX stands for FiberFrax and/or Lexan, T is temperature.

Table VII-32 (Page VII page 32) uses the assumption that heat transfer is 1-dimensional in the sand of the laboratory model. The original Prikryl coordinate system is used in Table VII-32, the origin is at the heat sink end, internal top of the drift. Heat transfer through different materials (or sections) of the experiment can be thought of as occurring in series; the heat transfer in each section should be equal. In our case, the heat transfer is better approximated as radial, but for the purposes of approximating a range of effective thermal conductivity of the sand, the one-dimensional approximation is believed to be sufficient.

Using the heat transfer approach (equating the flux through the sand to the flux across the Lexan (K=0.19) or FiberFrac K=0.035), the results in the table can be summarized into the following ranges for the sand thermal conductivity:
1.4 to 11.9 W/(m K) - using sand profile at 46.99 cm and heat transfer across the Lexan
1.9 to 7.7 W/(m K) - using sand profile at 57.15 cm and heat transfer across the Lexan

0.72 to 1.3 W/(m K) - using sand profile at 46.99 cm and heat transfer across the FiberFrac insulation
0.07 to 0.27 W/(m K) - using sand profile at 57.15 cm and heat transfer across the FiberFrac insulation

To hopefully average out errors with using either the Lexan or FiberFrac alone, I used a distance weighted bulk thermal conductivity of the Lexan/FiberFrac (bulk K=0.085) and came up with the following estimates:
0.47 to 0.89 W/(m K) - using the sand profile at 46.99 cm
0.12 to 0.44 W/(m K) - using the sand profile at 57.15 cm

Table VII-32. Estimates of thermal conductivity of the sand using heat transfer through Lexan/FiberFrac								
Ksand = KFF/LX * [deltaT across Lexan and or FiberFrac / distance FF/LX] * [distance sand / delta T in sand]								
	0.0847	= bulk K for FF/LX (W/mK)						
	0.012	= distance across Lexan (m)						
	0.0254	= distance across FiberFrax (m)						
	0.0992	= distance across sand (m)						
	Calculation of bulk thermal conductivity of FiberFrac and Lexan							
	0.19	= K of Lexan (LL)						
	0.035	= K of FiberFrac (FF)						
	0.08473262	= thickness weighted average K for FF/LX						
cttest11	delta T	delta T	delta T	delta T	delta T			
	across	across	across	top, sand	top, sand			
	insulation	Lexan, 57.15	Lexan, 46.99	at 57.15cm	at 46.99cm			
	-1	-2.18	-1.66	-1.81	-0.39			
	-3.1	-4.16	-3.23	-2.93	-0.78			
	-0.8	-1.07	-0.93	-0.78	-0.15			
cttest14	delta T			delta T	delta T			
	across			top, sand	top, sand			
	insulation			at 57.15cm	at 46.99cm			
	-1.2	-4.17	-3.35	-0.99	-0.44			
	-0.5	-1.25	-0.80	-0.25	-0.24			
	0	-0.51	-0.20	0.07	-0.22			
	-0.1	-0.40	-0.06	0.34	-0.25			
cttest11	calc Ksand	calc Ksand		calc Ksand	calc Ksand		calc	calc
	use lexan	use lexan		use FF	use FF		K sand	K sand
	at 57.15cm	at 46.99cm		at 57.15cm	at 46.99cm		T@57.15cm	T@46.99cm
	1.891014157	6.634486732		0.0755109	0.7577073		0.124	0.572
	2.228449203	6.494266771		0.1444779	0.7275986		0.238	0.891
	2.168701238	9.425927696		0.1406794	0.947694		0.231	1.161
cttest14								
	6.62774123	11.92899386		0.1661179	1.2930109		0.273	0.612
	7.735295955	5.234789035		0.270048	0.7127004		0.444	0.470
	-11.82491229	1.434802693		0	0.3164947		0.000	0.000
	-1.833795476	0.352871555		-0.040084	0.2135374		-0.066	0.088

Use of the sand profile at 46.55cm is preferable because the thermocouples on either side of the FiberFrac insulation are approximately located in the middle (not over the heater cartridge, which is where the profile at 57.15cm is located). The range in the estimates comes from the different steady state times (3 for cttest11 and 2 for cttest14; the other 2 steady state times for cttest14 were at times when the heater cartridge was set to a very low setting). For the temperature differences across the sand, I assumed that the top and bottom thermocouples reflected the complete gradient. However, the top-most thermocouple in the sand was not at the sand/Lexan interface; the bottom-most thermocouple in the sand did appear to be at the ceramic/sand interface). Note that this means the temperature difference across the Lexan was calculated using a thermocouple that may be as much as 1.5 cm below the sand/Lexan interface. To summarize, take these estimates with a grain of sand (i.e., only used to support literature or calibrated values).

Saturation Levels of the Sand

Uncertainty in saturation levels of the sand above the cylinder could lead to a large uncertainty of the effective thermal conductivity of the sand. Using the relation from Somerton (1981, see MULTIFLO documentation and reference list) for effective thermal conductivity as a function of saturation:

$k_{eff} = k_{dry} + \sqrt{S_l}\left(k_{wet} - k_{dry}\right)$ where S_l is the saturation and k is thermal conductivity.

If the sand desaturated to 25%, then the effective thermal conductivity would be much less than if it desaturated to 90%. We had used a TDR probe in early test phases (emplaced subhorizontal immediately above the cylinder to check the saturation). Jim Prikryl's scientific notebook contains comments on this measurement. It should only be considered supporting information since the probes were calibrated using different porous media, though ballpark (10%) accuracy is all that we need. The TDR probes indicated that the sand immediately above the cylinder was remaining >90% saturated, but check Jim's notebook for details.

Prikryl's notebook also contains the measurements of water content made on a column of sand. In Prikryl's lab measurement, 5 cm of water was placed in a 25 cm tall, round sample container. Silica sand was then added to the container to make a 20 cm tall column of sand and water. Samples were taken at 2 cm intervals and placed in plastic sample containers. Weights of containers and sample materials were recorded and are shown below. Liquid was removed from samples by heating at 90C.

The data suggests that the sand should remain fairly well saturated up to the top of the lexan box (~16.5 cm above the bottom of the cylinder). The sand was saturated to a level coinciding with the bottom of the cylinder. There is no reason to believe that the sand below the cylinder was not fully saturated throughout the test phases (no leakage was observed). Figure VII-33 contains the measured values from Prikryl and the pedotransfer function estimates described next.

Figure VII-33. Measured (symbols) compared to pedotransfer function estimates.

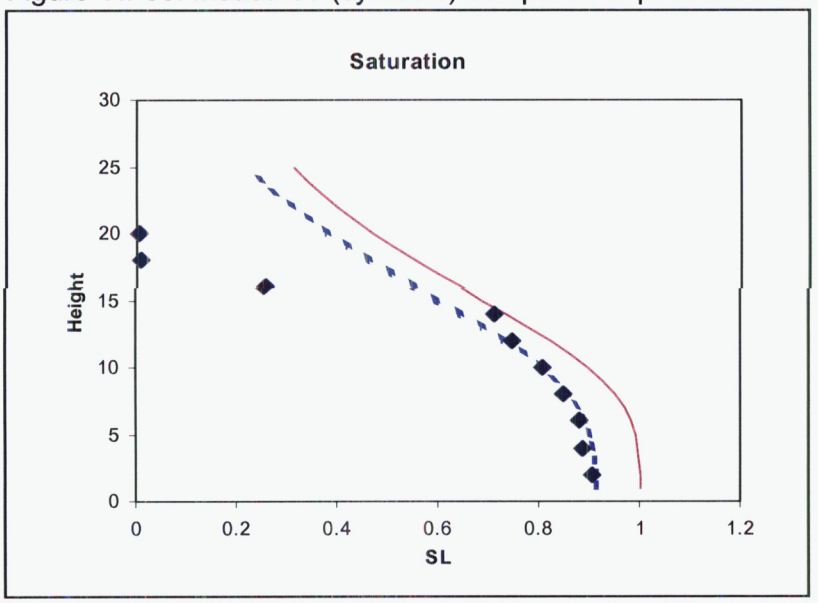

Particle size distribution and bulk density have been used to estimate the van Genuchten parameters for the water retention curve:

$S_e = [1+|\alpha\psi|^n]^{-m}$ where S_e (or SL in the figure) is the effective saturation, ψ is the capillary pressure head, and α, n, and m are coefficients (see van Genuchten, 1980, Soil Science Journal). The α term is the most important here because it controls the shape of the curve at low saturations. The Rosetta program version 1.2 from the U.S. Department of Agricultural (a product of Rien van Genuchten's Salinity Lab) was used to implement the pedotransfer functions. Rosetta just implements published algorithms using different types of inputs. I used the Depart. of Agricultural soil (texture) classification scheme and the bulk density. The soil texture and bulk density data were obtained from the sand supplier (T&S Materials, Inc). Figure VII-34 is a cumulative grain size curve, which is used to infer a pore size distribution. The grain size distribution curve in Figure VII-34 is from the "Estimates" worksheet in sand.xls. This figure shows that 9% of the sand is "very fine sand" (0.05 to 0.1 mm) and 87% is "fine sand (.01-0.25 mm), and the remainder is medium sand [see Klute-editor, Methods of Soil Analysis, Part 1, 1986, Soil Science Society of America; Jury, Gardner, and Gardner, 1991, Soil Physics].

The values of the van Genuchten obtained from the pedotransfer function and fitted to the Prikryl measured data are α=0.06 cm^{-1}, n=3.5, and m=0.714 (m =1-1/n). Using these values, the curves in Figure VII-33 were plotted; two curves are plotted to account for uncertainty in porosity (measured versus estimated from bulk density supplied by T&S Materials, Inc. The shift in porosity was a visually reasonable way to better match the data.

Figure VII-34. Cumulative grain size curve for the sand using data from Table VII-35.

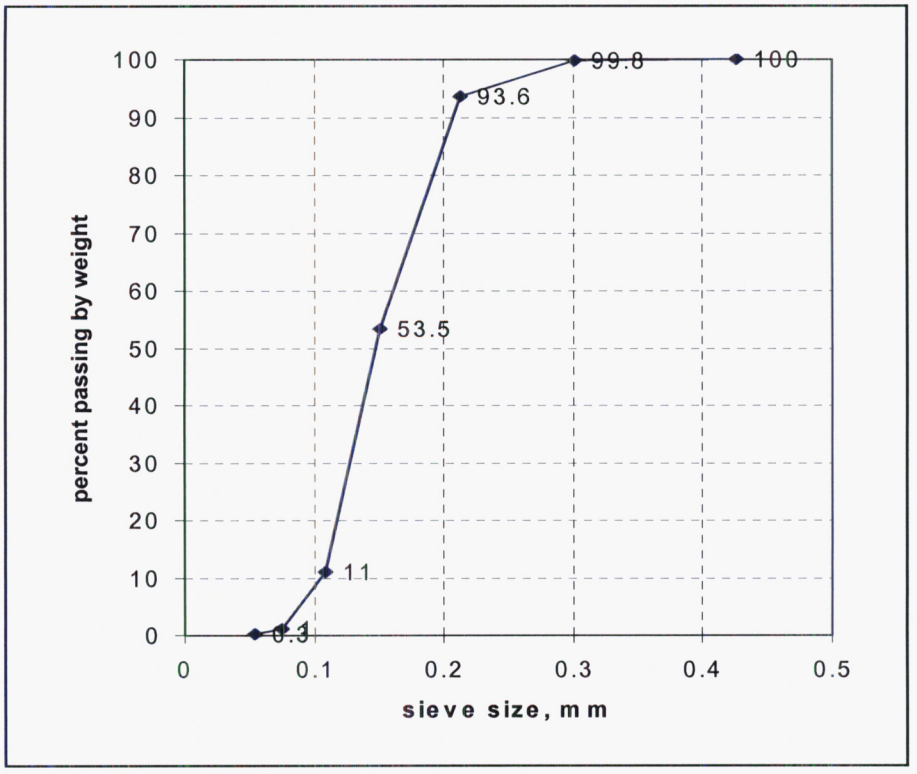

Table VII-35. Particle size data for the sand.

Darrell Sims 3/31/03, Fax on T & S Materials, Inc data on OK #1 sand		
USDA sieve	mm	passing (presumed by weight)
30	0.6	0
40	0.425	100
50	0.3	99.8
70	0.212	93.6
100	0.15	53.5
140	0.108	11
200	0.075	1
270	0.053	0.3
pan		0

Measured Values of Sand Thermal Conductivity

A bag of the sand (OK#1) was sent to Don Blackwell at Southern Methodist University. Considering the cost of setting up our own measurement system, and our lack of expertise in thermal conductivity measurements, Dr. Blackwell was an efficient approach. He is an acknowledged leader in the field; he has submitted an ASTM methodology for making such measurements (the divided bar approach).

Jim Prikryl put the report submitted by David Blackwell in the laboratory scientific notebook (#554). The measured values were 2.13 and 2.26 W/m-K for the water saturated samples and 0.33 and 0.34 W/m-K for the air saturated (dry) samples.

Steady State Profiles

From cttest11.xls, cttest14.xls, and cttest16b.xls, steady state profiles were extracted from the recorded data. For Test #11 and Test #14, a single time slice was extracted to use for plotting and for comparing with CFD simulation results. For Test #16, a time was selected as being at steady state, then 20 recorded time slices were averaged to use for CFD comparisons and plotting. Table VII-35 contains the power levels supplied to the heater cartridge for each steady state slice. The 4th phase of Test #14 had some peculiar sand temperatures that would affect the temperatures in the drift – this phase (at 1088.93 hours) should be excluded from comparisons with the CFD modeling.

Table VII-35. Power levels for Test #11, Test #14, and Test #16

	Time (hrs)	Power Setting	Power (watts)
Test #11	457.58	20	3.37
	735.37	25	5.251
	925.53	12	1.246
Test #14	284.98	20	3.37
	592.99	12	1.246
	783.22	6	0.343
	1088.93	2	0.057
Test #16d	-	20	3.52
Test #16e	-	25	5.51

Table VII-36, Table VII-39, and Table VII-41 contain the steady state slices for Test #11, Test #14, and Test #16 (d and e). Figure VII-42 contains 2 plots using selected thermocouples.

Table VII-36. Test #11 temperature data, steady state slices; uses old Prikryl coordinate system with origin at heat sink end of cylinder at inside top of drift.

Channel no		start time	----->	7/6/02 15:27	7/18/02 5:14	7/26/02 3:24
Thermocouple		hours	----->	457.584075	735.3657419	925.5276481
ID	x (cm)	y (cm)	z (cm)			
1	-1.905	-3.175	58.42	41.1781	51.84537	33.05496
2	0	-3.175	58.42	46.29116	62.28556	35.1638
3	1.905	-3.175	58.42	39.64968	47.96846	32.40895
4	-0.635	-1.905	58.42	47.86348	63.50646	35.52465
5	0.635	-1.905	58.42	42.75806	50.35131	34.37265
6	-1.27	-1.27	58.42	44.62497	59.77575	34.23965
7	0	-1.27	58.42	46.21467	61.5268	34.0168
8	1.27	-1.27	58.42	44.48262	53.75829	34.81575
9	-0.635	-0.3175	58.42	43.52301	57.29099	32.57877
10	0.635	-0.3175	58.42	42.02228	54.16846	32.09471
11	-1.905	-3.175	54.61	33.35506	38.30071	29.87211
12	0	-3.175	54.61	51.95407	67.92826	37.65773
13	1.905	-3.175	54.61	37.88166	44.77739	32.16328
14	-0.635	-1.905	54.61	43.90245	54.89777	34.75159
15	0.635	-1.905	54.61	42.78068	53.37944	33.88207
16	-1.27	-1.27	54.61	40.95464	50.80732	33.00101
17	0	-1.27	54.61	38.43228	47.16297	31.67129
18	1.27	-1.27	54.61	40.47603	49.84657	32.79505
19	-0.635	-0.3175	54.61	40.45761	50.06663	32.61442
20	0.635	-0.3175	54.61	36.94755	45.4008	30.66127
21	-1.905	-1.905	50.8	33.05038	38.35341	29.3739
22	0	-1.905	50.8	33.71485	40.19595	29.37975
23	1.905	-1.905	50.8	33.13459	39.02233	29.20809
24	-0.635	-0.635	50.8	34.97042	42.71809	29.701
25	0.635	-0.635	50.8	33.93431	40.86665	29.31777
26	0	-0.3175	50.8	31.1022	35.74501	28.39556
27	0	-4.7625	46.99	29.80112	33.28619	27.9277
28	-0.635	-4.445	46.99	29.54628	32.83951	27.86158
29	0.635	-4.445	46.99	29.70615	33.05983	27.91271
30	-1.905	-3.175	46.99	29.8512	33.41199	27.94959
31	0	-3.175	46.99	31.0097	35.49188	28.34391
32	1.905	-3.175	46.99	29.84045	33.31157	27.97177
33	-0.635	-1.905	46.99	31.49035	36.68591	28.35841
34	0.635	-1.905	46.99	31.58237	36.97579	28.34813
35	-1.27	-1.27	46.99	32.00455	37.76794	28.46032
36	0	-1.27	46.99	31.60984	37.16975	28.33718
37	1.27	-1.27	46.99	31.54921	37.00302	28.29816
38	-0.635	-0.3175	46.99	31.5992	37.43888	28.28911
39	0.635	-0.3175	46.99	30.29643	34.58441	27.99962
40	-1.905	-1.905	43.18	30.4255	34.80655	27.96998
41	0	-1.905	43.18	30.27691	34.69159	27.91562
42	1.905	-1.905	43.18	30.13252	34.33663	27.8647
43	-0.635	-0.635	43.18	29.90216	34.14224	27.77461
44	0.635	-0.635	43.18	29.89643	34.14446	27.79501

45	0	-0.3175	43.18	29.51625	33.16158	27.71317
46	-0.635	-4.7625	36.83	28.67588	31.51936	27.38302
47	0.635	-4.7625	36.83	28.6173	31.49888	27.32738
48	-1.27	-3.81	36.83	28.56409	31.37731	27.34691
49	0	-3.81	36.83	28.51461	31.30313	27.29672
50	1.27	-3.81	36.83	28.49377	31.21626	27.29491
51	-0.635	-3.175	36.83	28.6653	31.853	27.32846
52	0.635	-3.175	36.83	28.57036	31.44366	27.32661
53	-0.635	-1.905	36.83	28.89345	32.34942	27.32532
54	0.635	-1.905	36.83	28.93893	32.46056	27.36815
55	-1.27	-1.27	36.83	28.91063	32.54995	27.34156
56	0	-1.27	36.83	28.85668	32.33055	27.36267
57	1.27	-1.27	36.83	28.94735	32.63799	27.36839
58	-0.635	-0.3175	36.83	28.87816	32.40024	27.35844
59	0.635	-0.3175	36.83	28.86836	32.38092	27.33048
60	0	-4.7625	29.21	27.9399	30.48407	26.98458
61	-0.635	-4.445	29.21	28.10499	30.56632	27.17214
62	0.635	-4.445	29.21	28.04636	30.52738	27.14444
63	-1.905	-3.175	29.21	28.21405	30.84788	27.19841
64	0	-3.175	29.21	28.18293	30.76573	27.12219
65	1.905	-3.175	29.21	28.1244	30.7399	27.09247
66	-1.905	-1.905	29.21	28.15076	30.94093	27.06295
67	0	-1.905	29.21	28.04644	30.8322	26.99912
68	1.905	-1.905	29.21	28.2686	31.11285	27.12182
69	-0.635	-0.635	29.21	28.17943	31.01674	27.0635
70	0.635	-0.635	29.21	28.13401	30.97228	27.02637
71	0	-0.3175	29.21	28.0718	30.81081	27.03328
72	-0.635	-4.7625	20.32	27.34514	29.50301	26.64094
73	0.635	-4.7625	20.32	27.26457	29.40511	26.60804
74	-1.27	-3.81	20.32	27.25876	29.42025	26.60789
75	0	-3.81	20.32	27.30931	29.43856	26.62278
76	1.27	-3.81	20.32	27.19776	29.34779	26.57622
77	-0.635	-3.175	20.32	27.33496	29.58245	26.66182
78	0.635	-3.175	20.32	27.30223	29.53465	26.60472
79	-0.635	-1.905	20.32	27.35594	29.72064	26.61174
80	0.635	-1.905	20.32	27.41363	29.81421	26.61983
81	-1.27	-1.27	20.32	27.44249	29.88568	26.61675
82	0	-1.27	20.32	27.44812	29.89587	26.6112
83	1.27	-1.27	20.32	27.3725	29.8374	26.55955
84	-0.635	-0.3175	20.32	27.38531	29.78238	26.55818
85	0.635	-0.3175	20.32	27.35752	29.71252	26.5782
86	0	-4.445	10.16	26.50425	28.33162	26.03764
87	-1.27	-3.4925	10.16	26.64796	28.49392	26.1505
88	1.27	-3.4925	10.16	26.49833	28.32488	26.01306
89	-1.27	-1.5875	10.16	26.71344	28.6892	26.1857
90	1.27	-1.5875	10.16	26.68432	28.67429	26.12019
91	0	-0.635	10.16	26.72483	28.72063	26.2074
92	0	-4.1275	2.54	25.79383	27.58461	25.47964
93	0	-2.54	1.27	25.98882	27.71624	25.56824

94	0	-0.9525	2.54	26.2274	27.99854	25.7759
95	0	-5.715	57.15	33.29305	38.58984	29.21745
96	0	-6.985	57.15	32.4748	37.38732	28.88287
97	0	-8.255	57.15	31.69784	36.25758	28.63701
98	0	-9.525	57.15	31.16803	35.47448	28.42392
99	0	-10.795	57.15	30.82316	34.91045	28.29403
100	0	-12.065	57.15	30.64996	34.64814	28.21037
101	0	-5.715	46.99	29.78418	33.45782	27.84938
102	0	-6.985	46.99	29.8383	33.50899	27.82711
103	0	-8.255	46.99	29.8019	33.4541	27.82755
104	0	-9.525	46.99	29.71667	33.29901	27.78339
105	0	-10.795	46.99	29.6335	33.17862	27.73594
106	0	-12.065	46.99	29.59864	33.06408	27.76657
107	0	8.255	57.15	29.97945	33.76126	27.8733
108	0	6.985	57.15	30.10077	33.92054	27.9749
109	0	5.715	57.15	30.21125	34.16321	27.9547
110	0	4.445	57.15	30.42156	34.45941	28.09561
111	0	3.175	57.15	30.71054	34.91332	28.2193
112	0	1.905	57.15	31.13308	35.70356	28.37377
113	0	0.635	57.15	31.78969	36.69422	28.65063
114	0	8.255	46.99	29.46079	32.8324	27.72905
115	0	6.985	46.99	29.44736	32.84034	27.72251
116	0	5.715	46.99	29.49873	32.96558	27.73126
117	0	4.445	46.99	29.53921	33.03182	27.74193
118	0	3.175	46.99	29.65556	33.26392	27.79137
119	0	1.905	46.99	29.7907	33.51558	27.85928
120	0	0.635	46.99	29.85397	33.61417	27.88386
T1	0	-2.5	-2.5	25.7	25.5	26
T2	0	10	30	26.8	26.5	26
T3	0	12	30	27.8	29.6	26.8
T4	0	-2.5	63.5	26.6	26.5	25.8
T5	0	5	-1.5		22.8	22.2

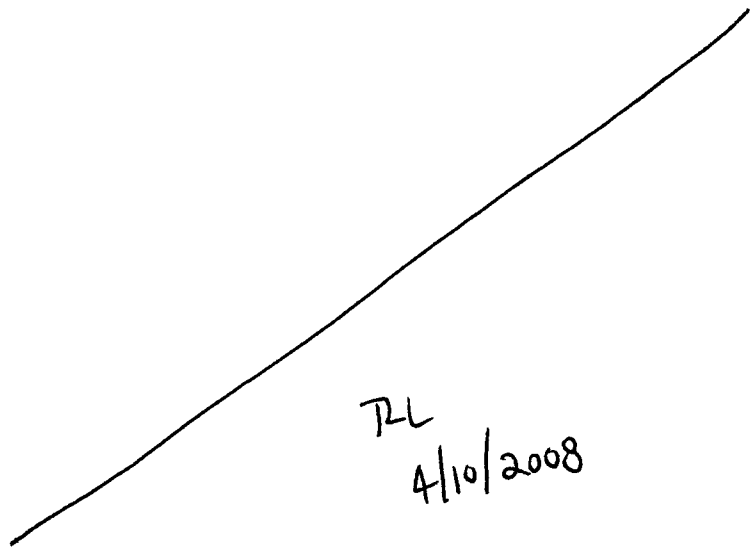

Table VII-39. Test #14 temperature data, steady state slices; uses old Prikryl coordinate system with origin at heat sink end of cylinder at inside top of drift.

Channel no		start time	----->	8/27/02 11:08	9/9/02 7:08	9/17/02 5:22	9/29/02 23:05
Thermocouple		hours	----->	284.9797	592.988	783.2175	1088.925
ID	x (cm)	y (cm)	z (cm)				
1	0	-3.175	58.42	52.14444	36.6067	28.604	25.33929
2	-1.27	-1.27	58.42	52.78992	35.87604	28.08357	25.12291
3	1.27	-1.27	58.42	44.54196	32.53519	27.0588	25.04298
4	-1.905	-3.175	54.61	38.51546	30.2109	26.62254	25.00461
5	1.905	-3.175	54.61	35.48307	29.48216	26.54546	25.06456
6	0	-1.27	54.61	41.88054	31.59799	26.82949	24.97368
7	-0.635	-0.3175	54.61	42.86834	31.64485	26.55181	24.83913
8	0.635	-0.3175	54.61	34.97725	28.425	25.84402	24.82186
9	0	-1.905	50.8	35.5464	28.41511	25.8052	24.81299
10	-0.635	-0.635	50.8	35.75593	28.28692	25.69083	24.78532
11	0.635	-0.635	50.8	36.0062	28.46065	25.82659	24.84208
12	0	-4.7625	46.99	30.15403	26.58571	25.39326	24.76043
13	-1.905	-3.175	46.99	30.55552	26.69186	25.38246	24.73331
14	1.905	-3.175	46.99	31.04156	26.77035	25.3855	24.74688
15	-0.635	-1.905	46.99	32.67846	27.33929	25.51526	24.74173
16	0.635	-1.905	46.99	32.11357	27.09081	25.41689	24.72734
17	0	-1.27	46.99	31.94116	26.97363	25.42184	24.73708
18	-1.905	-1.905	43.18	30.79189	26.5574	25.28997	24.65575
19	1.905	-1.905	43.18	31.00315	26.59262	25.30259	24.70455
20	0	-0.3175	43.18	30.31657	26.47748	25.28614	24.67939
21	-0.635	-4.7625	36.83	29.35693	26.27955	25.314	24.73687
22	0.635	-4.7625	36.83	29.31256	26.245	25.27529	24.72776
23	0	-3.81	36.83	29.47472	26.26122	25.26662	24.73137
24	-1.27	-1.27	36.83	29.71799	26.20205	25.18235	24.65051
25	0	-1.27	36.83	29.78456	26.23438	25.20927	24.64289
26	1.27	-1.27	36.83	29.75891	26.26677	25.25455	24.68372
27	0	-4.7625	29.21	28.60566	25.8868	25.08949	24.55896
28	-1.905	-3.175	29.21	28.60221	25.82812	25.01534	24.50321
29	1.905	-3.175	29.21	28.73937	25.8901	25.05943	24.56504
30	0	-1.905	29.21	28.7697	25.87138	25.03929	24.54344
31	-0.635	-0.635	29.21	28.83746	25.89222	25.05389	24.54023
32	0.635	-0.635	29.21	28.76848	25.87789	25.06015	24.53968
33	-1.27	-3.81	20.32	27.85126	25.49355	24.86536	24.40622
34	1.27	-3.81	20.32	27.83218	25.48931	24.84587	24.39215
35	-0.635	-1.905	20.32	27.94697	25.50177	24.86084	24.38968
36	0.635	-1.905	20.32	28.0298	25.51554	24.84855	24.37845
37	0	-1.27	20.32	28.005	25.48887	24.80044	24.35666
38	-0.635	-0.3175	20.32	27.9914	25.49098	24.82615	24.3846
39	0.635	-0.3175	20.32	28.02282	25.50914	24.83533	24.38646
40	0	-4.445	10.16	26.90998	24.9502	24.50081	24.11389
41	-1.27	-1.5875	10.16	27.44776	25.22543	24.69559	24.3347
42	1.27	-1.5875	10.16	27.2975	25.09259	24.55434	24.21981
43	0	-0.635	10.16	27.30305	25.10341	24.59981	24.21334
44	0	-4.1275	2.54	26.33648	24.45103	24.02713	23.6856

45	0	-2.54	0.635	26.35107	24.42645	23.9925	23.66704
46	0	-0.9525	2.54	26.58757	24.62109	24.17705	23.78738
47	0	-5.715	57.15	35.04161	28.4796	25.89266	24.7374
48	0	-6.985	57.15	33.30888	27.76808	25.7156	24.74428
49	0	-8.255	57.15	32.49576	27.46045	25.59672	24.69922
50	0	-9.525	57.15	31.92546	27.22713	25.52848	24.67258
51	0	-10.795	57.15	31.55324	27.0961	25.54198	24.70004
52	0	-5.715	46.99	30.36642	26.58138	25.31429	24.60561
53	0	-6.985	46.99	30.40291	26.60903	25.32923	24.60992
54	0	-8.255	46.99	30.39752	26.63936	25.37081	24.62282
55	0	-9.525	46.99	30.37785	26.61955	25.35098	24.61384
56	0	-10.795	46.99	30.30412	26.61567	25.36763	24.64795
57	0	0.635	57.15	32.25414	27.29952	25.54636	24.65713
58	0	1.905	57.15	31.86095	27.16215	25.50583	24.66401
59	0	3.175	57.15	31.44565	27.01299	25.46297	24.64803
60	0	4.445	57.15	31.13681	26.90362	25.45241	24.65293
61	0	5.715	57.15	31.2667	27.04643	25.61473	24.99815
62	0	0.635	46.99	30.88595	26.83581	25.52539	24.91213
63	0	1.905	46.99	30.86793	26.83046	25.51304	24.87539
64	0	3.175	46.99	30.76774	26.76694	25.45102	24.8466
65	0	4.445	46.99	30.59721	26.67347	25.39838	24.74325
66	0	5.715	46.99	30.44546	26.59675	25.30308	24.65726
T1	0	-2.5	-2.5	25.8	25.5	26.7	26.2
T2	0	10	30	25.9	25.3	25.1	24.5
T3	0	12	30	27.1	25.8	25.1	24.6
T4	0	-2.5	63.5	27.2	25.3	25.2	24.6
T5	0	5	-1.5	21.3	20.9	20.9	20.8

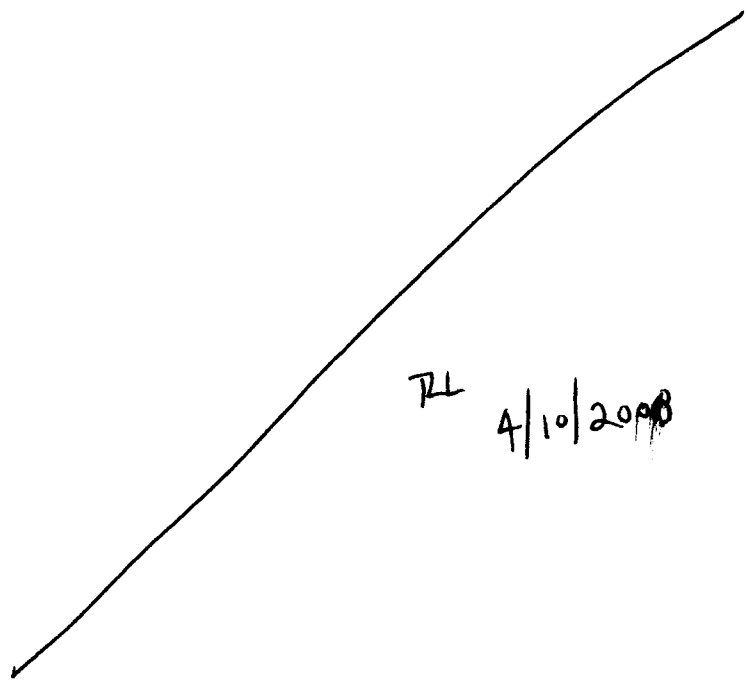

Table VII-41. Test #16d and #16e temperature data, steady state slices (average of 20 readings); **uses new coordinate system origin at center of drift.**

x (cm)	y (cm)	z (cm)	Thermocouple ID	Temperature, C	Temperature, C
26.65	0	-3.215	1	52.10	65.41
26.65	0	-4.485	2	45.57	55.62
26.65	0	-5.755	3	42.06	50.34
26.65	0	-7.025	4	39.69	46.73
26.65	0	-8.295	5	37.75	43.76
26.65	0	-9.565	6	36.15	41.40
26.65	0	-1.31	7	89.13	119.20
26.65	0	1.865	8	58.21	74.21
26.65	0	2.5	9	50.79	63.23
26.65	0	3.135	10	47.21	58.57
26.65	0	4.405	11	43.45	53.01
26.65	0	5.675	12	40.56	48.67
26.65	0	6.945	13	38.41	45.40
26.65	0	8.215	14	36.81	43.02
16.49	0	1.865	15	43.56	53.66
16.49	0	2.5	16	38.16	45.24
-12.72	0	1.865	17	27.06	29.46
-12.72	0	2.5	18	26.06	27.57
16.49	0	3.135	19	37.38	43.98
16.49	0	4.405	20	36.09	42.00
16.49	0	5.675	21	34.94	40.23
16.49	0	6.945	22	33.84	38.54
16.49	0	8.215	23	33.22	37.60
-12.72	0	3.135	24	26.17	27.68
-12.72	0	4.405	25	26.10	27.47
-12.72	0	5.675	26	25.88	27.14
-12.72	0	6.945	27	25.82	27.02
-12.72	0	8.215	28	25.71	26.85
31.095	0	-1.945	29	50.17	61.64
33	0	-1.945	30	43.51	51.61
35.54	0	-1.945	31	32.15	34.72
26.65	0	11.3138	32	33.15	37.54
16.49	0	11.3138	33	30.99	34.20
-12.72	0	11.3138	34	25.00	25.81
26.65	-8.255	-0.04	35	37.05	43.00
16.49	-8.255	-0.04	36	33.82	38.33
-12.72	-8.255	-0.04	37	25.89	26.95
26.65	0	13.0918	38	32.19	36.09
16.49	0	13.0918	39	30.25	32.98
-12.72	0	13.0918	40	25.26	26.07
26.65	0	15.6318	41	24.79	24.77
16.49	0	15.6318	42	25.70	25.66
-12.72	0	15.6318	43	24.06	23.61
external			44	24.23	23.73

Figure VII-42. Top is sample time profiles of temperature from Test #11 and bottom is from Test #14 with axial positions noted in the legends (uses new coord. sys, origin in center of drift).

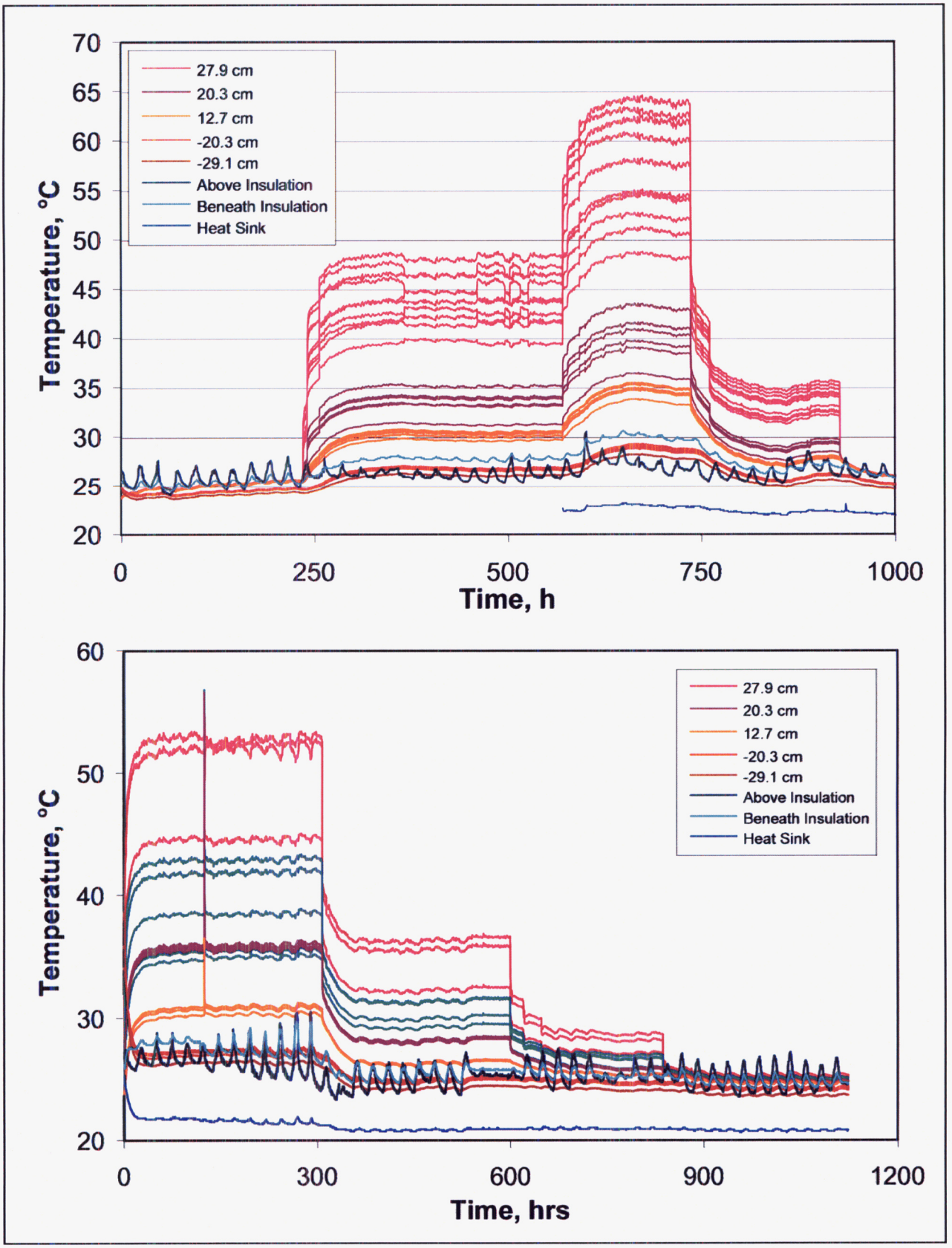

Sand Profiles in Cold-Trap Test

bubo E:\TEF-kti\ColdTrap\Test-11\cttest11.xls and cttest16b.xls
The files for Test #11includes the recorded data sent by Jim Prikryl in "Raw Data" and the processed data (by me) for sand profiles in the worksheet "ExternalProfiles". The file for Test #16 includes the recorded data sent by Jim Prikryl to Steve Svedeman. Five phases of Test #16 were run – numbered 16a, 16b, 16c, 16d, and 16e. Only the last two were compared with the CFD modeling. The worksheets in the file included the raw data with appropriately labeling noting the phase number (e.g., 16d) and separate worksheets with processed data and plots. The processing was done by Steve Svedeman, who did not have a scientific notebook for the desktop experiment. The primary reasons that the dry tests were done were to assess thermal conductivity of the sand and to check on power leakage. Both of these seem to be possible reasons for difficulty in matching CFD simulation results to measured data for the wet tests. Figure VII-43 contains the profiles at 46 and 57 cm (using the old coordinate system of Prikryl). Figure VII-44 contains the profiles for two different test phases for Test #16.

Figure VII-43. Sand profiles at 57.15 cm (near the heater) on the top, and at 46.99 cm axial position of the drift on the bottom of the figure box.

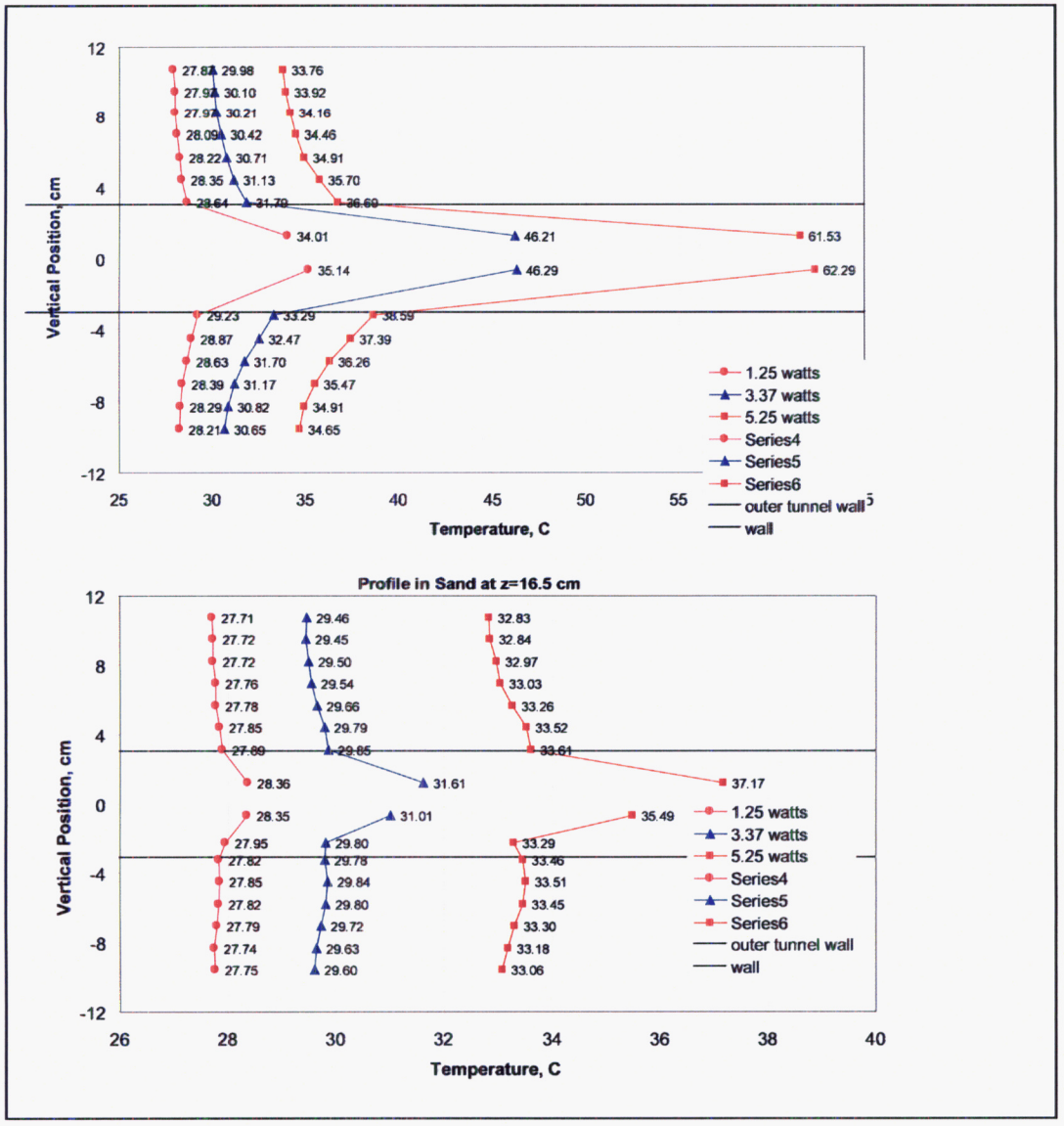

Figure VII-44. Sand profiles for Test 16 used in CFD comparison.

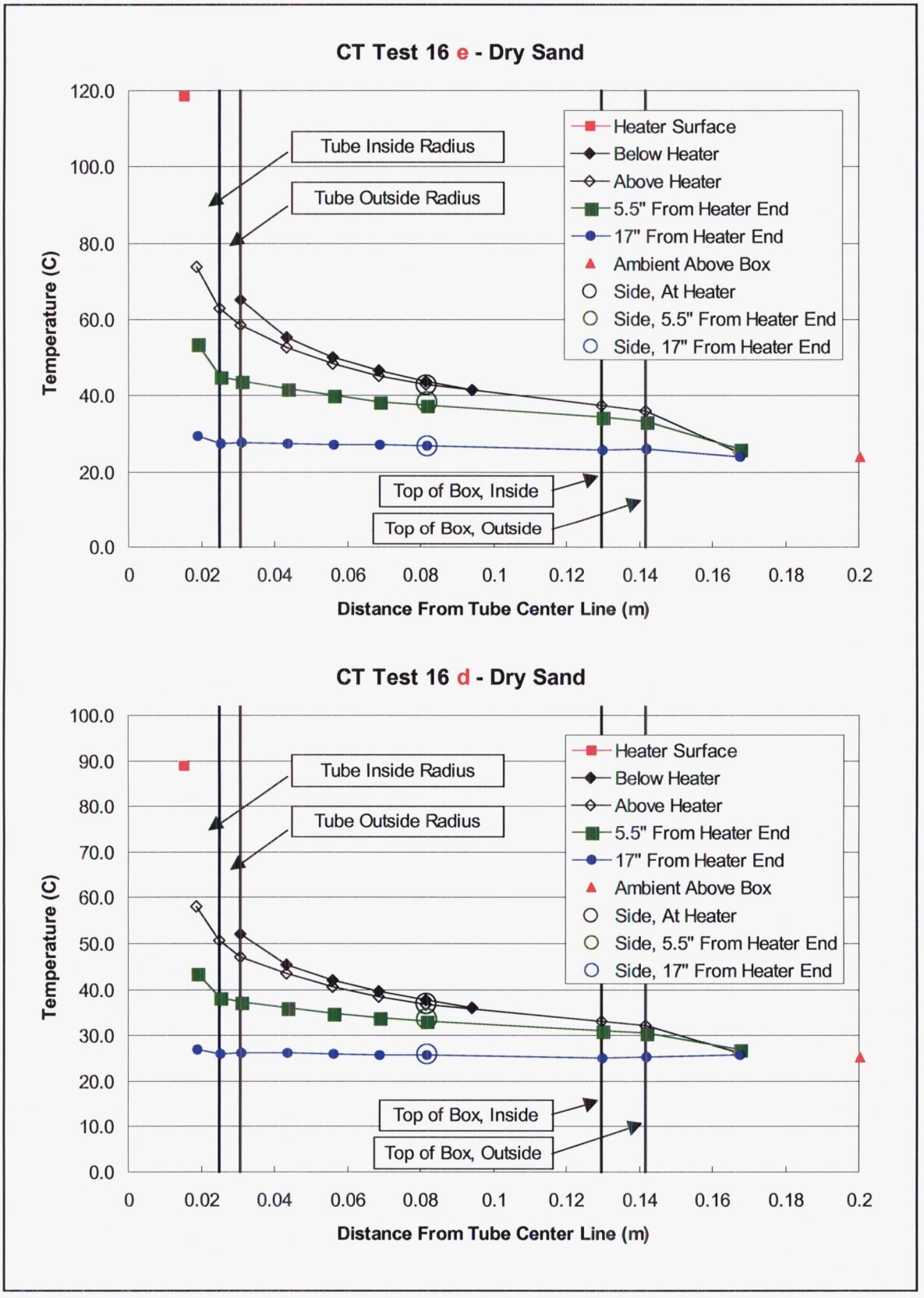

Cross-Sections of In-Drift Temperatures

Temperature data was extracted from:
bubo E:\TEF-kti\ColdTrap\Test-11\cttest11.xls
bubo E:\TEF-kti\ColdTrap\Test-14\cttest14.xls
for plotting in Tecplot 8.0-1.0 on Spock (SunOS). The extracted *.dat files and the Tecplot layouts are stored in
Spock: ~/ColdTrap/TestTemperature
./cttest11-March.dat and ./cttest14-March.dat
./Tsections11-???hrs.lay where ??? are the hours of the test 458, 735, and 926
./Tsections14-???hrs.lay where ??? are 285, 593, and 783 hours
Test 14 steady state at 1090 hours should not be used because the temperature gradients in the drift are too low and funny stuff may be going on with the heat sink and sand. Another thing to consider is the sensitivity of the thermocouples. Much of the data at the cold end cross-sections fall within the reliability of the thermocouples, thus caution should be exercised.

Rough drafts of the figures were created by Cheryl Patton following my examples from plotting of earlier test data. I checked her extraction of data from the original data set. The extracted data was put into the format needed by Tecplot (the *.dat files). The layouts just tell Tecplot how to plot the data. Figure VII-46 is the set of cross-sections for Test 11 at 485 hours, the last two cross-sections at the cold end were not included since there were only one or two thermocouples. Similarly, Figures VII-47 to VII-51 contain the cross-sections for the remaining 2 steady state times for Test #11 and the 3 times for Test #14.

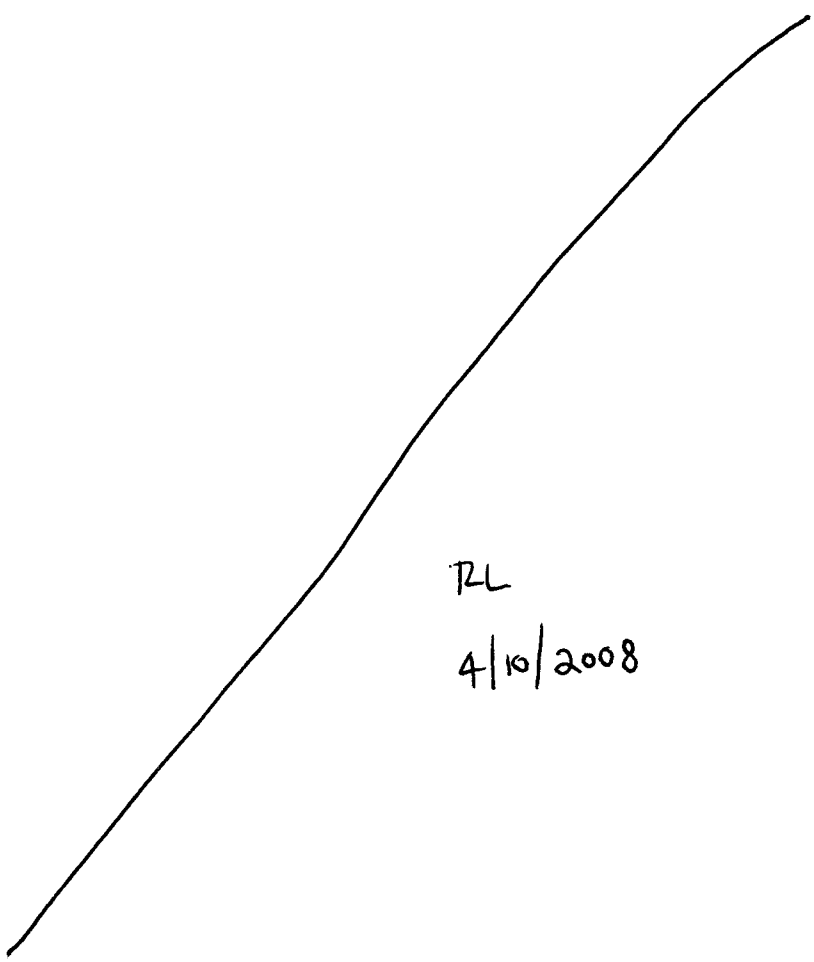

Figure VII-46. Cross-sections for Test #11 at 485 hours. The x-direction (axial position) along the drift is noted on each cross-section.

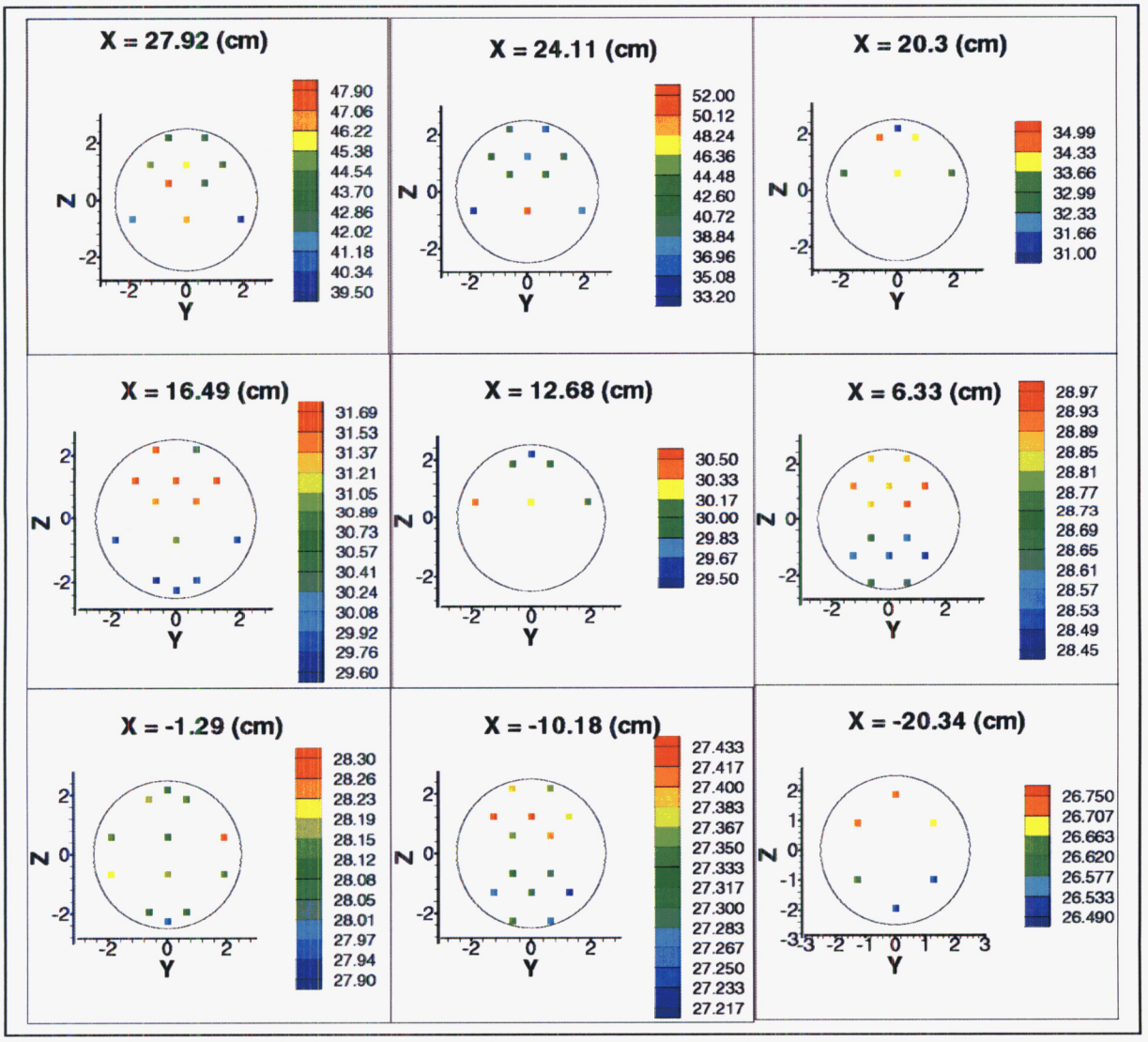

Figure VII-47. Cross-sections for Test #11 at 735 hours. The x-direction (axial position) along the drift is noted on each cross-section.

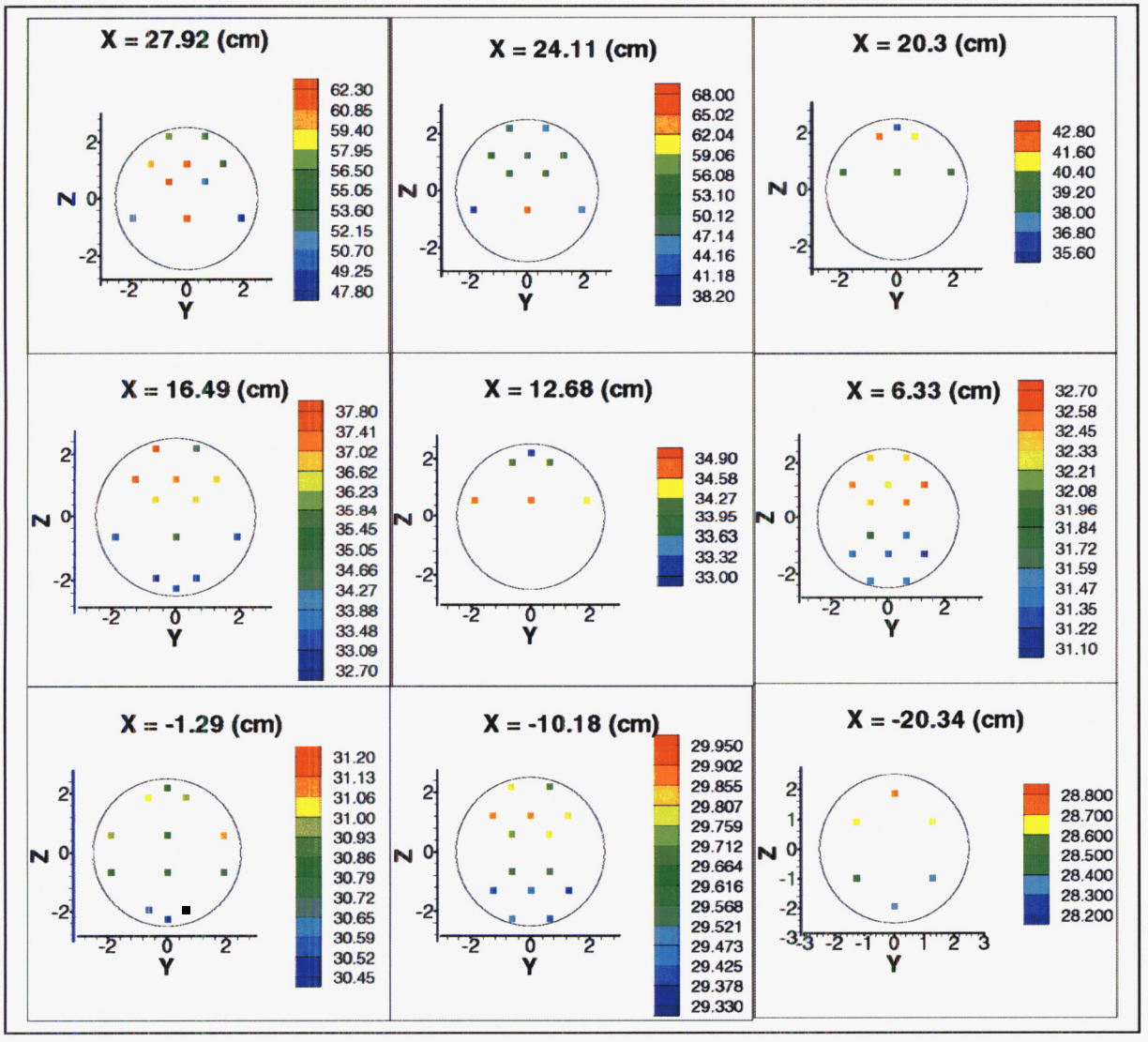

Figure VII-48. Cross-sections for Test #11 at 926 hours. The x-direction (axial position) along the drift is noted on each cross-section.

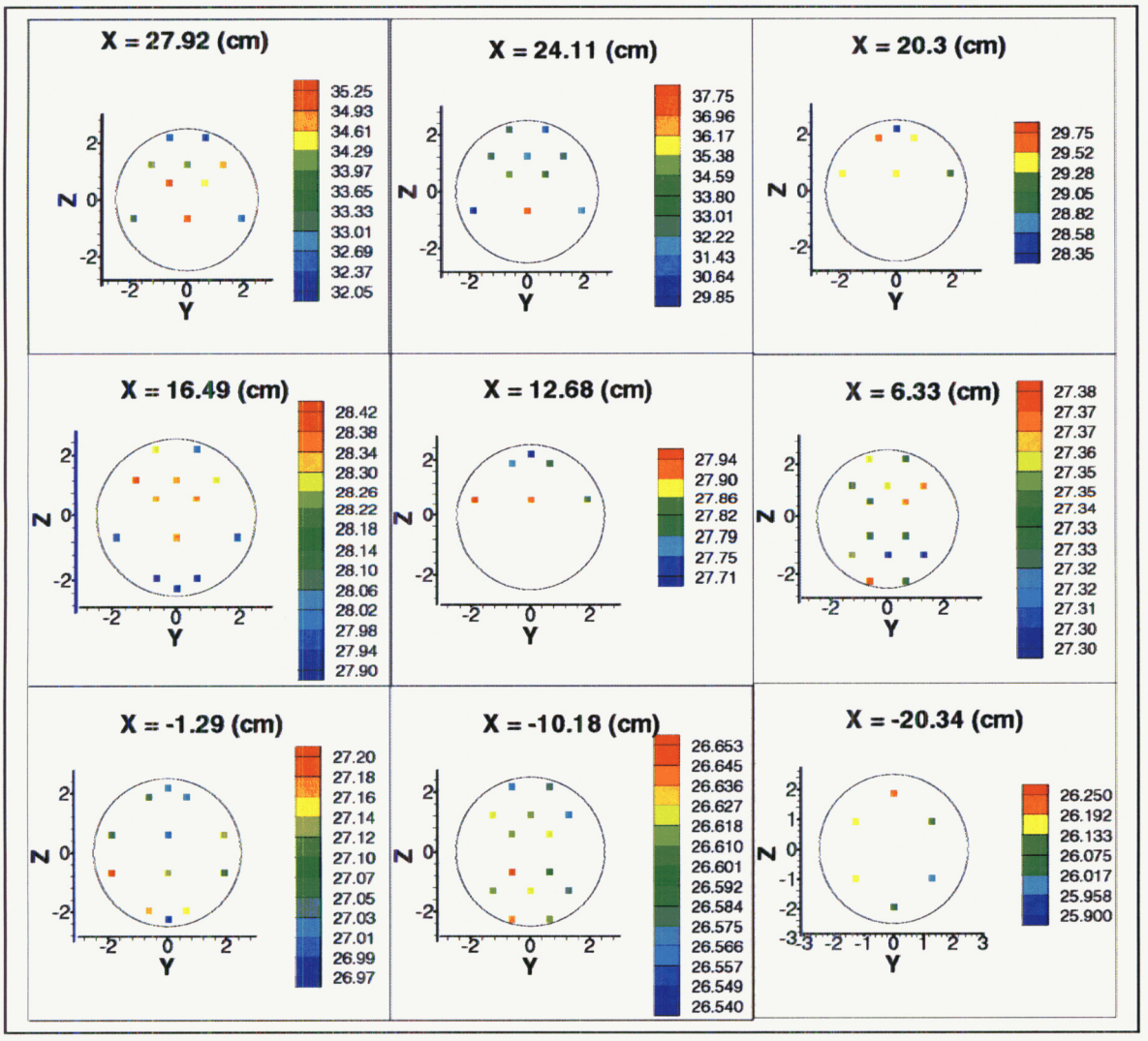

Figure VII-49. Cross-sections for Test #14 at 285 hours. The x-direction (axial position) along the drift is noted on each cross-section.

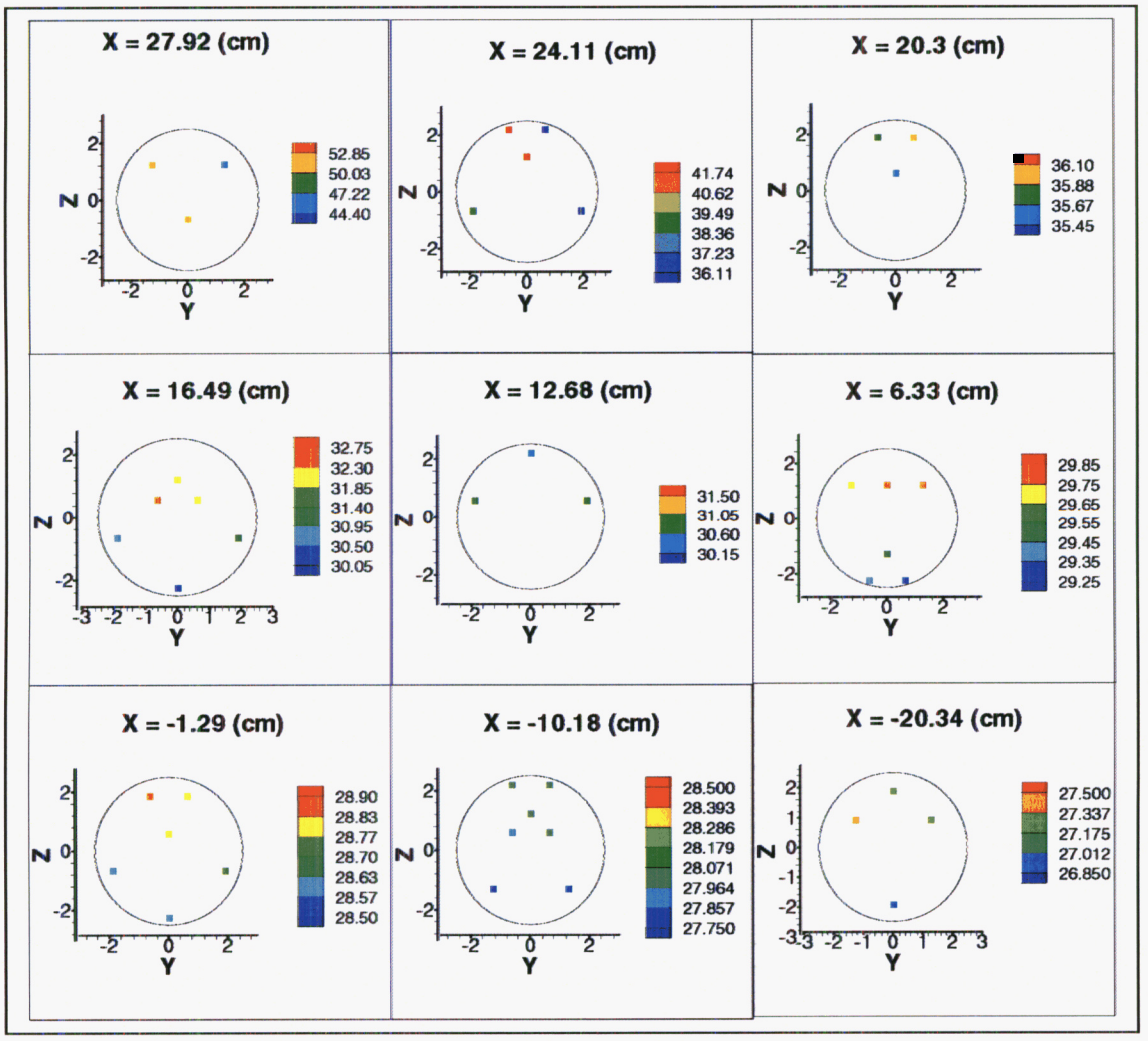

Figure VII-50. Cross-sections for Test #14 at 593 hours. The x-direction (axial position) along the drift is noted on each cross-section.

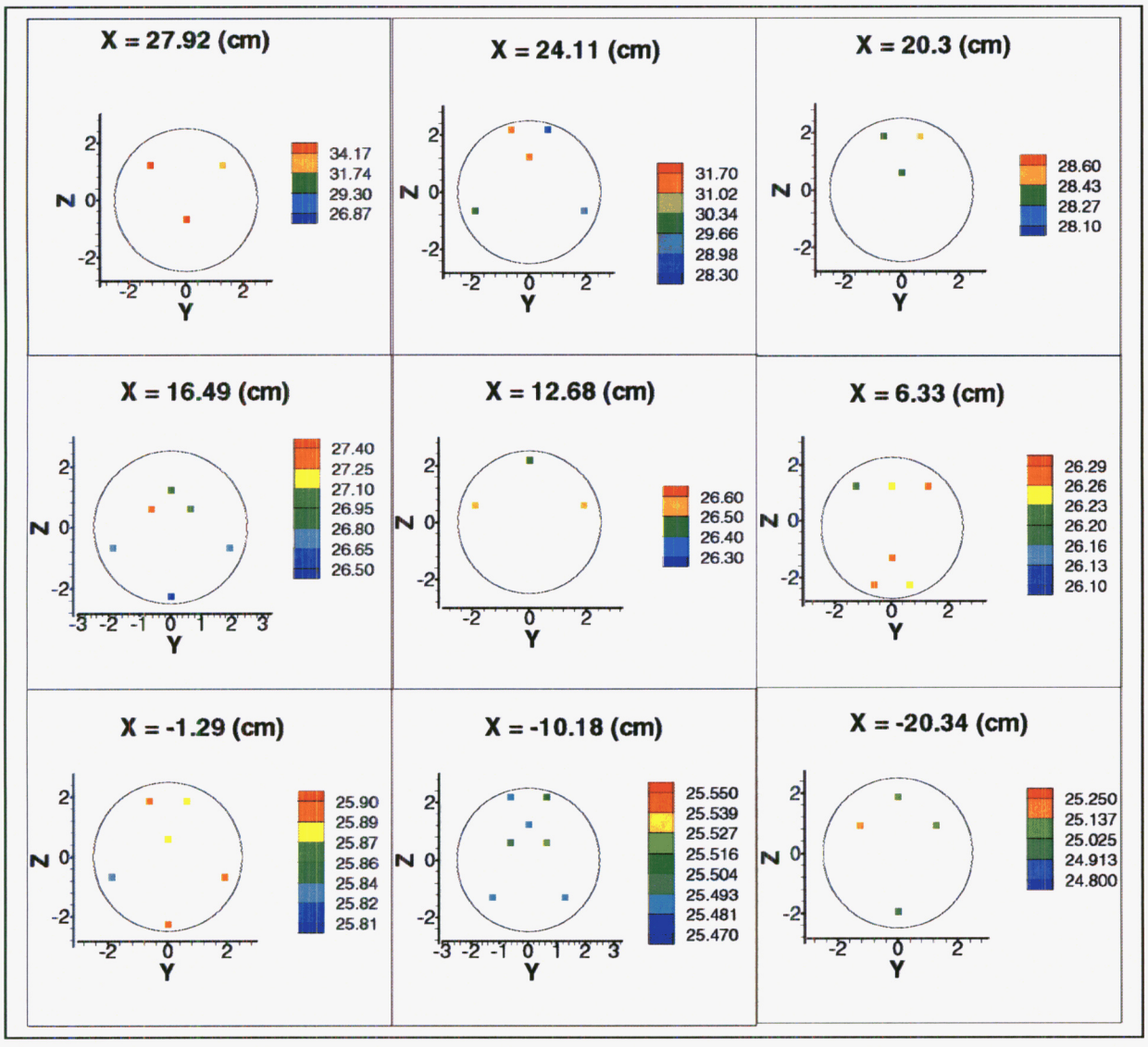

Figure VII-51. Cross-sections for Test #14 at 783 hours. The x-direction (axial position) along the drift is noted on each cross-section.

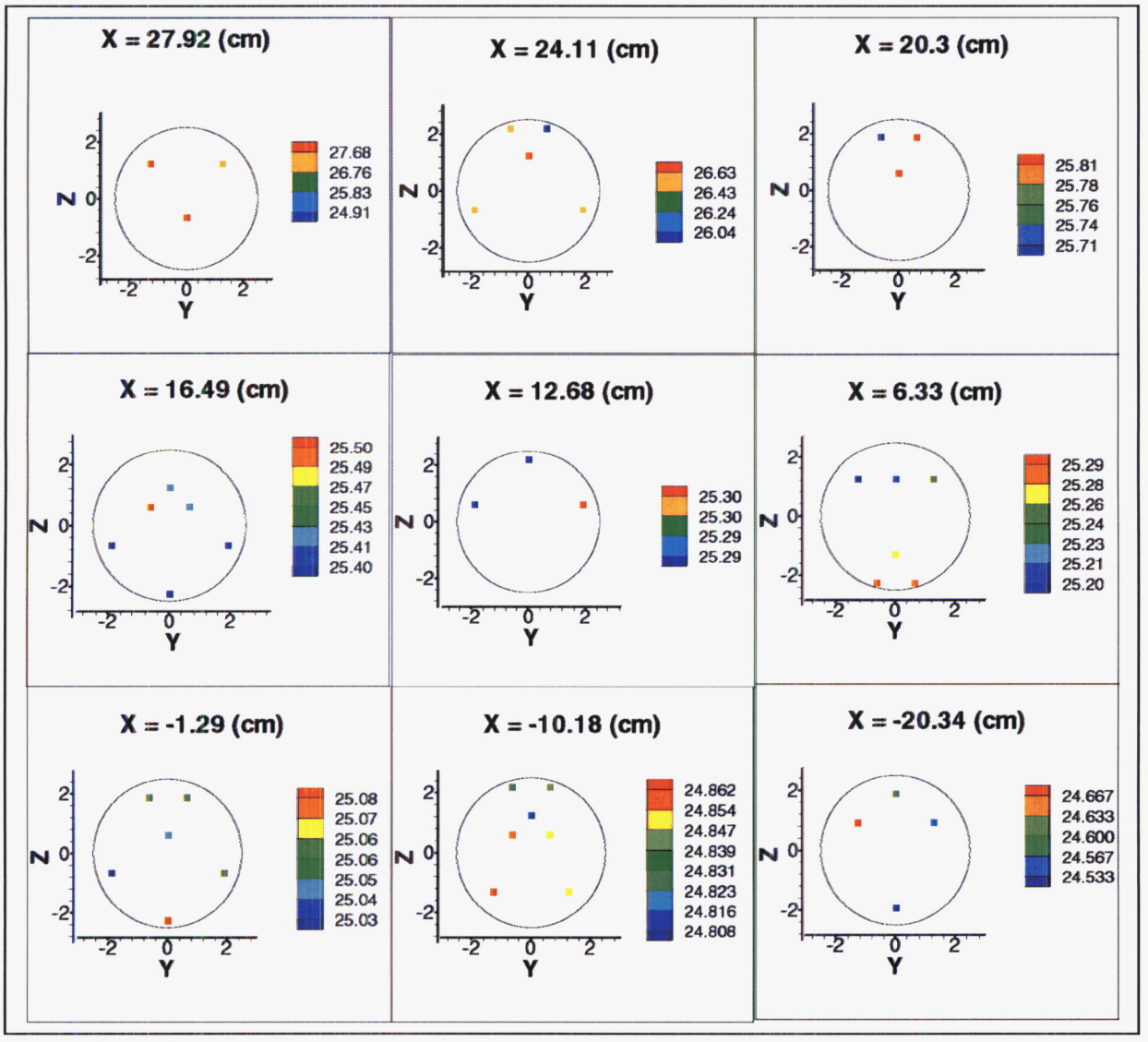

Test #11 Tecplot file (Spock: ~\ColdTrap\TestTemperatures\cttest11-March.dat):

```
TITLE = "Temperature distributions in 11 Cross-Sections"
VARIABLES = "x", "y", "z", "T=458Hrs", "T=735Hrs", "T=926Hrs"

ZONE T="CS1, z=27.92 [cm]", I=10, F=POINT
27.92  -1.905 -0.675 41.18  51.85  33.05
27.92  0      -0.675 46.29  62.29  35.16
27.92  1.905  -0.675 39.65  47.97  32.41
27.92  -0.635 0.595  47.86  63.51  35.52
27.92  0.635  0.595  42.76  50.35  34.37
27.92  -1.27  1.23   44.62  59.78  34.24
27.92  0      1.23   46.21  61.53  34.02
27.92  1.27   1.23   44.48  53.76  34.82
27.92  -0.635 2.1825 43.52  57.29  32.58
27.92  0.635  2.1825 42.02  54.17  32.09
ZONE T="CS2, z=24.11 [cm]", I=10, F=POINT
24.11  -1.905 -0.675 33.36  38.30  29.87
24.11  0      -0.675 51.95  67.93  37.66
24.11  1.905  -0.675 37.88  44.78  32.16
24.11  -0.635 0.595  43.90  54.90  34.75
24.11  0.635  0.595  42.78  53.38  33.88
24.11  -1.27  1.23   40.95  50.81  33.00
24.11  0      1.23   38.43  47.16  31.67
24.11  1.27   1.23   40.48  49.85  32.80
24.11  -0.635 2.1825 40.46  50.07  32.61
24.11  0.635  2.1825 36.95  45.40  30.66
ZONE T="CS3, z=20.3 [cm]", I=6, F=POINT
20.3   -1.905 0.595  33.05  38.35  29.37
20.3   0      0.595  33.71  40.20  29.38
20.3   1.905  0.595  33.13  39.02  29.21
20.3   -0.635 1.865  34.97  42.72  29.70
20.3   0.635  1.865  33.93  40.87  29.32
20.3   0      2.1825 31.10  35.75  28.40
ZONE T="CS4, z=16.49 [cm]", I=13, F=POINT
16.49  0      -2.2625       29.80  33.29  27.93
16.49  -0.635 -1.945 29.55  32.84  27.86
16.49  0.635  -1.945 29.71  33.06  27.91
16.49  -1.905 -0.675 29.85  33.41  27.95
16.49  0      -0.675 31.01  35.49  28.34
16.49  1.905  -0.675 29.84  33.31  27.97
16.49  -0.635 0.595  31.49  36.69  28.36
16.49  0.635  0.595  31.58  36.98  28.35
16.49  -1.27  1.23   32.00  37.77  28.46
16.49  0      1.23   31.61  37.17  28.34
16.49  1.27   1.23   31.55  37.00  28.30
16.49  -0.635 2.1825 31.60  37.44  28.29
16.49  0.635  2.1825 30.30  34.58  28.00
ZONE T="CS5, z=12.68 [cm]", I=6, F=POINT
12.68  -1.905 0.595  30.43  34.81  27.97
12.68  0      0.595  30.28  34.69  27.92
12.68  1.905  0.595  30.13  34.34  27.86
12.68  -0.635 1.865  29.90  34.14  27.77
12.68  0.635  1.865  29.90  34.14  27.80
12.68  0      2.1825 29.52  33.16  27.71
ZONE T="CS6, z=6.33 [cm]", I=14, F=POINT
6.33   -0.635 -2.2625       28.68  31.52  27.38
6.33   0.635  -2.2625       28.62  31.50  27.33
6.33   -1.27  -1.31  28.56  31.38  27.35
6.33   0      -1.31  28.51  31.30  27.30
6.33   1.27   -1.31  28.49  31.22  27.29
6.33   -0.635 -0.675 28.67  31.85  27.33
6.33   0.635  -0.675 28.57  31.44  27.33
6.33   -0.635 0.595  28.89  32.35  27.33
6.33   0.635  0.595  28.94  32.46  27.37
6.33   -1.27  1.23   28.91  32.55  27.34
6.33   0      1.23   28.86  32.33  27.36
6.33   1.27   1.23   28.95  32.64  27.37
6.33   -0.635 2.1825 28.88  32.40  27.36
6.33   0.635  2.1825 28.87  32.38  27.33
ZONE T="CS7, z=-1.29 [cm]", I=12, F=POINT
```

```
-1.29  0      -2.2625       27.94  30.48  26.98
-1.29  -0.635 -1.945 28.10  30.57  27.17
-1.29  0.635  -1.945 28.05  30.53  27.14
-1.29  -1.905 -0.675 28.21  30.85  27.20
-1.29  0      -0.675 28.18  30.77  27.12
-1.29  1.905  -0.675 28.12  30.74  27.09
-1.29  -1.905 0.595  28.15  30.94  27.06
-1.29  0      0.595  28.05  30.83  27.00
-1.29  1.905  0.595  28.27  31.11  27.12
-1.29  -0.635 1.865  28.18  31.02  27.06
-1.29  0.635  1.865  28.13  30.97  27.03
-1.29  0      2.1825 28.07  30.81  27.03
ZONE T="CS8, z=-10.18 [cm]", I=14, F=POINT
-10.18 -0.635 -2.2625       27.35  29.50  26.64
-10.18 0.635  -2.2625       27.26  29.41  26.61
-10.18 -1.27  -1.31  27.26  29.42  26.61
-10.18 0      -1.31  27.31  29.44  26.62
-10.18 1.27   -1.31  27.20  29.35  26.58
-10.18 -0.635 -0.675 27.33  29.58  26.66
-10.18 0.635  -0.675 27.30  29.53  26.60
-10.18 -0.635 0.595  27.36  29.72  26.61
-10.18 0.635  0.595  27.41  29.81  26.62
-10.18 -1.27  1.23   27.44  29.89  26.62
-10.18 0      1.23   27.45  29.90  26.61
-10.18 1.27   1.23   27.37  29.84  26.56
-10.18 -0.635 2.1825 27.39  29.78  26.56
-10.18 0.635  2.1825 27.36  29.71  26.58
ZONE T="CS9, z=-20.34 [cm]", I=6, F=POINT
-20.34 0      -1.945 26.50  28.33  26.04
-20.34 -1.27  -0.9925       26.65  28.49  26.15
-20.34 1.27   -0.9925       26.50  28.32  26.01
-20.34 -1.27  0.9125 26.71  28.69  26.19
-20.34 1.27   0.9125 26.68  28.67  26.12
-20.34 0      1.865  26.72  28.72  26.21
```

==========

Test #14 Tecplot file (Spock: ~\ColdTrap\TestTemperatures\cttest14-March.dat):

```
TITLE = "Temperature distributions in 11 Cross-Sections"

VARIABLES = "x", "y", "z", "T=285Hrs", "T=593Hrs", "T=783Hrs", "T=1090Hrs"

ZONE T="CS1, z=58.42 [cm]", I=3, F=POINT
27.92  0      -0.675 52.14  36.61  28.60  25.34
27.92  -1.27  1.23   52.79  35.88  28.08  25.12
27.92  1.27   1.23   44.54  32.54  27.06  25.04
ZONE T="CS2, z=54.61 [cm]", I=5, F=POINT
24.11  -1.905 -0.675 38.52  30.21  26.62  25.00
24.11  1.905  -0.675 35.48  29.48  26.55  25.06
24.11  0      1.23   41.88  31.60  26.83  24.97
24.11  -0.635 2.1825 42.87  31.64  26.55  24.84
24.11  0.635  2.1825 34.98  28.43  25.84  24.82
ZONE T="CS3, z=50.8 [cm]", I=3, F=POINT
20.3   0      0.595  35.55  28.42  25.81  24.81
20.3   -0.635 1.865  35.76  28.29  25.69  24.79
20.3   0.635  1.865  36.01  28.46  25.83  24.84
ZONE T="CS4, z=46.99 [cm]", I=6, F=POINT
16.49  0      -2.2625       30.15  26.59  25.39  24.76
16.49  -1.905 -0.675 30.56  26.69  25.38  24.73
16.49  1.905  -0.675 31.04  26.77  25.39  24.75
16.49  -0.635 0.595  32.68  27.34  25.52  24.74
16.49  0.635  0.595  32.11  27.09  25.42  24.73
16.49  0      1.23   31.94  26.97  25.42  24.74
ZONE T="CS5, z=43.18 [cm]", I=3, F=POINT
12.68  -1.905 0.595  30.79  26.56  25.29  24.66
12.68  1.905  0.595  31.00  26.59  25.30  24.70
12.68  0      2.1825 30.32  26.48  25.29  24.68
ZONE T="CS6, z=36.83 [cm]", I=6, F=POINT
6.33   -0.635 -2.2625       29.36  26.28  25.31  24.74
6.33   0.635  -2.2625       29.31  26.25  25.28  24.73
```

```
6.33   0      -1.31  29.47  26.26  25.27  24.73
6.33   -1.27  1.23   29.72  26.20  25.18  24.65
6.33   0      1.23   29.78  26.23  25.21  24.64
6.33   1.27   1.23   29.76  26.27  25.25  24.68
ZONE T="CS7, z=29.21 [cm]", I=6, F=POINT
-1.29  0      -2.2625       28.61  25.89  25.09  24.56
-1.29  -1.905 -0.675 28.60  25.83  25.02  24.50
-1.29  1.905  -0.675 28.74  25.89  25.06  24.57
-1.29  0      0.595  28.77  25.87  25.04  24.54
-1.29  -0.635 1.865  28.84  25.89  25.05  24.54
-1.29  0.635  1.865  28.77  25.88  25.06  24.54
ZONE T="CS8, z=20.32 [cm]", I=7, F=POINT
-10.18 -1.27  -1.31  27.85  25.49  24.87  24.41
-10.18 1.27   -1.31  27.83  25.49  24.85  24.39
-10.18 -0.635 0.595  27.95  25.50  24.86  24.39
-10.18 0.635  0.595  28.03  25.52  24.85  24.38
-10.18 0      1.23   28.01  25.49  24.80  24.36
-10.18 -0.635 2.1825 27.99  25.49  24.83  24.38
-10.18 0.635  2.1825 28.02  25.51  24.84  24.39
ZONE T="CS9, z=10.16 [cm]", I=4, F=POINT
-20.34 0      -1.945 26.91  24.95  24.50  24.11
-20.34 -1.27  0.9125 27.45  25.23  24.70  24.33
-20.34 1.27   0.9125 27.30  25.09  24.55  24.22
-20.34 0      1.865  27.30  25.10  24.60  24.21
ZONE T="CS10, z=2.54 [cm]", I=2, F=POINT
-27.96 0      -1.6275       26.34  24.45  24.03  23.69
-27.96 0      1.5475 26.59  24.62  24.18  23.79
ZONE T="CS11, z=0.635 [cm]", I=1, F=POINT
-29.865       0      -0.04  26.35  24.43  23.99  23.67
```

Thermocouple Calibration Checks

Two calibration checks on thermocouples were made, one after Test #11 and one after Test #14. Thermocouples were calibrated before each test as recorded in Prikryl's scientific notebook. Regression equations for electrical signal to temperature were calculated for each thermocouple. After the test was completed, the thermocouples were put in the temperature baths again and the readings were recorded. Table VII-54 contains a summary of the post-test checks. Two standard deviations is a typical approach for estimating reliability of readings. Table VII-54 summarizes calculations made at the bottom of "PostTest-CalibChk" worksheet in cttest11.xls and in "Thermocouple-Calib-Oct9" worksheet in cttest14.xls.

Table VII-5. Data From Calibration Checks of the Thermocouples.

Test # 11, July 30, 2002						
Known Temperature, C	23.80	30.85	38.00	44.90	51.00	57.90
Minimum Error	-0.24	-0.20	-0.22	-0.18	-0.18	-0.32
Maximum Error	0.16	0.24	0.16	0.16	0.26	0.23
Average Error	-0.08	-0.04	-0.06	-0.06	-0.02	-0.01
Standard Deviation	0.093	0.084	0.073	0.074	0.092	0.116
Test #14, October 9, 2002						
Known Temperature, C	23.35	29.75	36.05	43.65	49.95	56.20
Minimum Error	-0.39	-0.28	-0.22	-0.28	-0.45	-0.32
Maximum Error	1.27	0.44	0.33	0.33	0.42	0.50
Average Error	-0.06	0.01	0.01	0.00	-0.10	0.10
Standard Deviation	0.292	0.243	0.172	0.134	0.131	0.129

4/10/03 RF

Large-Scale Cold-Trap Experiment - Development

Geometric scaling:

After scrounging around, it was decided that we have to go with the same tunnel/canister dimensions as were used in the Atlas Facility Convection test. The DOE is changing the design, and we do not know what the specs will be for the license application design. Thus for our ~20% scale model with the concrete culverts, we'll use:

Actual tunnel diameter = 5.5 m
canister length = 5.17 m
canister diameter = 1.59 m
canister power (waste package power) = 600 watts (@ 300yrs)
(we will be backing off from this power for relevancy to cold trap process,
so please also consider at lesser watts, i.e., longer/larger number years for aging the waste)

cement culvert internal diameter = 42 inches = 1.067 m
cement culvert wall thickness = 4.5 inches = 11.4 cm
laboratory scaled model length = 10 m

Frank's Scaling Analysis Memo:

MEMO

DATE: March 17, 2003
TO: Randy Fedors
FROM: Frank Dodge
SUBJECT: Thermal scaling methods for Large-Scale Cold Trap Experiment

The large-scale Cold Trap Experiment is supposed to have a geometric scale factor (ratio of model drift dimensions to corresponding full scale dimensions) in the range of 1/3 of full-scale. The experiment will be considerably larger than the bench scale Cold Trap Experiment. To design the large scale experiment it is necessary to know how to scale the electrical power of the simulated waste packages. To make this determination, it is assumed that the scale-model tests are conducted in such a way that the temperature differences ΔT between various locations in the scale-model drift are equal to the full scale values. It is also assumed that:

1. simulated waste packages are geometrically scaled (i.e., the same shape but smaller) with respect to the actual waste packages;
2. "far-field" temperatures (i.e., outer walls) of the scale-model drift are maintained equal to the far-field temperatures of the actual drifts; and
3. relative humidity of the air in the scale-model drift is maintained at 100% by a water source within the drift.

These assumptions should be readily achievable in the tests. Assumption 3 is not actually required for thermal scaling but is needed to demonstrate the desired Cold Trap phenomenon (transport and

condensation of moisture). In the following discussion, the geometric scale factor is denoted by λ (e.g., 1/3 or whatever).

The heat added to the drift air by the waste packages eventually is transmitted to the surrounding rock (except for the small fraction needed to vaporize any liquid water within the drift). The energy balance between the heat q liberated by a waste package and the heat transferred to the air is expressed as:

$$q = hA_s\Delta T \tag{1}$$

Here, h is the convection heat transfer coefficient, A_s is the surface area of the waste package, and ΔT is the temperature difference between the outer surface of the waste package and the inner surface of the drift. As mentioned above, it is desired to conduct the scale-model tests such that the ΔT's measured in the scale model tests can be interpreted as full scale temperature differences and likewisw the heart transfer coefficients can also be "scaled up". The scale model surface areas are λ^2 times the full scale areas. If the scale factor for the heat transfer coefficient is denoted as λ_h and the scale factor for the scale model heater powers is denoted by λ_q, then from Equation (1):

$$\lambda_q = \lambda_h\lambda^2 \tag{2}$$

The thermal scaling of the waste packages thus reduces to the question of how the heat transfer coefficient h is scaled. The 2-D analysis of the Cold Trap model problem (described in a previous memo) indicated that the heat transfer coefficient increased as the geometric scale factor decreased. The experiments and analyses of Kuehn and Goldstein[1] for a similar geometry also demonstrated that the heat transfer coefficient increases as the scale factor decreases:

$$\lambda_h = \lambda^{-n} = \lambda^{-0.25} \tag{3}$$

If Eq. (3) holds for the Cold Trap geometry, the electrical power of the geometrically similar heaters has to be reduced in proportion to:

$$\lambda_q = \lambda^{1.75} \tag{4}$$

That is, the heater power is reduced more than the reduction in heater surface area.

Because of the uncertainty in the exact value of n in Eq. (3) for the Cold Trap experiment, it is recommended that the experiment be numerically simulated in advance. The simulations could be conducted for several values of the geometric scale factor λ, in which the exponent n be varied until a value of n is obtained that results in the equal values of ΔT at similar scaled locations for the various cases.

It is noted that scaling the heater power by the method described herein will not necessarily result in air velocities in the drift that can be easily interpreted in terms of full scale values. Presumably the recommended numerical simulations will shed some light on the velocity scaling. However, velocity scaling is not a crucial limitation for the experiments since the air velocity primarily determines the overall rate at which moisture is transported and condensed within the drift. The lack of a definite velocity scaling does not limit the validity of the experiments to demonstrate the Cold Trap phenomena nor will it compromise the ability to scale up the heat transfer results and the heat transfer coefficients to full scale.

[1] "An Experimental and Theoretical Study of Natural Convection in the Annulus Between Horizontal Concentric Cylinders," J. Fluid Mechanics, vol. 74, part 4, pp. 695-719, 1976.

A short memo from Frank Dodge:

SCALING TO REPOSITORY CONDITIONS

The fluid mechanics and heat transfer phenomena occurring in the drift depend on many interrelated parameters, but the primary dimensionless parameters that govern the drift response are the geometrical shapes of the drift and the waste packages, and the Rayleigh Number which governs the natural convection flows set up by the heat released by the waste packages. The Rayleigh Number is defined as $Ra = g\beta\Delta TL^3/\nu\alpha$, where g = gravity, β = thermal expansion coefficient of the drift fluid (i.e., air), ΔT = the temperature difference between the waste package surfaces and the drift fluid, L = a characteristic dimension (drift diameter), and ν = kinematic viscosity and α = thermal diffusivity of the drift fluid. Since Ra is a function of L^3, it is not possible to have exactly the same value of Ra for a reduced-scale model of the drift as for the repository (unless ΔT is increased substantially or a fluid different that air is used to fill the model drift). Consequently, some compromises must be made in the model, and the model tests must be conducted at different geometric scales or with different ΔTs, or empirical relations must be used, or the test results have to be interpreted with the aid of numerical simulations, in order to scale up the model experiments to repository conditions. Even with these restrictions, scale model tests can be conducted in such a way that, for example, the heat transfer coefficients h that apply between the waste packages and the drift fluid can be determined from the tests and scaled to the repository conditions: $h_{repository} = h_{model}(L_{model}/L_{repository})(Ra_{repository}/Ra_{model})^n$, where $n \approx 0.25$. In order to accomplish this scaling, the heat output of the simulated waste packages has to be adjusted appropriately, as discussed elsewhere in this report. Similarly, the airflow velocities and moisture transport can be interpreted (but not scaled up directly) to predict repository conditions. The two-dimensional analytical "model" problem demonstrates these conclusions quantitatively.

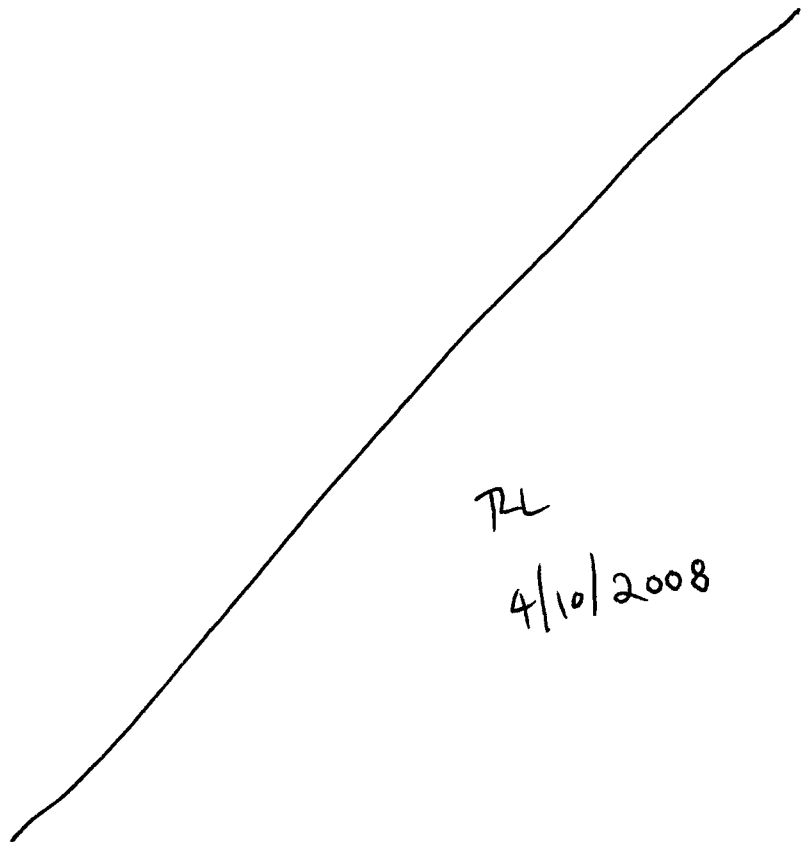

4/14/03 RF

Frank's New Condensation Model, Discretized Condensation Rate along the tunnel length is the only difference for this new version of the MathCad2000 worksheet:
E:\TEF-kti\ColdTrap\AnalyticalSoln\coldTrap modelProblem-moistureDistribution-2000.mcd

ANALYSIS OF COLD-TRAP EXPERIMENT

This is an analysis of a "model" problem tha is meant to aid in designing and interpreting the Cold Trap experiment. It replaces the actual cylindrical experiment drift with a two-dimensional drift. the model probelm also replaces the heater by a uniform hot wall. The object of the analysis is to predict the magnitudes of the overall circulation in the drift and the rate at which moisture might be condensed on a target near the cold wall.
Various values of the parameters can be input (as indicated by the **red text** below) to investigate their effects.

The overall geometry of the model problem is shown in the illustration.

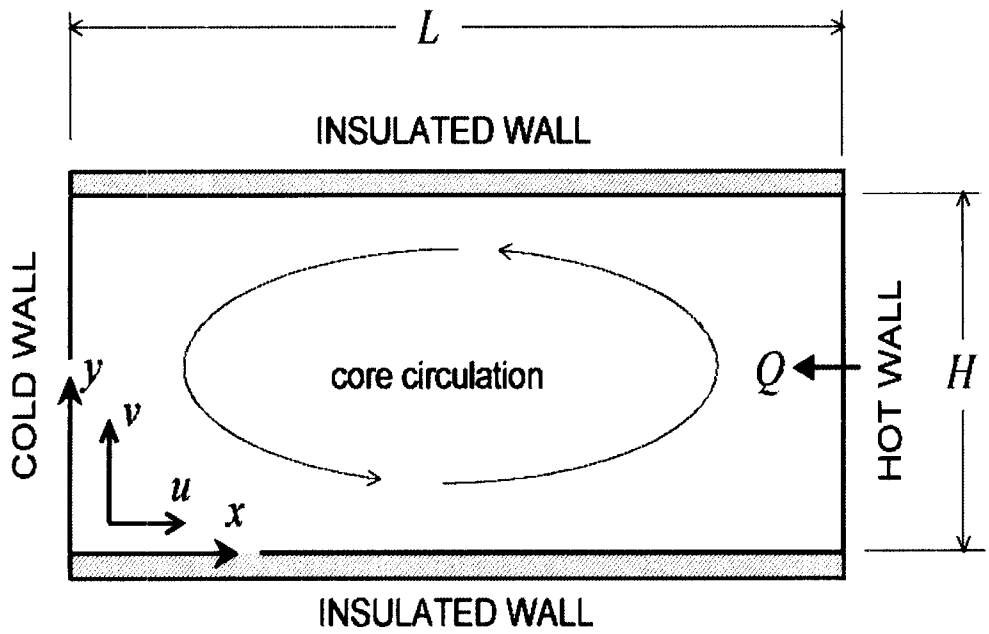

The main assumptions used in the *flow* analysis are:

2-D x,y geometry
heat Q added at the hot wall and removed at the cold wall
walls at $y = 0$ and $y = H$ are insulated
steady flow
Boussinesq approximation is used to estimate buyoyancy effects
The equations of motion are made nondimensional using the following scheme

$X = x/L$ $\quad Y = y/H$ = non-dimensional coordinates

$U = u\,(\nu_0 L)(g\beta_o H^3 \Delta T_o)^{-1}$ = non-dimensional velocity in x-direction

$V = v\,(\nu_0 L^2)(g\beta_0 H^4 \Delta T_0)^{-1}$ = non-dimensional velocity in y-direction

$\theta = (T - T_c)/\Delta T_0$ = non-dimensional temperature

The symbols are defined as:

ΔT_o = temperature difference between hot and cold walls
T = air temperature at time t at location x,y
T_c = temperature of the cold wall at $x = 0$
g = gravitational acceleration
β_o = thermal expansion coeffcient of air at the reference temperature
ν_o = kinematic viscosity of air at the reference temperature

Other symobls that will be used subsequently are defined as:
α_o = thermal diffusivity of air, $k_o/\rho_o C_{po}$, at the reference temperature
δ^* = boundary layer thickness parameter
ρ_o = density of air at the reference temperature
C_{po} = specific heat of air at the reference temperature
k_o = thermal conductivity of air at the reference temperature
p = pressure
Pr = Prandtl number, ν_o/α_o
Q = heat input at hot wall (per unit width of the drift)
Ra = Rayleigh number, $g\beta_o H^3 \Delta T_o/(\alpha_o \nu_o)$
t = time

With these definitions and non-dimensional variables, we expect that the **non-dimensional variables will have a maximum value of one and a minimum of zero**:

$0 <= X <= 1$ $0 <= Y <= 1$ $0 <= |U| <= 1$ $0 <= |V| <= 1$ $0 <= |\theta| <= 1$

GOVERNING DIFFERENTIAL EQUATIONS

The circulatory flow within the 2-D drift is governed by the following diffferenital equations, which express the conservation of mass, momentum, and energy requirements:

conservation of mass:

$$\frac{\partial U}{\partial X} + \frac{\partial V}{\partial Y} = 0$$

combined x and y conservation of momentum (combining the equations eliminates pressure as a variable)

$$\left(\frac{H}{L}\right)^4 \left(\frac{Ra}{Pr}\right)\left[\frac{\partial}{\partial X}\left(U\frac{\partial U}{\partial X} + V\frac{\partial U}{\partial Y}\right)\right] - \left(\frac{H}{L}\right)^2 \left(\frac{Ra}{Pr}\right)\left[\frac{\partial}{\partial Y}\left(U\frac{\partial V}{\partial X} + V\frac{\partial V}{\partial Y}\right)\right] =$$

$$\frac{\partial \theta}{\partial X} - \frac{\partial^3 U}{\partial Y^3} + \left(\frac{H}{L}\right)^2 \left[\frac{\partial}{\partial Y}\left(\frac{\partial^2 V}{\partial X \partial Y} - \frac{\partial^2 U}{\partial X^2}\right)\right] + \left(\frac{H}{L}\right)^4 \frac{\partial^3 V}{\partial X^3}$$

conservation of energy

$$Ra\left(\frac{H}{L}\right)^2 \left(U\frac{\partial \theta}{\partial X} + V\frac{\partial \theta}{\partial Y}\right) = \frac{\partial^2 \theta}{\partial Y^2} + \left(\frac{H}{L}\right)^2 \frac{\partial \theta}{\partial X^2}$$

The **boundary conditions** for these differential equations are expressed as:

$U = V = 0$ for $X = 0$ and $X = 1$, and for $Y = 0$ and $Y = 1$ ("no - slip")

$$\frac{\partial \theta}{\partial Y} = 0 \quad \text{for } Y = 0 \text{ and } Y = 1 \text{ (insulated walls)}$$

$\theta = 0$ for $X = 0$; $\theta = 1$ for $X = 1$

Considering the form of these equations and the fact that $(H/L)^2 << 1$, it is natural to try to find a **solution expressed in powers of $(H/L)^2$** since higher order terms can be negelected. Thus, we assume:

$$U = U_o + \left(\frac{H}{L}\right)^2 U_1 + \left(\frac{H}{L}\right)^4 U_2 + \ldots.$$

$$V = V_o + \left(\frac{H}{L}\right)^2 V_1 + \left(\frac{H}{L}\right)^4 V_2 + \ldots.$$

$$\theta = \theta_o + \left(\frac{H}{L}\right)^2 \theta_1 + \left(\frac{H}{L}\right)^4 \theta_2 + \ldots.$$

These expressions are substituted into the differential equations for mass, momentum, and energy conservation given above. We collect the terms in powers of the parameter $(H/L)^2$. Since $(H/L)^2$ in principle can have any value, it is necessary that the expressions multiplied by the various powers of $(H/L)^2$ must each be satisfied individually. This process gives the following set of differential equations.

Zeroth order $(H/L)^0$ equations

$$\frac{\partial U_o}{\partial X} + \frac{\partial V_o}{\partial Y} = 0$$

$$\frac{\partial \theta_o}{\partial X} - \frac{\partial^3 U_o}{\partial Y^3} = 0$$

$$\frac{\partial^2 \theta_o}{\partial Y^2} = 0$$

First order $(H/L)^2$ equations

$$\frac{\partial U_1}{\partial X} + \frac{\partial V_1}{\partial Y} = 0$$

$$-\frac{Ra}{Pr}\left[\frac{\partial}{\partial Y}\left(U_o \frac{\partial U_o}{\partial X} + V_o \frac{\partial U_o}{\partial Y}\right)\right] = \frac{\partial \theta_1}{\partial X} - \frac{\partial^3 U_1}{\partial Y^3} + \frac{\partial^3 V_o}{\partial X \partial Y^2} - \frac{\partial^3 U_o}{\partial Y \partial X^2}$$

$$Ra\left(U_o \frac{\partial \theta_o}{\partial X} + V_o \frac{\partial \theta_o}{\partial Y}\right) = \frac{\partial^2 \theta_o}{\partial X^2} + \frac{\partial^2 \theta_1}{\partial Y^2}$$

Second order $(H/L)^4$ equations

$$\frac{\partial U_2}{\partial X} + \frac{\partial V_2}{\partial Y} = 0$$

$$\frac{Ra}{Pr}\left[\frac{\partial}{\partial X}\left(U_o \frac{\partial U_o}{\partial X} + V_o \frac{\partial U_o}{\partial Y}\right)\right] - \frac{Ra}{Pr}\left[\frac{\partial}{\partial Y}\left(U_o \frac{\partial U_1}{\partial X} + V_o \frac{\partial U_1}{\partial Y} + U_1 \frac{\partial U_o}{\partial X} + V_1 \frac{\partial U_o}{\partial Y}\right)\right] =$$

$$\frac{\partial \theta_2}{\partial X} - \frac{\partial^3 U_2}{\partial Y^3} + \frac{\partial^3 V_1}{\partial X \partial Y^2} - \frac{\partial^3 U_1}{\partial Y \partial X^2} + \frac{\partial^3 V_o}{\partial X^3}$$

$$Ra\left(U_o \frac{\partial \theta_1}{\partial X} + V_o \frac{\partial \theta_1}{\partial Y} + U_1 \frac{\partial \theta_o}{\partial X} + V_1 \frac{\partial \theta_o}{\partial Y}\right) = \frac{\partial^2 \theta_2}{\partial Y^2} + \frac{\partial^2 \theta_1}{\partial X^2}$$

The third and higher order equations are similar to the second order equations.

SOLUTION TO DIFFERENTIAL EQUATIONS FOR THE <u>CORE</u> FLOW

The solution of the differential equations correct through the first order terms is:

$$U(K_1, Y) := \frac{1}{6} \cdot K_1 \cdot \left(Y^3 - \frac{3}{2} \cdot Y^2 + \frac{1}{2} \cdot Y\right)$$

$$V(K_1, Y) := 0$$

$$\theta(K_1, K_2, Ra, H, L, X, Y) := K_2 + K_1 \cdot X + \frac{1}{120} \cdot Ra \cdot K_1^2 \cdot \left(\frac{H}{L}\right)^2 \cdot \left(Y^5 - \frac{5}{2} \cdot Y^4 + \frac{5}{3} \cdot Y^3\right)$$

where K_1 and K_2 are integration constants to be determined.

These equations represent the **<u>core</u>** flow away from the $X = 0$ and $X = 1$ ends of the channel. Note that U is not identically zero at $X = 0$ and $X = 1$ as the boundary conditions require. However, the average value of U across the

channel height is zero, so the $X = 0$ and $X = 1$ boundary conditions are satisfied in an average sense. Similarly, the temperature θ is not constant at either the hot end or the cold end. The way the solutions are corrected to meet the boundary more exactly is described later.

HEAT FLOW FROM HOT END TO COLD END OF CHANNEL

The net heat flow from the hot end of the channel to the cold end is a combination of conduction through the air and the energy carried by the flow. It is given by the following integral. Note that the integral does not depend on position X in the channel.

$$Q = \int_0^H \left(k_o \frac{\partial T}{\partial X} - \rho_o C_{po} u T \right) dy$$

Carrying out the integration gives

$$Q(k_o, H, L, Ra, K_1, \Delta T_o) := k_o \cdot \Delta T_o \cdot \left(\frac{H}{L}\right) \cdot \left[K_1 + \frac{K_1^3}{362880} \cdot \left(\frac{H}{L} \cdot Ra\right)^2 \right]$$

EVALUATION OF INTEGRATION CONSTANTS TO MEET BOUNDARY CONDITIONS

A simple way to evaluate K_1 and K_2 is to set the average value of θ equal to 0 at $X = 0$ and equal to 1 at $X = 1$. This procedure gives $K_1 = 1$ and $K_2 = 0$. This satisfies the boundary conditions at X = 0 and X = 1 only in an average sense. We can do better by correcting the previous expressions by including the equations for higher powers of $(H/L)^2$ or we can consider the end effects separately by a boundary layer approach. The boundary layer approach is selected because it converges more quickly. Furthermore, an "integral" formulation is used. The boundary layer thickness at the end walls is denoted by δ. From symmetry, δ is the same on the cold wall and the hot wall. Thus, we will impose symmetry about the center of the drift and consider just the cold wall. The end conditions are denoted by the subscript "*e*."

The symmetry condition of θ = 0.5 for X =0.5, Y = 0.5 requires that:

$$K_2 + \frac{1}{2} K_1 + Ra\left(\frac{H}{L}\right)^2 \frac{K_1}{1440} = \frac{1}{2}$$

The boundary conditions at the cold wall are: (a) all velocities be zero; and (b) the temperature be constant and equal to the cold wall temperature. These conditions require that:

$$U_e = V_e = \theta_e = 0 \qquad \frac{\partial \theta_e}{\partial Y} = 0 \qquad \text{at} \quad X = 0$$

There are also conditions required to match the boundary layer to the core flow at the edge of the boundary layer and to make the boundary layer flow merge smoothly with the core flow; these conditions are expressed as:

$$U_e = U \qquad V_e = V = 0 \qquad \theta_e = \theta \qquad \text{at } X = \delta$$

$$\frac{\partial U_e}{\partial X} = \frac{\partial U}{\partial X} \qquad \frac{\partial V_e}{\partial X} = \frac{\partial V}{\partial X} = 0 \qquad \frac{\partial \theta_e}{\partial X} = \frac{\partial \theta}{\partial X} \qquad \text{at} \quad X = \delta$$

For an "integral" solution, we assume physically reasonable functions for the velocities and temperature, which are then made to satisfy the governing equations in an integral sense. The unknown in these functions is the boundary layer thickness, δ.

Suitable fundtional forms for the velocities and temperature that satisfy all the above B.C.s are:

$$U_e = K_1 \left(Y^3 - \frac{3}{2} Y^2 + \frac{1}{2} Y \right) \left(\frac{X}{\delta}\right)^2 \left[1 - \frac{4}{3}\left(\frac{X}{\delta}\right) + \frac{1}{2}\left(\frac{X}{\delta}\right)^2 \right]$$

$$V_e = \frac{K_1}{2\delta} \left(Y^4 - 2Y^3 + Y^2 \right) \left(\frac{X}{\delta}\right) \left(1 - \frac{X}{\delta}\right)^2$$

$$\theta_e = \left[K_2 + K_1 X + \frac{Ra}{120} K_1^2 \left(\frac{H}{L}\right)^2 \left(Y^5 - \frac{5}{2} Y^4 + \frac{5}{3} Y^3 \right) \right] \left(\frac{X}{\delta}\right) \left(2 - \frac{X}{\delta}\right)$$

Furthermore, the expressions for U_e and V_e satisfy the conservation of mass differential equation. Thus, only the conservation of momentum and conservation of energy equations remain to be satisfied. These equations are put into

an integral form by integrating them across the boundary layer thickness. The result, for example, for the **conservation of energy** differential equation is:

$$Ra\left(\frac{H}{L}\right)\int_0^{\delta}\int_0^{1} U_e\frac{\partial\theta_e}{\partial X}\,dXdY + Ra\left(\frac{H}{L}\right)^2\int_0^{\delta}\int_0^{1} V_e\frac{\partial\theta_e}{\partial Y}\,dXdY = \int_0^{\delta}\int_0^{1}\left[\left(\frac{H}{L}\right)^2\frac{\partial^2\theta_e}{\partial X^2}+\frac{\partial^2\theta_e}{\partial Y^2}\right]dXd$$

Some of the integrations can be done by parts to give the final result:

$$Ra\int_0^{1} U_e\theta_e\big|_{X=\delta}\,dY = K_1 - \int_0^{1}\left.\frac{\partial\theta_e}{\partial Y}\right|_{X=\delta} dY$$

Similarly, the **conservation of momentum** integral reduces to:

$$\int_0^{1}\theta_e\big|_{X=\delta}\,dY - \int_0^{\delta}\left.\frac{\partial^2 U_e}{\partial Y^2}\right|_{Y=0}^{Y=1} dX - \left(\frac{H}{L}\right)^4\int_0^{1}\left.\frac{\partial^2 V_e}{\partial X^2}\right|_{X=0}^{X=\delta} dY = 0$$

By substituting in the previous functional expressions and performing the integrations, we derive the following two equations that relate the unknown parameters:

$$\frac{2}{5}\left(\frac{H}{L}K_1\right)\left[\frac{1}{4}-(\delta')^4\right] = \left[K_2 + \frac{Ra}{1440}\left(\frac{H}{L}K_1\right)^2\right](\delta')^3$$

$$\frac{Ra^2}{725{,}760}\left(\frac{H}{L}K_1\right)^3\delta' = K_2 + \frac{Ra}{1440}\left(\frac{H}{L}K_1\right)^2$$

where $\delta' = \delta(L/H)$ is a scaled boundary layer thickness that is more convenient for numerical work since it is not so small as δ.

These two expressions and the previous expression for the symmetry condition are sufficient to determine the three unknowns: K_1, K_2, and δ'.

NUMERICAL RESULTS

Input values for drift dimensions, air properties, and desired temperature difference from the hot end to the cold end of the drift (properties are evaluated at about 60 deg C).

Air viscosity:

$\nu_o := 0.191\cdot\frac{cm^2}{s}$

Air diffusivity:

$\alpha_o := 0.268\cdot\frac{cm^2}{s}$

Air conductivity:

$k_o := 0.000283\cdot\frac{watt}{cm\cdot K}$

Drift height:

$H := 5\cdot cm$

Drift length:

$L := 24\cdot 2.54\cdot cm$

Gravity:

$g := 980\cdot\frac{cm}{s^2}$

Cold wall temperature:

$T_c := 295\cdot K$

Temperature difference:

$\Delta T_o := 32\cdot K$

Computed parameters

Air expansion coefficient:

$$\beta_o := \frac{1}{T_c + \Delta T_o}$$

$$\beta_o = 3.058 \times 10^{-3} \frac{1}{K}$$

Rayleigh number:

$$Ra := \frac{g \cdot \beta_o \cdot H^3 \cdot \Delta T_o}{\nu_o \cdot \alpha_o}$$

$$Ra = 2.342 \times 10^5$$

Equations are solved by inputting guesses and then finding the solution

(Because of limitations in Mathcad's font selection for equations, δ' will be replaced by δ_x for numerical work)

Guesses:

$K_1 := 1$

$K_2 := 0$

$\delta_x := 1$

Given

$$K_2 + 0.5 \cdot K_1 + \left(\frac{H}{L} \cdot K_1\right)^2 \cdot \frac{Ra}{1440} = 0.5$$

(symmetry condition)

$$0.4 \cdot \left(\frac{H}{L} \cdot K_1\right) \cdot \left(0.25 - \delta_x^{\,4}\right) = \delta_x^{\,3} \cdot \left[K_2 + \left(\frac{H}{L} \cdot K_1\right)^2 \cdot \frac{Ra}{1440}\right]$$

(conservation of energy)

$$\left(\frac{H}{L} \cdot K_1\right)^3 \cdot \frac{Ra^2 \cdot \delta_x}{725760} = K_2 + \left(\frac{H}{L} \cdot K_1\right)^2 \cdot \frac{Ra}{1440}$$

(conservation of momentum)

$$\begin{pmatrix} KK_1 \\ KK_2 \\ \delta\delta \end{pmatrix} := \text{Find}(K_1, K_2, \delta_x)$$

(This is MathCad's solution technique)

$K_1 := KK_1$

$K_2 := KK_2$

$\delta_x := \delta\delta$

The numerical results are:

$K_1 = 0.339$

$K_2 = 0.204$

$\delta_x = 0.203$

PLOTS OF CORE FLOW AND TEMPERATURE

Plotting range:

$Y := 0, .02 .. 1$

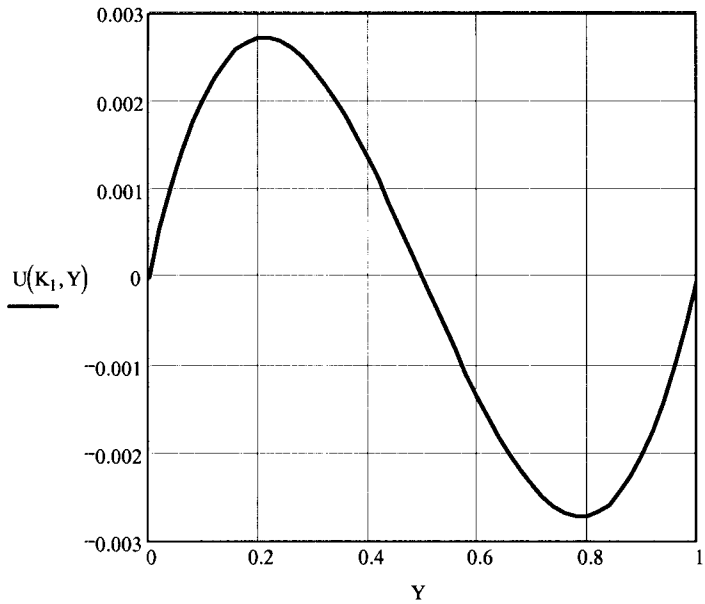

X-velocity (non-dimensional)

(Velocity in upper half of the drift
is from the hot end to the cold end,
and in the reverse direction for the
lower half)

Peak velocity (dimensional) from the graph:

$$u_{max} := 0.0016 \cdot \left(\frac{g \cdot \beta_o \cdot H^3 \cdot \Delta T_o}{\nu_o \cdot L} \right)$$

$$u_{max} = 0.016 \frac{m}{s}$$

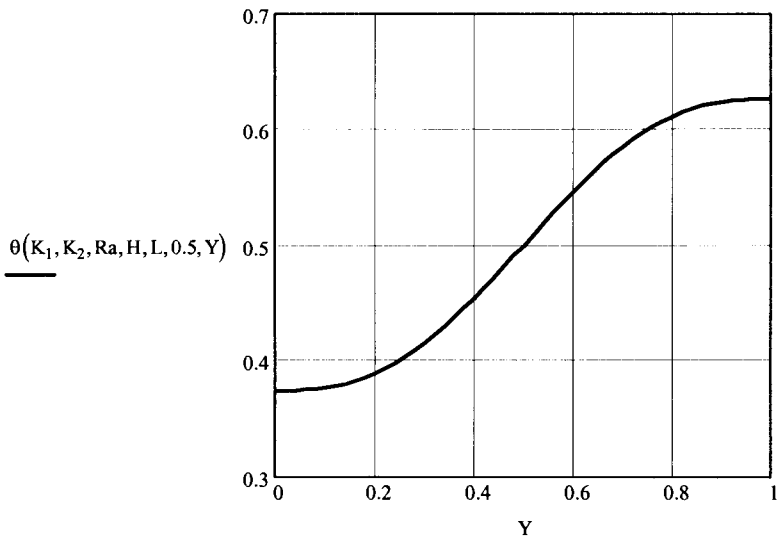

Nondimensional temperature distribution at X = 0.5

PLOTS OF FLOW AND TEMPERATURE IN THE END WALL REGION

Definition of end-wall X and Y velocities:

$$U_e(K_1,\delta_x,X,Y) := K_1\cdot\left(Y^3-\frac{3}{2}\cdot Y^2+\frac{1}{2}\cdot Y\right)\cdot\left(\frac{X}{\delta_x}\right)^2\cdot\left[1-\frac{4}{3}\cdot\left(\frac{X}{\delta_x}\right)+\frac{1}{2}\left(\frac{X}{\delta_x}\right)^2\right]$$

$$V_e(K_1,\delta_x,X,Y) := \frac{K_1}{2\cdot\delta_x}\cdot\left(\frac{X}{\delta_x}\right)\cdot\left(1-\frac{X}{\delta_x}\right)^2\cdot\left(Y^4-2\cdot Y^3+Y^2\right)$$

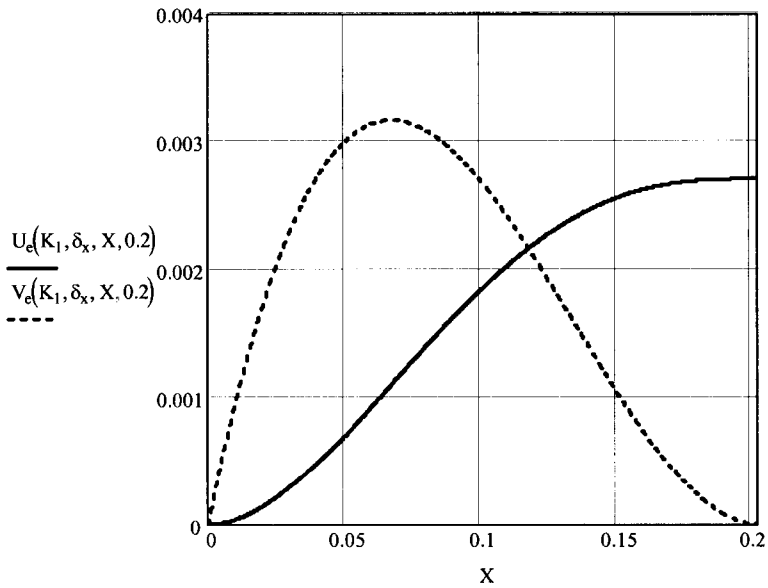

Plot of velocities in the end wall region $0 < X < \delta_X$ at the Y elevation that corresponds to the peak core flow velocity. Note that the X-velocity blends smoothly to the core velocity for $X = \delta_X$ and the the V-velocity decreases to zero at $X = \delta_X$.

Definition of end-wall temperature distribution:

$$\theta_e(K_1,K_2,Ra,\delta_x,H,L,X,Y) := \left(\frac{X}{\delta_x}\right)\cdot\left(2-\frac{X}{\delta_x}\right)\cdot\theta(K_1,K_2,Ra,H,L,X,Y)$$

$\theta_e(K_1, K_2, Ra, \delta_x, H, L, X, 0.5)$

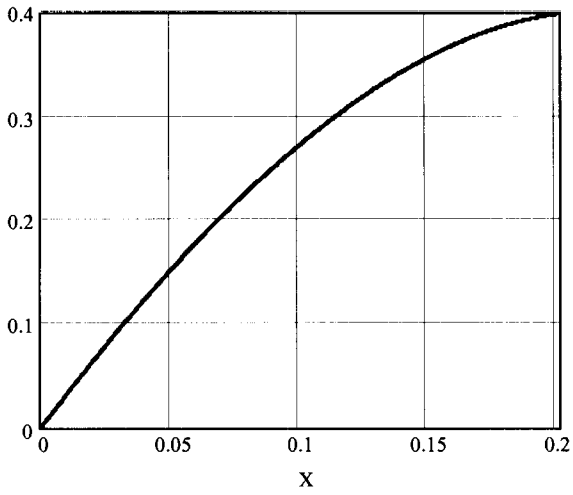

Plot of end wall temperature for $Y = 0.5$. Not that the temp. gradually increases from its value at $X = \delta_X$ to a value of 0.5 at $X = 0.5$, for this value of $Y = 0.5$.

MOISTURE TRANSPORT

The moisture transport is computed using the following observations and assumptions.

1. The flow from the hot end to the cold end carries wetter air to the cold end.
2. The reverse flow from the cold end to the hot end carries drier air back to the hot end
3. The air has a 100% relative humidity a the hot end. When the air gets to the cold end, if will be supersaturated and some moisture will condense on the target. The air will still have a 100% relative humidity but because it is colder, the actual mass of water in the air will be less.
4. The air flow from one end to the other is equal to the average density of the air times the average velocity in either the upper (hot to cold) or lower (cold to hot) half of the tube.
5. Same air flow rate occurs in the circular channel as in the 2-D channel

INPUT FROM THERMODYNAMICS AND FROM THE STEAM TABLES

Relative humidity:

$RH := 1$

Moisture vapor pressures at various temperatures (curve fit to the steam table data over a range of temperatures):

$A := 0.0259 \cdot K^{-1}$

$B := 460 \cdot K$

$C := 0.075 \cdot psi$

$PV(T) := C \cdot e^{A \cdot \left(\frac{9}{5}T - B\right)}$

psia

Partial pressure of the air in the air-moisture mixture:

$P_o := 14.7 \cdot psi$

$P(T) := P_o - PV(T)$

psia

Absolute humidity of the air at temperature T

$\omega_o := 0.622 \cdot \frac{gm}{gm}$

$$\omega(T) := \omega_o \cdot \frac{PV(T)}{P(T)} \cdot RH$$

grams of moisture per gram of dry air

Average density of the dry air for cold air at temperature T and hot air at temperature T+ΔT:

$$R := 41.65 \cdot \frac{cm^3 \cdot psi}{K \cdot gm}$$

$$\rho(T, \Delta T) := \frac{(P(T + \Delta T) + P(T))}{(2 \cdot T + \Delta T) \cdot R}$$

grams per cubic centimeter

AIR MASS FLOW RATE

Reference air velocity:

$$UU := \frac{g \cdot \beta_o \cdot H^3 \cdot \Delta T_o}{6 \cdot \nu_o \cdot L}$$

Average velocity in the hot or cold half of the channel (by integrating the core velocity distribution):

$$U_{ave} := \frac{1}{32} \cdot UU \cdot K_1$$

$$U_{ave} = 1.819 \frac{cm}{s}$$

Mass flow rate of core air flow in the upper or lower half of the channel:

$$m_{air}(T, \Delta T_o) := \rho(T, \Delta T_o) \cdot U_{ave} \cdot \frac{\pi}{4} \cdot \frac{H^2}{2}$$

$$m_{air}(T_c, \Delta T_o) = 0.018 \frac{gm}{s}$$

MOISTURE FLOW RATE

The amount of moisture condensed at a location is the difference in absolute humidities at the hot end and the channel location in question times the flow rate of dry air:

$$m_{cond}(T, \Delta T) := m_{air}(T, \Delta T) \cdot (\omega(T + \Delta T) - \omega(T))$$

gram moisture per second

$$m_{cond}(T_c, \Delta T_o) = 1.533 \times 10^{-3} \frac{gm}{s}$$

$$\Delta m_{total} := m_{cond}(T_c, \Delta T_o)$$

CONDENSED MOISTURE PER HOUR

*The amount of moisture condensed **per hour** on the target can be no larger than:*

$$M := 3600 \cdot s \cdot m_{cond}(T_c, \Delta T_o)$$

$$M = 5.518\,gm$$

(NEW STUFF)

MOISTURE DISTRIBUTION ASSUMING CONTIONUOUS FALL OUT

Assume ten spatial increments along the axis of the model drift

$L = 0.61\,m$

Boundary layer thickness:

$$\delta := \delta_x \cdot H$$

$$\delta = 0.01\,m$$

$$x_1 := 0.5 \cdot \delta$$

$$x_2 := \delta$$

$$x_{10} := L$$

$$x_9 := L - 0.5 \cdot \delta$$

$x_8 := L - \delta$

$i := 1,2..6$

$x_{i+2} := \delta + \frac{L - 2\cdot\delta}{6}\cdot i$

$j := 1,2..10$

$x_j =$

$5.075\cdot10^{-3}$	m
0.01	
0.108	
0.207	
0.305	
0.403	
0.501	
0.599	
0.605	
0.61	

$T_1 := \theta_e\left(K_1, K_2, Ra, \delta_x, H, L, \frac{\delta_x}{2}, 0.5\right)\cdot\Delta T_o + T_c$

$T_1 = 303.756\,K$

$T_2 := \theta_e\left(K_1, K_2, Ra, \delta_x, H, L, \delta_x, 0.5\right)\cdot\Delta T_o + T_c$

$T_2 = 307.776\,K$

$\delta_x = 0.203$

$T_{10} := \Delta T_o + T_c$

$T_{10} = 327\,K$

$T_9 := T_{10} - \left(T_1 - T_c\right)$

$T_9 = 318.244\,K$

$\frac{x_3}{L} = 0.178$

$T_8 := T_{10} - \left(T_2 - T_c\right)$

$T_8 = 314.224\,K$

$i := 1,2..6$

$j := 1,2..10$

$T_{i+2} := \frac{T_8 - T_2}{6}\cdot i + T_2$

T_j =

303.756	K
307.776	
308.851	
309.925	
311	
312.075	
313.149	
314.224	
318.244	
327	

Relative humidity:

$RH := 1$

Moisture vapor pressures at various temperatures (curve fit to the steam table data over a range of temperatures):

$A := 0.0259 \cdot K^{-1}$

$B := 460 \cdot K$

$C := 0.075 \cdot psi$

$PV(T) := C \cdot e^{A \cdot \left(\frac{9}{5} T - B\right)}$

psia

Partial pressure of the air in the air-moisture mixture:

$P_o := 14.7 \cdot psi$

$P(T) := P_o - PV(T)$

psia

Absolute humidity of the air at temperature T

$\omega_o := 0.622 \cdot \frac{gm}{gm}$

$\omega(T) := \omega_o \cdot \frac{PV(T)}{P(T)} \cdot RH$

grams of moisture per gram of dry air

Average density of the dry air for cold air at temperature T and hot air at temperature T+ΔT:

$R := 41.65 \cdot \frac{cm^3 \cdot psi}{K \cdot gm}$

$\rho(T, \Delta T) := \frac{(P(T + \Delta T) + P(T))}{(2 \cdot T + \Delta T) \cdot R}$

grams per cubic centimeter

AIR MASS FLOW RATE

Reference air velocity:

$U_c(\Delta T_o) := \frac{g \cdot \beta_o \cdot H^3 \cdot \Delta T_o}{6 \cdot \nu_o \cdot L}$

Average velocity in the hot or cold half of the channel (by integrating the core velocity distribution):

$U_{ave}(\Delta T_o) := \frac{1}{32} \cdot U_c(\Delta T_o) \cdot K_1$

$U_{ave}(\Delta T_o) = 1.819 \frac{cm}{s}$

Mass flow rate of air in the upper or lower half of the channel:

$$m_{air}(T,\Delta T_o) := \rho(T,\Delta T_o)\cdot U_{ave}(\Delta T_o)\cdot\frac{\pi}{4}\cdot\frac{H^2}{2}$$

$$m_{air}(T_c,\Delta T_o) = 0.018\,\frac{gm}{s}$$

MOISTURE FLOW RATE

The amount of moisture condensed from the hot end to a location in the channel is the difference in absolute humidities at the hot end and the channel location in question times the flow rate of dry air:

$m_{cond}(T) := m_{air}(T,\Delta T_o)\cdot(\omega(T_c+\Delta T_o)-\omega(T))$

gram moisture per second

$i := 1,2..11$

$TT_i := T_{11-i}$

$T_c = 295\,K$

$TT_{11} := T_c$

$m_{cond}(TT_i) =$

	gm/s
0	
$5.36\cdot10^{-4}$	
$7.561\cdot10^{-4}$	
$8.115\cdot10^{-4}$	
$8.653\cdot10^{-4}$	
$9.176\cdot10^{-4}$	
$9.684\cdot10^{-4}$	
$1.018\cdot10^{-3}$	
$1.065\cdot10^{-3}$	
$1.232\cdot10^{-3}$	
$1.533\cdot10^{-3}$	

$i := 1,2..10$

Amount condensed at each x location:

$\Delta m_{cond}(i) := m_{cond}(TT_{i+1}) - m_{cond}(TT_i)$

$\Delta m_{cond}(i) =$

	gm/s
$5.36\cdot10^{-4}$	
$2.201\cdot10^{-4}$	
$5.532\cdot10^{-5}$	
$5.381\cdot10^{-5}$	
$5.229\cdot10^{-5}$	
$5.079\cdot10^{-5}$	
$4.93\cdot10^{-5}$	
$4.783\cdot10^{-5}$	
$1.663\cdot10^{-4}$	
$3.009\cdot10^{-4}$	

$x_i =$

0.507	cm
1.015	
10.837	
20.658	
30.48	
40.302	
50.123	
59.945	
60.453	
60.96	

$$\sum_{i=1}^{10} \Delta m_{cond}(i) = 1.533 \times 10^{-3} \frac{gm}{s}$$

Percent of total condensation at each location

$$\Delta mPercent(i) := \frac{\Delta m_{cond}(i)}{\Delta m_{total}}$$

$\Delta mPercent(i)$

0.35
0.144
0.036
0.035
0.034
0.033
0.032
0.031
0.109
0.196

$x_i =$

0.507	cm
1.015	
10.837	
20.658	
30.48	
40.302	
50.123	
59.945	
60.453	
60.96	

4/20/03 RF

Condensation Calculations – Desktop Model

bubo:
E:\TEF-kti\ColdTrap\AnalyticalSoln\coldTrap modelProblem-moistureDistribution-2000.mcd
E:\TEF-kti\ColdTrap\Test-14\cttest14.xls (worksheet "steady-summary")

By changing inputs on page VII-62 (primarily cold wall temperature and temperature difference), and reading the results at the end of the MathCad2000 sheet the tables in the "steady-summary" worksheet were created. Distribution along the drift and cumulative distribution along the drift were created. Figure VII-72 contains the plotted results for different temperature gradients from the analytical model. As expected given the assumed condensation model, most of the condensation occurs near the heater and near the heat-sink wall. In-between these points, there is little temperature variation along the drift as predicted by the analytical solution. Note, however, that the analytical solution does not account for the variation in heat flux out the cylinder along the drift length (higher heat flux near the heater, less heat flux near the cold end).

Figure VII-72. Condensation rate at points along the drift. Here the cold end is the "0" distance and the heater cartridge end is at 61 cm (Prikryl's original coordinate system origin at the cold end).

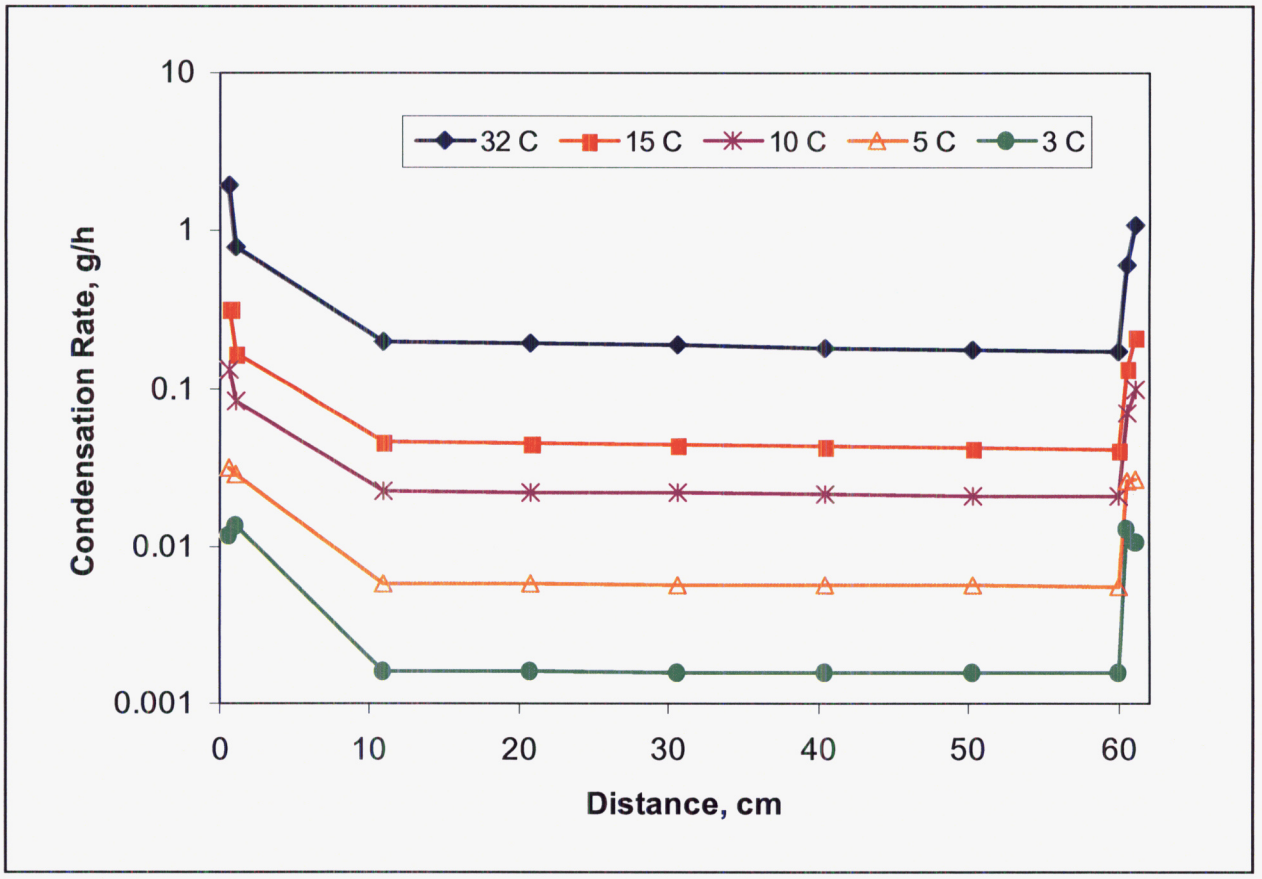

Figure VII-73a contains the cumulative distribution of the same data as used in Figure VII-72, The condensation rate is accumulated starting from the heat-sink end (cold end) of the drift in Figure VII-73a.

Figure VII-73a

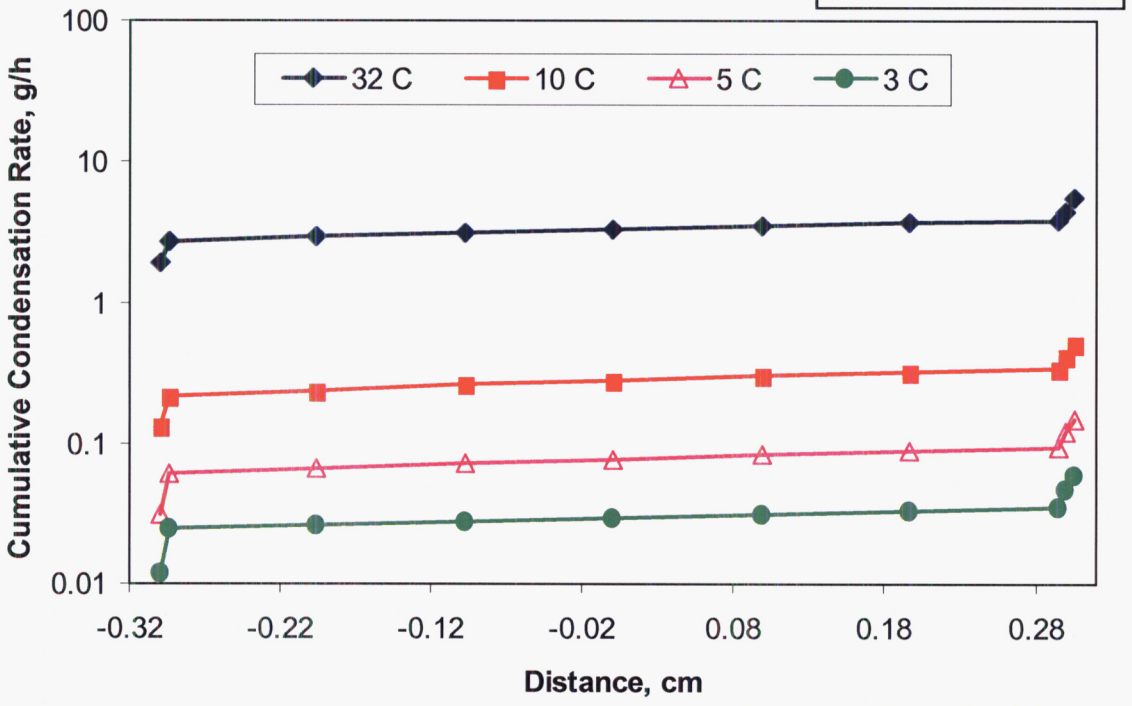

In Figure VII-73b. the simulated condensation at the cold end of the tunnel is compared with the measured condensation coming off the heat sink wall. The closeness of the match is likely to be misleading because the CFD modeling being done by David Walter (Sci Ntbk #576) seems to indicate that the condensation should all occur near the heat source, where the largest temperature gradient occurs. The CFD results show little temperature variation along the cold half of the drift; the airflow vectors are very small in the cold half versus the hot half of the drift (half, as in the axial direction). Also, the first measured data point (ΔT=4 C) should probably be considered reliable because of overall temperatures in the sand and drift. Temperatures in the room were influencing the sand temperatures, both of which were higher than those of the heat sink.

Figure VII-73b

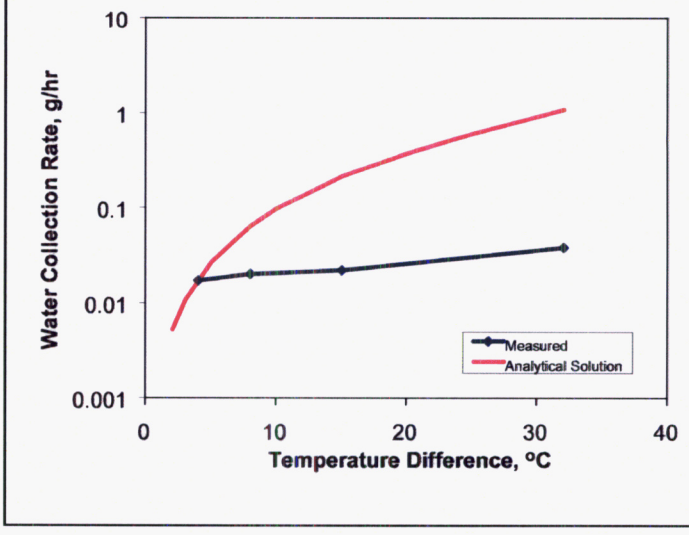

==========

10/03/03 RF

Entries made into Scientific Notebook #432E for the period April 3, 2002 to September 30, 2003 have been made by Randall Fedors (October 3, 2003).

No original text or figures entered into this Scientific Notebook has been removed

RF 10/03//2003

==========

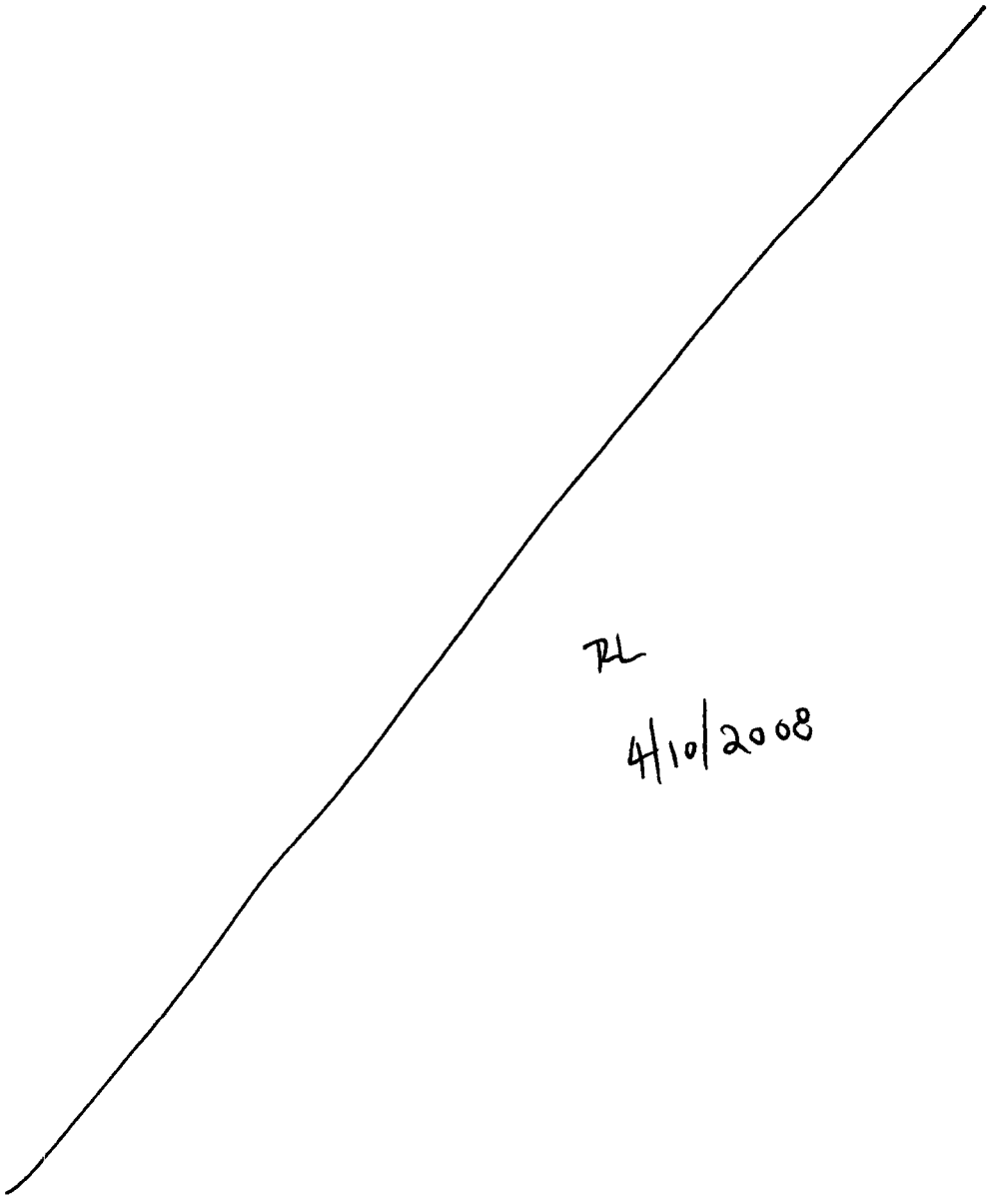

Volume VII – TEF Cold Trap

RF 12/17/03

Gustavo's Integration Meeting

For Gustavo integration meeting Dec 18, 2003, provide temperature conditions conducive to localized corrosion.

Using info from files
edge-effectCM_final.xls (Chandrika file)
Psat.xls (used with simple model to determine that RH=.247 when T=140C; presuming boiling at T=97C)
early_east-temperatureprofile1.xls (see SciNtbk #432e Vol VIII, and SciNtbk #532)
EdgeEffectDegradation.xls (see SciNtbk #432e Vol VIII, and SciNtbk #532)
Dft25west_results.xls (Chandrika file)
Dft25west_RHresults.xls (Chandrika file)

These spreadsheets are in bubo: E:\TEF-kti\Sensitivity-June2003\RevisionsAug2003

Information Relevant to Waste Package Environment	Peak Temperature	Duration of Time 80<T °C<140	Onset Year of Temperature Window
Center - No Degradation[1]	160	4638	215
East Edge - No Degradation[1]	82	393	70
Center - Base Case Drift Degradation[2]	223	5430	731
West Edge - Base Case Drift Degradation[2]	137	2330	51

Entries ignore early period during rise in temperatures.
At 140 °C, RH=0.247 using simple assumption.
1. TH result only
2. TH input to in-drift model.

12/18/03 RF

Preliminary Boundary Conditions for CFD Drift Modeling

Computational fluid dynamics model of 200-m segment (Steve Green's) needs temperature boundary condition in the wallrock along the entire length of the drift. Until the 3D thermohydrology modeling is (started and) completed, the 3D mountain scale model for conduction will be used (TPA conduction mountain scale model).

Comments